

Nonlinear Modeling, Identification and Control of Membrane Bioreactors

Guilherme Araujo Pimentel

▶ **To cite this version:**

Guilherme Araujo Pimentel. Nonlinear Modeling, Identification and Control of Membrane Bioreactors. General Mathematics [math.GM]. Université Montpellier; Université de Mons, 2015. English. NNT : 2015MONTS219 . tel-01130312v2

HAL Id: tel-01130312

https://inria.hal.science/tel-01130312v2

Submitted on 5 Mar 2019

HAL is a multi-disciplinary open access archive for the deposit and dissemination of scientific research documents, whether they are published or not. The documents may come from teaching and research institutions in France or abroad, or from public or private research centers.

L'archive ouverte pluridisciplinaire **HAL**, est destinée au dépôt et à la diffusion de documents scientifiques de niveau recherche, publiés ou non, émanant des établissements d'enseignement et de recherche français ou étrangers, des laboratoires publics ou privés.

Nonlinear Modeling, Identification and Control of Membrane Bioreactors

Guilherme Araujo Pimentel
Graduate Automation and Control Engineer
Master Electrical Engineer
(Pontifícia Universidade Católica do Rio Grande do Sul - BRA)

Ph.D. Thesis
submitted at the
Université de Mons and Université de Montpellier 2
in fulfilment of the requirements for the degree of

Docteur en Sciences de l'Ingénieur (UMons)
Docteur en Mathématiques et Modélisation (UM2)

Jury Members

Prof. Dr. A.-L. Hantson	(Université de Mons, Belgium) - *Secretary*
Prof. Dr. J.-L. Vasel	(Université de Liège , Belgium) - *Jury President*
Prof. Dr. I. Queinnec	(LAAS-CNRS, France) - *Rapporteur*
Prof. Dr. Ph. Bogaerts	(Université Libre de Bruxelles, Belgium) - *Rapporteur*
Prof. Dr. M. Heran	(Université Montpellier 2, France) - *Examiner*
Dr. J. Harmand	(Institut National de Recherche Agronomique, France) - *Examiner*
Dr. A. Rapaport	(Institut National de Recherche Agronomique, France) - *Advisor (FRA)*
Prof. Dr. A. Vande Wouwer	(Université de Mons, Belgium) - *Advisor (BEL)*

To my wife, Bruna.

A tarefa de viver é dura, mas fascinante.
Ariano Suassuna (1927–2014)

Acknowledgments

I would like to express my deepest gratitude to Dr. Alain Vande Wouwer, my advisor in Belgium, and Dr. Alain Rapaport, my advisor in France, for giving me the opportunities to be part of the Automatic Control Laboratory of the University of Mons (Belgium) and the MODEMIC INRA-INRIA team in the UMR MISTEA Research Laboratory (France). I am grateful for their advice in the scientific and life domains.

I give special appreciation to my two thesis rapporteurs, Dr. Isabelle Queinnec and Dr. Philippe Bogaerts, and to the jury members, Dr. Anne-Lise Hantson, Dr. Jean-Luc Vasel, Dr. Marc Heran and Dr. Jérôme Harmand, for their invaluable comments and advice for improving my thesis.

I acknowledge the Interuniversity Attraction Pole DYSCO and INRA-INRIA for the support and funding sources that made my research work possible.

A special thanks to my colleagues Pedro, Micaela, Ines, Cristina, Paul, Sofia, Giannina, Radhouanne, Mihaela, Laurent, Vincent, William, M. Remy, Christine, Véronique, Razvan, Coralie, Amel, Amine, José, Laurence, Céline, Tewfik and Fabien for all their advice and the nice talks in the years working with them. My gratitude also goes to Ciler, Jonathan and Thomas for their help in the revision and the improvement of my thesis manuscript.

Likewise, a big thank you to all the people I have met in the last few years in Mons and Montpellier who have helped me to maintain high spirits in the hardest of moments and have fun in the brightest ones.

I also thank my friends in Brazil who have encouraged me every step of the way. Finally, I thank my lovely wife Bruna for her support, patience and unconditional love, as well as my family who have supported me from the moment I decided to embark on a PhD until the very end.

Summary

This thesis proposes a simple submerged membrane bioreactor (sMBR) dynamic model that comprises physical and biological process behaviors. Filtration (physical aspect) is represented by a resistance-in-series model composed of a reversible resistance, linked to the sludge cake formation (that can be detached by air scouring) and an irreversible fouling resistance. The biological process is described by a simple chemostat model. The model asymptotic behavior, observability, controllability and fast and slow dynamics are analyzed. The latter analysis, based on Tikhonov's theorem, reveals the possibility decouple the dynamics in three time-scales, i.e. long-term fouling evolution (slow dynamic), biological degradation (fast dynamic) and fouling cake formation (ultrafast dynamic).Therefore, a parameter identification is organized in three steps corresponding to the three time-scales obtained from the analytical analysis. The parameter identification is implemented using a weighted least-squares cost function and a lower bound on the covariance matrix of the parameter estimates, which is used to obtain the parameters confidence intervals, is computed by the inverse of the Fisher Information Matrix (FIM). The model capacity to predict trans-membrane pressure and biological degradation is proved by model identification and cross-validation results.

As sMBR processes are relativity new, experimental process data are scarce. Thus, a lab-scale recirculating aquaculture system with an sMBR is designed, built and automated. Process online measurements, such as temperature, total suspended solids (TSS), ammonia and nitrate effluent concentrations, air cross- and effluent flow rates and trans-membrane pressure, are gathered in order to validate the proposed model. In addition, experimental data from a pilot plant located in Spain are also used to further analyze and validate the model.

Concerning the process control theoretical study of two different approaches are presented: a nonlinear model predictive control (NMPC) is

implemented in order to optimize the effluent production rate and maximize the period between two chemical cleaning procedures and a partial-linearizing feedback Lyapunov controller is designed in order to stabilize the fouling by actuating in the air cross- and effluent flows.

The results included in this thesis show the importance of analytical model studies in order to gain process insight and deduce model simplification.

Another important point is the simple dynamic model structure with a small number of parameters, which is adequate to implement advanced control strategies on sMBR processes and, similarly, to predict biological degradation and fouling build-up dynamics.

Résumé de la Thèse

Cette thèse propose un modèle dynamique d'un BioRéacteur à Membrane Submergée (BRMS) incluant les comportements physiques et biologiques du processus. La filtration (aspect physique) est représentée par un modèle avec des résistances en série, composé de la résistance réversible (liée au processus de formation d'un gâteau qui peut être enlevé grâce à un débit d'air) et de la résistance au colmatage irréversible. Le comportement biologique est décrit par un modèle de chémostat simple. L'analyse du modèle comprend : l'analyse asymptotique, l'observabilité, la contrôlabilité et l'étude dynamique lente et rapide. Cette dernière, basée sur le théorème de Tikhonov, révèle la possibilité de simplifier la dynamique du modèle en découplant le processus en trois échelles de temps : l'évolution du colmatage à long terme (dynamique lente), la dégradation biologique (dynamique rapide) et la formation du gâteau (dynamique ultrarapide). Par conséquent, une identification des paramètres est organisée en trois étapes correspondant aux trois échelles de temps obtenues à partir de l'analyse analytique. L'identification des paramètres est implémentée en utilisant d'une part une fonction de coût basée sur la méthode des moindres carrés pondérés et d'autre part, l'inverse de la matrice d'information de Fisher (FIM) qui est utilisée pour obtenir les intervalles de confiance des paramètres calculés. La capacité du modèle à prédire la pression transmembranaire et la dégradation biologique est prouvée par la validation du modèle et la validation croisée des résultats. Comme les processus BRMS sont relativement nouveaux, les données expérimentales publiées dans la littérature restent relativement rares. C'est pourquoi un procédé de laboratoire a été conçu, construit et automatisé. Des mesures en ligne des variables du procédé, telles que la température, les matières en suspension (MES), les concentrations en ammoniaque et en nitrate, les débits d'air et de l'effluent liquide ainsi que la pression transmembranaire sont rassemblées afin de valider le modèle proposé. De plus, des données expérimentales collectées dans un procédé pilote situé en Espagne sont utilisées pour con-

solider la validation du modèle. Concernant le contrôle du processus, deux approches différentes sont présentées : une commande prédictive non linéaire (NMPC) est mise en œuvre afin d'optimiser le taux de production d'effluent et de maximiser la période entre deux opérations de nettoyage chimique et un contrôleur linéarisant basé sur la théorie de Lyapunov est conçu afin de stabiliser le colmatage en manipulant le débit d'air et d'effluent liquide. Les résultats présentés dans cette thèse montrent l'importance des études analytiques sur les modèles afin d'améliorer la compréhension et de permettre la simplification de ces modèles. Un autre point important est la simplicité de la structure du modèle dynamique et le nombre réduit de paramètres. Ce travail montre que cette structure est suffisante pour mettre en œuvre des stratégies de contrôle avancées sur les processus BRMS et même de prédire la dégradation biologique et la dynamique de croissance du colmatage.

Modèle BRMS proposée Un des plus grands défis des processus de traitement BRMS est le développement d'un modèle intégré (comprenant les phénomènes biologiques et un mécanisme de filtration). En outre, ces modèles comprennent de nombreux paramètres qui peuvent être difficiles à estimer à partir des données expérimentales et sont, en général, trop complexes pour être utilisés à des fins de contrôle. En règle générale, il est toujours nécessaire de faire un compromis entre la complexité du modèle et la capacité prédictive dynamique. A des fins de contrôle, le modèle choisit devrait être le plus simple modèle permettant de réaliser la tâche désirée (Kokotović et al, 1986). Dans ce contexte, il n'y a que peu de propositions de modèles BRMS, qu'ils soient basés sur des approches empiriques (Khan et al, 2009), sur une boîte noire évaluant le rendement de filtration (Dalmau et al, 2013) ou construits par des réseaux de neurones artificiels (Choi et al, 2012).

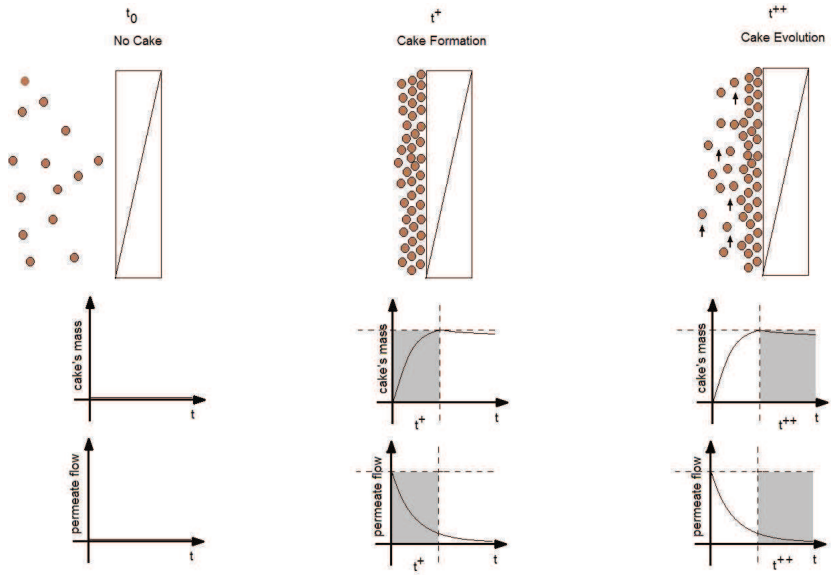


Figure 1: Evolution temporelle de la masse du gâteau et du débit de l'effluent : au t_0, $Q_{out} = 0$; à t^+, le gâteau est formé; l'intervalle de temps jusqu'à t^{++} montre en outre l'évolution du gâteau

La modélisation d'un processus de colmatage en bioréacteur BRMS est sélectionnée comme point de départ. Cette étude estime que le dépôt des particules crée une résistance à l'écoulement au travers de la membrane. La résistance de colmatage total (R_{total} $[m^{-1}]$) est représentée par l'équation (1). R_m $[m^{-1}]$ est la résistance intrinsèque, R_{irrev} est la résistance irréversible qui ne peut être éliminée que par nettoyage chimique , R_{rev} désigne la résistance réversible qui est affectée par le débit d'air et δ_R est utilisé pour représenter la perturbation de résistance totale (résultant du biofilm), la polarisation de concentration et les résistances d'échelle.

$$R_{total} = R_m + R_{rev} + R_{irrev} + \delta_R \tag{1}$$

Le effluent est donné par $Q_{out} = A\ TMP/\eta R_{total}$, où TMP $[mbar]$ est la pression transmembranaire et η $[mbar.d]$ est la viscosité apparente de l'eau, (Figure 2). La résistance réversible du gâteau de boue est gouverné par

$$R_{rev} = \rho_{rev}\frac{m + m0}{A} \tag{2}$$

où ρ_{rev} $[m \cdot g^{-1}]$ est la résistance spécifique du gâteau de boue, m_0 $[g]$ est la masse initiale du gâteau de boue, A est la superficie de la membrane et m $[g]$

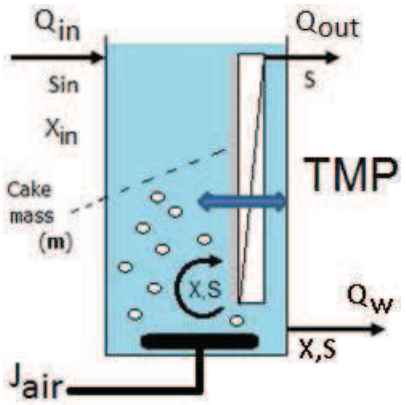


Figure 2: Croquis du processus BRMS.

est la masse du gâteau de boue instantanée. La dynamique de ce dernier peut être décrite par l'équation (3).

$$\frac{dm}{dt} = Q_{out}X - J_{air}\mu_{air}(m)m, \quad \text{avec } \mu_{air}(m) = \beta\frac{m}{K_{air}+m} \tag{3}$$

La partie droite de l'équation (3) possède deux termes. Le premier terme représente l'attachement de biomasse sur la surface de la membrane dépendant de la vitesse des effluents Q_{out} $[m^3/d]$ et de sa concentration X $[g/m^3]$. L'échelle de temps est représentée dans la Figure 1 par t^+, montrant que les particules en suspension près de la membrane sont rapidement attirées contre le filtre. Le deuxième terme de l'équation (3) représente le détachement du gâteau de boue proportionnel au flux d'air. Le paramètre β $[m^{-1}]$ est lié à la résistance du gâteau de boue de détachement. Ce dernier mécanisme est bien sûr également influencé par J_{air}, mais aussi par la masse du gâteau. Avec une masse de plus en plus attachée, le détachement devient plus probable et son évolution est représentée par une équation de 'Monod', c'est à dire une loi monotone avec saturation. Cette structure du modèle garantit que la masse du gâteau n'atteindra jamais des valeurs négatives, chose physiquement impossible. La dynamique du gâteau de boue est si rapide qu'elle peut être vue comme instantanée par rapport aux autres dynamiques du processus.

La résistance irréversible R_{irrev} est proportionnelle à la quantité d'effluent produit et est calculée en utilisant les termes (ρ_{irrev}), proposés par Di Bella et al (2008).

$$R_{irrev} = \rho_{irrev}\sum\frac{Q_{out}}{A}t_f \tag{4}$$

où t_f est la durée de la période de filtration.

L'activité biologique est décrite en utilisant un modèle simple de chémostat (Smith and Waltman, 1995), impliquant une biomasse croissante sur un substrat limitant (5). Il est important de souligner que cette structure simple de modèle biologique peut être facilement étendue à plus d'une réaction biologique. Cependant, l'augmentation de la complexité induit un étalonnage du modèle plus délicat et réduit l'utilité du modèle pour le développement de contrôleurs.

$$\begin{cases} \dfrac{dS}{dt} = -\dfrac{1}{Y}\mu(S)X + \dfrac{Q_{in}}{V}(S_{in} - S) & \text{(5a)} \\ \dfrac{dX}{dt} = \left(\mu(S) - \dfrac{Q_w}{V}\right)X + \dfrac{Q_{in}}{V}X_{in} - \dfrac{Q_{out}}{V}X + \dfrac{J_{air}}{V}\mu_{air}(m)m & \text{(5b)} \end{cases}$$

L'équation (5a) représente la consommation du substrat par la biomasse en suspension, gouvernée par une loi de Monod $\mu(S) = \mu_{S,max}\frac{S}{S+K_S}$, et le transport de substrat entrant et sortant du réservoir. Notez que le substrat n'est pas affecté par la membrane sachant que seule la matière solide est retenue par celle-ci.

L'équation (5b) montre qu'il existe une interaction entre les solides en suspension et le gâteau. La première partie de l'équation représente la croissance de la biomasse libre qui consomme le substrat. Le transport de la biomasse induit l'attachement du gâteau décrit par $\frac{-Q_{out}}{V}X$ ainsi que le détachement du gâteau et sa "conversion" instantanée en matière solide en suspension suivant l'équation $+\frac{J_{air}}{V}\mu_{air}(m)m$. Le flux des déchets est représenté par Q_w et le débit entrant est défini comme $Q_{in} = Q_w + Q_{out}$. L'échelle de temps biologique est régie par le taux de consommation de substrat et, par conséquent, la croissance de la biomasse. Ce taux est représenté par une loi de Monod ($\mu(S)$) et est normalement exprimée en jours.

Les procédés de traitement de l'eau sont normalement actionnés dans un mode continu. De ce fait, l'évolution à long terme du gâteau est observée et peut être modélisée par

$$\frac{d\beta}{dt} = \gamma\beta \tag{6}$$

Le paramètre β $[m^{-1}]$ représente la facilité (ou difficulté) de détacher le gâteau de la membrane à l'aide d'un courant transversal d'air. Dans un pro-

cessus avec une pression transmembranaire constante, le flux sortant diminue avec le temps, β est donc croissant et $\gamma[d^{-1}]$ est positif. Cela signifie aussi que l'efficacité de J_{air} augmente à la suite de la perte de la force de traction de la membrane permettant le dépôt des particules. En revanche, si le processus a un débit sortant constant, la capacité de J_{air} pour détacher le gâteau baisse, β diminue, donc γ a une valeur négative. Ce phénomène peut également être lié au coefficient de compression du gâteau proposé par Li and Wang (2006). Cette évolution est normalement mesurée en semaines ou en mois.

Regroupant les équations précédentes, le modèle intégré est représenté par l'équation (7), où β, S, X et m sont toujours positives et bornées.

$$\begin{cases} \dfrac{d\beta}{dt} = \gamma\beta & \text{(7a)} \\ \dfrac{dS}{dt} = -\dfrac{1}{Y}\mu(S)X + \dfrac{Q_{in}}{V}(S_{in} - S) & \text{(7b)} \\ \dfrac{dX}{dt} = \left(\mu(S) - \dfrac{Q_w}{V}\right)X + \dfrac{Q_{in}}{V}X_{in} - \dfrac{Q_{out}}{V}X + \dfrac{J_{air}}{V}\mu_{air}(m)m & \text{(7c)} \\ \dfrac{dm}{dt} = Q_{out}X - J_{air}\mu_{air}(m)m & \text{(7d)} \end{cases}$$

$$\text{avec } \mu(S) = \mu_{S,max}\frac{S}{K_S + S}, \quad \mu_{air}(m) = \beta\frac{m}{K_{air} + m}$$

Notez que le modèle peut être étendu à un processus avec plus d'espèces et de substrats sans grand effort. Cela signifierait que S pourrait être modélisé comme NO_3 ou NH_4. La variable X, quant à elle, pourrait être considérée comme la population de bactéries hétérotrophes ou de bactéries autotrophes.

Analyse du modèle Trois échelles de temps différentes ont été déduites du comportement du processus : la première est liée à l'attachement et au détachement du gâteau, la seconde est induite par la dynamique biologique du procédé et la dernière par l'évolution du gâteau à long terme.

Pour démontrer cette hypothèse, l'approche par des perturbations singulières est utilisée. La présence de petits paramètres dans la description du modèle dynamique, pouvant ou ne pouvant pas être fixés comme étant égales à zéro, révèle la possibilité de réduction du modèle en une plus petite dimension (Kokotović et al, 1986; Saksena et al, 1984). L'apparition simultanée de phénomènes lents et rapides contribue à une dynamique complexe,

à une rigidité du modèle et à un effort de calcul pour la simulation. Il est intéressant de détecter les différents résultats des échelles de temps dans les modèles réduits, où le phénomène à la dynamique la plus lente est dominant. Cela peut être considéré comme une boucle de processus interne et externe. La dynamique rapide, également nommée couche limite, représente l'écart au comportement lent prédit.

L'outil mathématique utilisé pour faire face aux différentes échelles de temps est le théorème de Tikhonov qui permet de réduire la complexité du système par approximations convenables (Khalil, 2002). Un système lent-rapide peut être mis sous forme d'une perturbation singulière quand il peut être exprimé en utilisant les coordonnées appropriées, de manière à distinguer deux sous-systèmes comprenant un petit paramètre positif ϵ.

Dans le modèle BRMS, trois échelles de temps peuvent être identifiées : l'attachement du gâteau est considéré comme l'échelle de temps ultrarapide, la croissance de la biomasse libre et la consommation de substrat comme l'échelle de temps rapide, et l'évolution du gâteau comme l'échelle de temps lente. Il en résulte la représentation générique suivante :

$$\begin{cases} \frac{d\beta}{dt} = \gamma\beta & \longrightarrow \dot{x}_{sl} \\ \frac{dS}{dt} = -\frac{1}{Y}\mu(S)X + \frac{Q_{in}}{V}(S_{in} - S) & \longrightarrow \dot{y}_1 \\ \frac{dX}{dt} = (\mu(S) - \frac{Q_w}{V})X + \frac{Q_{in}}{V}X_{in} - \frac{Q_{out}}{V}X + \beta\frac{J_{air}}{V}\frac{m^2}{K_{air}+m} & \longrightarrow \dot{y}_2 \\ \frac{dm}{dt} = Q_{out}X - \beta J_{air}\frac{m^2}{K_{air}+m} & \longrightarrow \dot{z} \end{cases} \tag{8}$$

où x_{sl} est la variable d'état lente, y la variable d'état rapide, et z la variable d'état ultrarapide. Les petits paramètres sont supposés être $\epsilon_1 = |\gamma|$ et $\epsilon_2 = \frac{1}{V}$. Deux hypothèses sont prises: γ **est petit** et **le volume** V **est grand**.

Ce principe de trois échelles de temps du processus est utilisé pour développer une analyse analytique plus détaillée du modèle et procéder à l'identification des paramètres. Tout ceci est finalement validé par les données expérimentales de deux processus différents dans le Chapitre 4.

Basé sur l'analyse lente-rapide, l'identification des paramètres peut être organisée en trois étapes correspondant aux trois échelles de temps. En effet, une identification directe de tous les paramètres est délicate et conduit à l'apparition de plusieurs minima locaux. Une approche diviser-pour-mieux-régner, où les sous-ensembles de paramètres sont estimés en premier, est donc utilisée et l'ensemble des paramètres est ensuite réestimé à partir sur base de ces estimations. Les paramètres sont alors beaucoup plus proches de l'optimum et cela diminue sévèrement les efforts de calcul.

Validation du modèle avec données expérimentales Le modèle proposé a été comparé avec des modèles BRMS bien connus dans la recherche, montrant sa capacité à imiter ces modèles en dépit de sa structure simple et de sa petite quantité de paramètres. Des analyses analytiques et numériques ont été effectuées et les résultats ont montré la possibilité d'utiliser ce modèle comme référence pour le fonctionnement des processus et leur maintenance. Dans les procédures de conception de modélisation, la dernière et la plus importante des étapes est celle de validation du modèle utilisant les données obtenues à partir de processus expérimentaux. Dans cette section, le modèle est validé par deux processus différents : (i) un système BRMS de recirculation de l'aquaculture pour l'enlèvement de l'ammoniaque (RAS-sMBR) et (ii) une usine de traitement BRMS des eaux usées. Il est important de souligner que les deux processus ont des caractéristiques différentes (i.e. caractéristiques de l'eau d'entrée, concentration totale de solides en suspension et caractéristiques des effluents). De la même manière, ces validations montrent la pertinence du modèle proposé.

RAS-sMBR Le système de recirculation de l'aquaculture (RAS) est défini comme un processus où l'eau du bassin est traitée puis réinjectée en continu. A cette recirculation peut s'ajouter quotidiennement un volume d'eau fraiche qui ne dépasse en aucun cas 10 % du volume total du bassin(Hutchinson et al, 2004). La recirculation, cependant, provoque l'accumulation d'ammoniaque, nitrate et de matières organiques qui doivent être supprimés avant de retourner dans le système. L'élimination de l'azote pour le RAS comprend normalement des technologies de filtrage comme des contacteurs biologiques rotatifs (RBC), des lits bactériens et des biofiltres à sable fluidisé (Crab et al, 2007). L'une de ces techniques de filtration est le bioréacteur à membrane immergé (BRMS). Comme les données des installations BRMS d'aquaculture sont très difficiles à obtenir, une installation pilote RAS a été conçue, automatisée et analysée. L'ensemble de données enregistrées est utilisé pour valider le modèle proposé.

La dynamique ultra-rapide étant liée à l'attachement et au détachement réversible des boues, elle influence également les mesures *TMP*. Pour cette échelle de temps, ni la dégradation biologique ni l'évolution à long terme du colmatage n'ont été prises en compte. De plus, leur évolution est considérée comme constante en raison de leur comportement dynamique lent. L'identification des paramètres est réalisée par une simulation portant sur

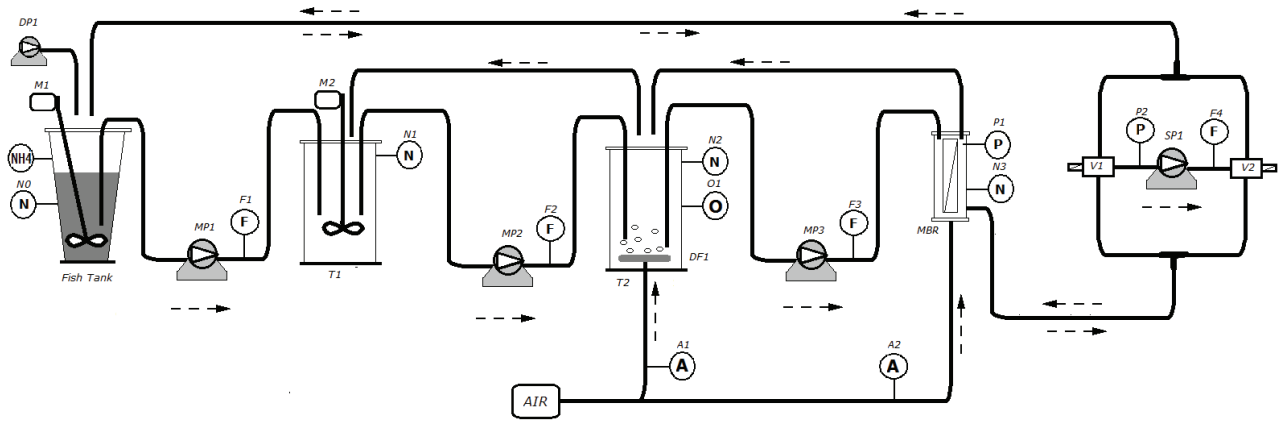


Figure 3: Schèma des systèmes d'aquaculture de recirculation équipé d'un BRMS.

une heure de données. Les paramètres identifiés sont K_{air}, ρ_{rev} et m_0.

La dynamique rapide est basée sur les réactions biologiques du système. Par conséquent, la dégradation de l'ammoniaque et la croissance de la biomasse ont été prises en compte. Comme le procédé fonctionne en régime stationnaire, avec apport d'ammoniaque constant, une impulsion a été ajoutée à l'afflux d'ammoniaque pour extraire des informations sur sa dynamique de dégradation. Les paramètres Y, $\mu_{S,max}$ et K_{air} ont été identifiés sur environ $3,5$ *jours*.

La dynamique lente est liée à l'évolution du gâteau à long terme. On l'exprime en utilisant la couche irréversible de boue, le paramètre ρ_{irrev}, l'évolution à long terme du gâteau de boue γ et les paramètres de viscosité apparente A_1 et A_2. L'identification à long terme utilise un ensemble de données plus vaste de 16 *jours*. La valeur moyenne de chaque cycle est calculée et utilisée dans la procédure d'identification.

Usine pilot de traitement BRMS des eaux usées L'usine pilote BRMS des eaux usées permet biologiquement d'éliminer les matières organiques, l'azote et le phosphore (Figure 4).

Dans cette étude, l'attention est concentré uniquement sur le mécanisme de colmatage, et un modèle dynamique encore plus simple est proposé, calibré et validé grâce aux données expérimentales recueillies à partir de l'installation pilote. L'influence de la variation de la température ambiante sur *TMP* est également prise en compte afin de prédire plus précisément l'accumulation du colmatage.

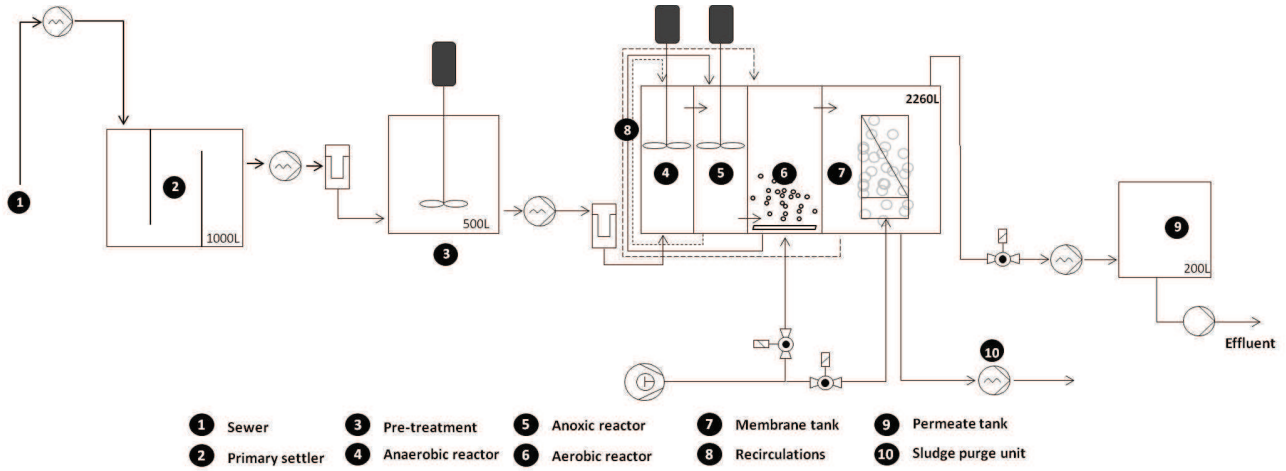


Figure 4: Schéma de l'installation pilote expérimentale.

Basé sur l'analyse de la dynamique lente-rapide, l'identification des paramètres est organisée en deux étapes correspondant aux deux échelles de temps. L'ensemble des paramètres θ est divisé en deux sous-ensembles de paramètres à identifier. La procédure d'identification court terme utilise $\theta_{short} = [K_{air}, \rho_{rev}, m_0]$ avec β et η considérés comme des valeurs constantes. Notez que la viscosité (η) peut être mesurée et β devrait être estimée approximativement par quelques simulations préliminaires.

La procédure d'identification des paramètres est réglée sur une demi-journée de données pour identifier K_{air}, ρ_{rev} et m_0, passant de $20,0$ jours à $20,5$. Les paramètres à court terme identifiés sont ensuite utilisés dans l'identification des paramètres à long terme du sous-ensemble $\theta_{long} = [\gamma, A_1, A_2]$.

Pour la identification à long terme, un plus grand ensemble de données est utilisé, c'est-à-dire entre le 20ème et le 50ème jours. Les paramètres γ, A_1 et A_2 sont ainsi identifiés. Il faut noter que le modèle suit les variations de température quotidiennes. Il est important de souligner que si ces oscillations ne sont pas prises en compte et que le processus n'est pas analysé sur le long terme, une mauvaise interprétation de la mesure *TMP* pourrait être faite. Si le *TMP* décline, cela peut s'expliquer par le fait que la température de l'eau affecte la viscosité apparente et non en raison de certaines mises en œuvre d'une stratégie de contrôle. La prise en compte de ces variations naturelles peut en effet conduire à une meilleure prévision du colmatage lors des stratégies de contrôle.

L'analyse de validation croisée est effectuée avec un ensemble de données qui n'ont pas été utilisées à des fins d'identification. Même si ces 10 jours de données n'ont pas été utilisées pour la routine d'identification, la *TMP*

possède un facteur de corrélation de $R^2 = 0,9512$, montrant la capacité du modèle à prédire la *TMP* sur l'échelle de temps à long terme du système.

Stratégies de contrôle pour BRMS Le problème du contrôle BRMS peut être divisé en contrôleurs boucle ouverte ou boucle fermée, qui agissent soit dans la filtration ou dans l'aspect biologique, ou soit dans les deux processus. Le dispositif de commande en boucle ouverte est normalement obtenu par essais du procédé, ce qui entraîne une valeur fixe pour les actionneurs au cours du temps. Les contrôleurs en boucle fermée utilisent des mesures du procédé pour calculer une action de commande qui est introduite dans le système par un dispositif d'actionnement (par exemple, pompe, valve, minuterie, etc.).

Dans les deux études suivantes, une commande prédictive non linéaire (NMPC), et une commande de linéarisation partielle, avec une fonction quadratique de Lyapunov, sont élaborées en utilisant le modèle intégré proposé afin de stabiliser l'évolution du gâteau.

NMPC-BRMS L'objectif de cette étude est de concevoir une commande prédictive non linéaire (NMPC) pour une installation de traitement des eaux usées avec un bioréacteur à membrane submergée afin de minimiser la résistance irréversible tout en maintenant la pression transmembranaire constante. Cette dernière est en effet un bon indicateur pour conserver l'épaisseur du gâteau sur la membrane à un niveau acceptable. A cet effet, les variables manipulées sont le flux de sortie et le débit d'air qui permet à la couche de matériau formée sur la membrane (le « gâteau de boue ») de se détacher. La stratégie de contrôle est testée en tenant compte d'un simulateur détaillé comme processus de référence et du modèle d'ordre réduit proposé comme prédicteur.

La fonction de coût est définie comme :

$$F(x,u) = (Q_{out}t^2)^2 + (TMP - TMP^*)^2 \tag{9}$$

où l'effluent, multiplié par le carré du temps, est réduit au minimum afin de contrôler la résistance irréversible et en même temps de maintenir la pression transmembranaire à la consigne TMP^* souhaitée. Notez que la résistance irréversible, qui dépend du flux de sortie et du temps, doit être minimisée pour agrandir l'intervalle entre les nettoyages chimiques. Les contraintes suivantes sont ajoutées : (i) $Q_{out} \geq 0$ et (ii) $J_{air} \geq 0$ pour garantir respectivement

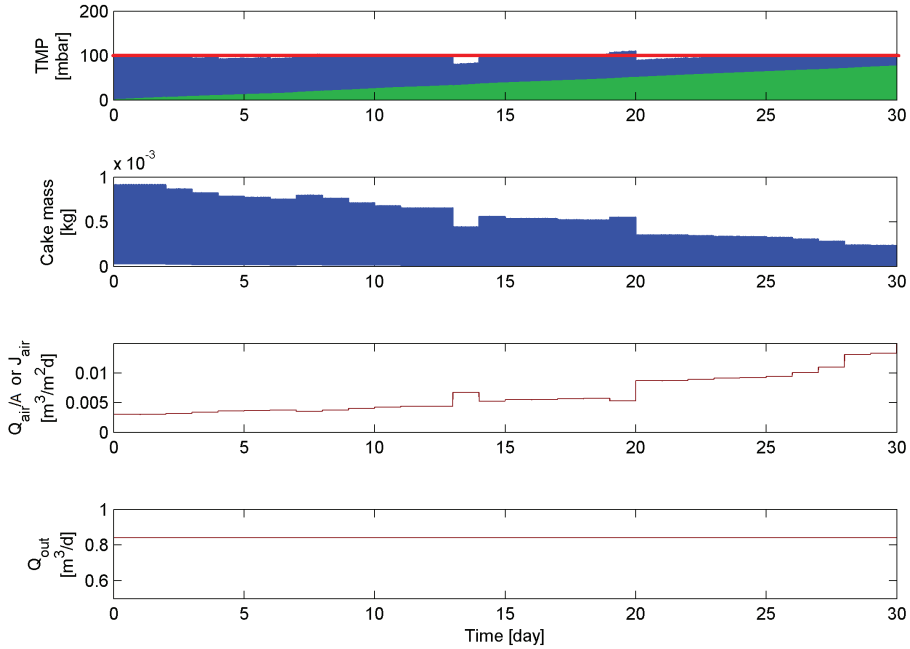


Figure 5: NMPC agissant sur le processus descriptif.

un débit d'effluent liquide et un débit d'air positifs. La méthodologie est appliquée en utilisant le code *Matlab* présenté par Grüne and Pannek (2011).

Les résultats présentés dans la Figure 5 sont obtenus en supposant que toutes les variables d'état sont mesurées. Le NMPC utilise un temps d'échantillonnage d'une journée, un horizon de prédiction $T_p = 3$ jours et un intervalle de contrôle $T_c = 1$ jour.

Le premier graphique de la Figure 5, représente la *TMP* calculée avec la résistance totale. Notez que, en bleu, il est possible de voir l'influence de la résistance réversible et, en vert, l'influence de la résistance irréversible sur la valeur *TMP*. La consigne TMP^* est représentée par une ligne rouge, qui est fixée à 100 *mbar*. Pour maintenir la consigne désirée, le contrôleur augmente le débit d'air (Q_a/A ou J_{air}) et, en même temps, diminue le flux de de l'effluent (Q_{out}). Ces valeurs d'entrée sont présentées dans les deux derniers graphiques de la Figure 5. La décroissance de la masse du gâteau de boue, observée dans le deuxième graphique, montre que la résistance du gâteau de boue (R_{rev}) est beaucoup plus importante que la résistance irréversible au début du processus. Cela respecte les observations de Mannina et al (2011). Il est important de souligner que les actions du contrôleur maintiennent la consigne souhaitée même si certaines non-linéarités ne sont pas modélisées dans le modèle simplifié.

Les résultats montrent que le procédé peut être réglé jusqu'à ce que la

résistance irréversible joue le rôle principal dans la résistance au colmatage. Lorsque cet état est atteint, un nettoyage chimique est nécessaire, ou une pression transmembranaire plus grande doit être utilisée.

"State-feedback linearization" avec une fonction quadratique de Lyapunov Basée sur une fonction quadratique de Lyapunov il est possible de réécrire deux lois de contrôle positives pour contrôler l'évolution de la masse du gâteau.

$$\begin{cases} m > m^* & \bar{u}_{Q_{out}} = \frac{\omega}{X} & \bar{u}_{J_{air}} = \frac{\lambda(m-m^*)+\omega}{\mu_{air}(m)m} \\ m < m^* & \bar{u}_{Q_{out}} = \frac{-\lambda(m-m^*)+\omega\mu_{air}(m)m}{X} & \bar{u}_{J_{air}} = \frac{\omega}{\mu_{air}(m)m} \end{cases} \tag{10}$$

Un $\omega > 0$ est ajouté dans la loi de commande afin d'avoir deux entrées positives durant tout le processus.

La figure 6 montre les entrées du processus, Q_{out} et J_{air}, permettant de maintenir la masse du gâteau à la valeur désirée (m^*). Le processus commence par une masse de gâteau de $0,5\ g$ avec une consigne à $0,4\ g$ jusqu'au 10ème jour, où il est ajusté à $0,5\ g$. Comme il y a deux actionneurs différents, le paramètre λ doit être distingué entre les deux entrées : $\lambda = 50$ pour J_{air} et $\lambda = 1$ pour Q_{out}. Il faut noter que les deux entrées restent constantes pour l'échelle de temps à court terme. Après 17 *jours*, l'évolution du colmatage devient plus important et le contrôleur doit augmenter J_{air} pour maintenir la valeur du gâteau constante.

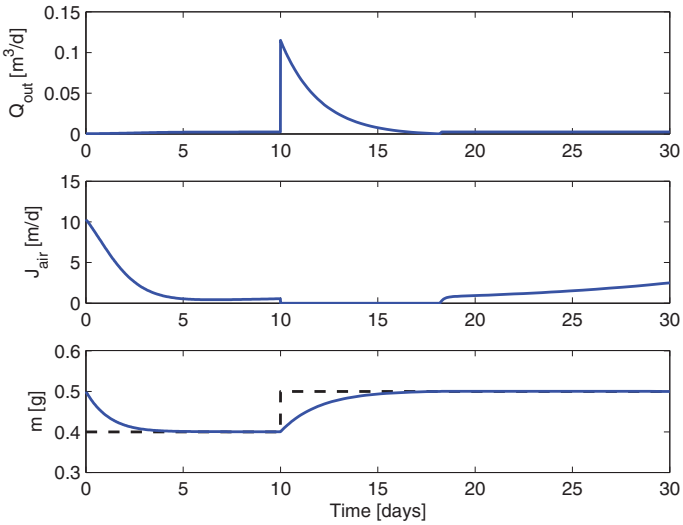


Figure 6: Contrôleur Quadratic Lyapunov. La valeur de référence (m^*) est en noir.

List of Publications

Journal articles

[1] Araujo Pimentel Guilherme, Vande Wouwer Alain, Harmand Jérôme, Rapaport Alain, "Design, Analysis and Validation of a Simple Dynamic Model of a Submerged Membrane Bioreactor" Water Research Journal, (70) 97 - 108, 2015;

[2] Guilherme A. Pimentel, Pedro Almeida, Anne-Lise Hantson, Alain Rapaport, Alain Vande Wouwer, "Design, Automation, Operation and Modeling of a RAS-sMBR Pilot Plant" to be submitted to Chemical Engineering Journal, 2015;

Conferences with proceedings

[3] Araujo Pimentel Guilherme, Vande Wouwer Alain, Rapaport Alain, Harmand Jérôme, "Modeling of submerged membrane bioreactor with a view of control" in 11th IWA Conference on Instrumentation Control and Automation, Narbonne, France, 2013;

[4] Miranda Almeida Pedro, Araujo Pimentel Guilherme, Vasel Jean-Luc, Hantson Anne-Lise, Rapaport Alain, Harmand Jérôme, Vande Wouwer Alain, "Analysis of two recirculating aquaculture systems (RAS): Submerged membrane bioreactor and fixed bed biofilter technologies" in 3rd IWA Benelux Young Water Professional Regional Conference, Belval, Luxembourg, 2013;

[5] G. Araujo Pimentel, M. Dalmau, A. Vargas, J. Comas, I. Rodriguez-Roda, A. Rapaport, A. Vande Wouwer, "Validation of a simple fouling model for submerged membrane bioreactor" MATHMOD 2015 - 8th Vienna International Conference on Mathematical Modelling, Vienna, Austria, 2015;

[6] G. Araujo Pimentel, A. Rapaport, A. Vande Wouwer, "Nonlinear Model Predictive Control of a Wastewater Treatment Process Fitted with a Submerged Membrane Bioreactor" accepted to International Symposium on Advanced Control of Chemical Processes (AdChem2015), Whistler, Britsh Columbia, Canada, 2015;

Conferences without proceedings

[7] Araujo Pimentel Guilherme, Vande Wouwer Alain, Coutinho Ferreira Daniel, Rapaport Alain, "Some Preliminary Results on Modeling and Control of MBR Process" in 31st Benelux Meeting on Systems and Control, Heijen, Pays-Bas, 2012;

[8] Araujo Pimentel Guilherme, Benavides Castro Micaela, Retamal Cristina, Dewasme Laurent, Vande Wouwer Alain, Coutinho Daniel, "Robust Partial Feedback Linearizing Control of Bioreactor in Fed-Batch Mode" in IAP DYSCO Study Day : Dynamical systems, control and optimization, Mons, Belgium, 2013 Poster

[9] Araujo Pimentel Guilherme, Harmand Jérôme, Vande Wouwer Alain, Rapaport Alain, "Time Scaling Study Using Tikhonov's Theorem in a Submerged Membrane Bioreactor" in IAP DYSCO Study Day : Dynamical systems, control and optimization , Bruxelles, Belgium, 2013 Poster

[10] Araujo Pimentel Guilherme, Vande Wouwer Alain, Rapaport Alain, Harmand Jérôme, "A simplified model of a submerged membrane bioreactor" in 32nd Benelux Meeting on Systems and Control, Houffalize, Belgium, 2013

[11] Araujo Pimentel Guilherme, Hantson Anne-Lise, Rapaport Alain, Vande Wouwer Alain, "Lab-scale aquaculture plant fitted with sMBR: design, data collection and sMBR modeling" in IAP DYSCO Study Day, Namur, Belgique, 2014 Poster

[12] Araujo Pimentel Guilherme, Vande Wouwer Alain, Rapaport Alain, "Stabilizing the cake evolution for a class of submerged membrane bioreactors using a Lyapunov controller" in 33rd Benelux Meeting on Systems and Control, Heijden, The Netherlands, 2014

[13] Araujo Pimentel, G., Dalmau, D., Vargas, A, Comas, J., Rodriguez-Roda, I., Rapaport, A., Vande Wouwer, A. "Modelling the influence of temperature in the long-term fouling process of a submerged membrane bioreactor" in IAP DYSCO Study Day, Ghent, Belgique, 2014 Poster

Preface

Within the last decades, progress in many areas of research has been responsible for a better quality of life and has increased worldwide human life expectancy. A common tool that can be identified in all these areas of research is mathematical modeling. Before mathematics became recognized and understood worldwide, observations were used as a tool to predict seasons, time, planting and harvest periods. These observations have since been able to be translated into a universal language of mathematics. Mathematics intrinsically carries the exercise of abstractions and formalizations. The transformation of complex problems into simple problems has been a central focus in problem-solving. In addition, the power of abstraction imposed by analytical analysis has helped find solutions. With better knowledge about process trajectories and behaviors, interest to change these trajectories and behaviors in order to drive it to a desired value has arisen. These ideas founded the basis of control theory that, stated as simple tool, maintain a certain behavior or change a certain behavior to a desired one, for instance. Over time, this simple concept has become a powerful tool, which is used to guarantee process stability, time of convergence and/or minimum time problem resolution.

Numerical tools have also been extraordinarily important for human development, and the flourishing of this tool has come with the numerical revolution fomented by the introduction of computational processing innovation. Executing thousands of computations over a very short time span and the development of models that closely mimic real dynamics, enable the development of simulators that help the operation, control, optimization and design of complex systems. Virtual system simulators are fundamental to the assessment of new control strategies into real processes, not exposing the physical system structure to risk.

The migration from simulator results to real applications has been possible only due to the instrumentation and actuator developments for process

automations. Merging simulation results and automation have increased process profitability, security and reliability. Furthermore, the development of optimization tools has allowed not only a certain process to be driven to a certain region, but it has also enabled a certain process to be driven faster and/or through a smaller path. Many mathematical tool developments have guaranteed that these optimizations have global or local asymptotic stability, increasing the process robustness. An optimal, i.e. more efficient and conscious, utilization of natural element resources has an extremely important role as these resources have started to become scarce and polluted in an astonishing velocity in the last century. One of these vital elements is water. The growth of the population at such a rate and the use of water for industrial, domestic, food production and agricultural processes, have alerted water quality organizations. The most efficient way to oppose the inevitable water shortage is to educate and inform society, particularly industry, about the importance of water. Another crucial way, is to optimize the existing water treatment processes to increase the effluent volume and quality in order to reuse treated water. Both are demanding tasks and really important for present and future generations.

Water quality was not an important issue until the discovery of pathogens transmitted by contaminated water. This was responsible for huge mortality in permanent settlements throughout the history of mankind and, unfortunately, even today it poses a major risk to public health. Sanitation and the use of biotechnologies in water treatment has gained attention due to its relatively easy implementation, avoiding large health problems and environmental risks. Many different technologies have been developed to increase water quality, and one of these new technologies is Membrane bioreactors. The combination of a membrane, that is characterized to filter microscopical particles, i.e. virus and dissolved salt, to mention a few, with a biological degradation in water treatment plants, increased the discharged water quality, increasing the possibility for direct water reuse. Despite this advantage, this technology has the drawback of the fouling process that decreases the process efficiency. The modeling of this process and the implementation of a model-based controller are extremely important in fully accepting the reliability of this new technology. The interdisciplinary aspect of water treatment is approached in this thesis. The modeling of submerged membrane bioreactors (sMBRs) for water treatment is an important step for water treatment process control and optimization. To study water sustainability, a recirculating aquaculture system pilot plant is designed, built, automated and modeled

in order to illustrate the importance of sMBRs for water reuse.

Contents

1 MBR Fundamentals **33**
1.1 The History of Membranes in Water Treatment Processes . . . 33
1.1.1 Definitions and Descriptions 35
1.1.1.1 The Membrane Classification 36
1.1.2 Membrane Process Configurations 38
1.2 MBR Market 40
1.3 Conventional Activated Sludge vs. sMBR 41
1.3.1 sMBR Advantages 42
1.3.2 sMBR Drawbacks 43
1.4 Fouling Formation 44
1.4.1 Backwash, Relaxation and Chemical Cleaning 46

2 Modeling sMBR **49**
2.1 Mathematical Modeling of Biological Systems 49
2.2 Mathematical Model Types 51
2.2.1 Black-box Models 51
2.2.2 White-box Models 52
2.2.3 Gray-box Models 53
2.3 Motivation for Modeling sMBRs 53
2.4 sMBR Model Types 54
2.4.1 sMBR Biological Modeling 54
2.4.2 sMBR Physical Modeling 57
2.4.3 sMBR Integrated Modeling 59
2.5 Proposed Simple Integrated sMBR Model 60

3 Analysis, Parameter Identification & Simulation **67**
3.1 Introduction 67
3.2 Full Model Analysis 67

3.2.1 Fast and Slow Dynamics 68
3.2.1.1 Singular Perturbations 68
3.2.1.2 Three-time-scale Singular Perturbation 69
3.2.2 Asymptotic Analysis 73
3.2.3 Study of the Linearized Dynamics - Short-term 73
3.2.4 Observability 75
3.2.4.1 SL_2H applied to sMBR Model 76
3.2.5 Controllability 77
3.2.5.1 *Lie Brackets* Applied to sMBR Model 78
3.3 Biological Aspect Simulations and Analysis 79
3.3.1 Global Stability Study 79
3.4 Physical Aspect Simulation and Analysis 81
3.5 Model Simulation and Parameter Identification 85

4 Model Validation with Experimental Data 96
4.1 Recirculating Aquaculture System Fitted with sMBR Pilot Plant Design 96
4.1.1 Process Description 97
4.1.2 Experimental Setup 98
4.1.3 Data Logging and Instrumentation 102
4.1.4 Recirculating Aquaculture System and sMBR 103
4.1.5 Critical Flux 105
4.1.6 Air Cross-Flow Study 106
4.1.7 Model Identification and Cross-validation 107
4.1.7.1 Ultra-fast Dynamic Identification 109
4.1.7.2 Fast Dynamic Identification 111
4.1.7.3 Slow Dynamic Identification 112
4.1.7.4 Cross-validation 113
4.2 Wastewater Treatment Pilot Plant[1] 114
4.2.1 Pilot Plant Description 115
4.2.2 Recorded Data 116
4.2.3 *TMP* Long-term Exponential-like Behavior 118
4.2.4 Permeate and *TMP* Amplitude 118
4.2.5 Relaxation 119
4.2.6 Temperature Influence 119
4.2.7 Air-blowers Temperature 120

[1]Experimental data provided by LEQUiA Group, Laboratory of Chemical and Environmental Engineering, University of Girona, Catalonia, Spain

4.2.8 Model Identification and Cross-validation 120
4.2.8.1 Short-term Identification 121
4.2.8.2 Long-term Identification 123
4.2.8.3 Cross-validation 124
4.3 Analysis of the Identified Parameters 126

5 Control Strategies for sMBRs 130
5.1 NMPC to a WWTP fitted with an sMBR 132
5.1.1 NMPC-sMBR Process Control 133
5.1.2 Simulation Results 135
5.2 Partial state-feedback linearizing control based on a quadratic control-Lyapunov function 139
5.2.1 Formula for Feedback 141
5.2.1.1 Control-Lyapunov Function 141
5.2.1.2 Partial state-feedback linearization 142
5.2.2 Stabilizing Sludge Cake Mass 143

6 Conclusions & Directions for Further Research 147

A About Lyapunov Controllers for Bioreactors 166
A.1 Biological Stabilization Based on Lyapunov Controllers Theory 166
A.1.1 Comparison of two Control-Lyapunov Functions . . . 169
A.1.2 Simulation Tests 169

List of Figures

1 Evolution temporelle de la masse du gâteau et du débit de l'effluent : au t_0, $Q_{out} = 0$; à t^+, le gâteau est formé; l'intervalle de temps jusqu'à t^{++} montre en outre l'évolution du gâteau . . 9
2 Croquis du processus BRMS. 10
3 Schèma des systèmes d'aquaculture de recirculation équipé d'un BRMS. 15
4 Schéma de l'installation pilote expérimentale. 16
5 NMPC agissant sur le processus descriptif. 18
6 Contrôleur Quadratic Lyapunov. La valeur de référence (m^*) est en noir. 19

1.1 Membrane Classification based on the pore size. 35
1.2 Generic application of submerged MBR representation. 36
1.3 The left shows submerged membrane configuration while right side shows the side-stream membrane. 38
1.4 A study carried out by Yang et al (2006) on the utilization of side-stream MBR or submerged MBR in North America. . . . 39
1.5 Global Market trends 40
1.6 Industrial process water treatment in Japan (2009): percentage of MBR installation by industry 41
1.7 Conventional Activated Sludge *versus sMBR* 42
1.8 Energy demand distribution 44
1.9 Cake formation and particle trajectory: (a) air cross-flow; (b) backwash 46
1.10 Filtration mechanisms with their schemas, equation and linear representation 46
1.11 Concentration Polarization Layer (CP Layer) 47
1.12 Physical and Chemical Cleaning Methods 48
1.13 Pressure transient for constant flux operation of a dead-end filter 48

2.1 ASM1 Scheme 55
2.2 Time evolution of cake mass and effluent flow: at t_0, $Q_{out} = 0$; at t^+, the cake is formed; the time interval up to t^{++} shows the further cake evolution 61
2.3 sMBR process sketch. 63

3.1 Evolution of function g related to y_1. 72
3.2 Relation between fouling, trans-membrane pressure and ϕ. . . 75
3.3 Strictly Linked Lower Hessenberg System (SL_2H). Adapted from Mailier et al (2010) 76
3.4 Bioreactor with membrane, ϕ is the permeate flux factor and α is the withdrawal of the biomass factor. 80
3.5 Nullcline Arrows PPlane. $Q_{in} = 1.1$, $S_{in} = 6$, $\alpha = 0.4$, $\phi = 0.6$, $K_S = 10$, $Y = 0.67$ and $\mu_{S,max} = 4$. The nullcline orange is the substrate and the violet is the biomass 80
3.6 Comparison: left - GPS-X blocks. Right - proposed model and Li and Wang (2006) model. 82
3.7 Comparision between the models. Blue: Li Model, Red: GPS-X model and Green:Proposed Model. 84
3.8 Comparision between the models with air cross-flow. Blue: Li Model, Red: GPS-X model and Green:Proposed Model. 84
3.9 The blue dynamic is with air and the red dynamic without air. 85
3.10 GPS-X simulation: Time Simulation with cake evolution. . . . 87
3.11 GPS-X simulation: Phase plane plot. Trajectories from three different initial conditions. 88
3.12 Dotted line: GPS-X with full ASM1 model; solid line: proposed simplified model. Orange window - ultrafast; Green window - fast; Blue window - slow. 90
3.13 Identification Procedure. The columns represent the procedure and the line the parameters to be estimated. 92
3.14 Cross-validation with different initial values and set-points. Dotted line: GPS-X with full ASM1 model; solid line: proposed simplified model. 93
3.15 L1-norm of parametric sensitivities 94

4.1 The recirculating aquaculture systems scheme fitted with an sMBR. 98

4.2 Pilot Description. Where, DP is ammonia dosing pump, M are the mixers, NH4 is the point of ammonia measurement, N are the tank level sensors, MP are the magnetic pumps, F are the liquid flow-meter sensors, T are the tanks, DF is the air diffuser, A are the air flow-meters, O is the measuring point for oxygen, P are the pressure sensors, V are the direction valves and SP is the suction pump. 99
4.3 Relaxation and permeate cycles, t_{relax} and $t_{permeate}$ minutes. . . . 99
4.4 Microdyn-Nadir: 0.35 m^2 and 150 $MWCO[kDa]$. 101
4.5 Layers of automation. 102
4.6 Water samples. On the left permeate sample and on the right sMBR tank sample 103
4.7 Measurements from an experiment in August. 104
4.8 Measurements from an experiment in October. 104
4.9 Fouling onto membrane surface. 105
4.10 Five-minute trial steps varying $8.14 L/m^2h$ 106
4.11 Comparison of the different air cross-flow. In blue J_{air} = 53.85 m^3/m^2d and in green J_{air} = 22.85 m^3/m^2d 107
4.12 *TMP* short-term behavior, ultra-fast dynamic. 109
4.13 Biological degradation direct identification (Fast Dynamic): blue is the model and green is the real data. 111
4.14 Figure on the top shows slow dynamic cross-validation: the blue stands for the model and the green dots are the mean value of each cycle computed from the real data. Figure on bottom-left shows the initial values in detail and Figure on bottom-right shows the end values in detail 112
4.15 Cross-validation of the ultra-fast dynamic.Red line is the experimental data and in blue the model. 113
4.16 Cross-validation of the fast dynamic.Red line is the experimental data and in blue the model. 114
4.17 Experimental pilot plant schematic. 116
4.18 Chemical cleaning periods. Plotted values are daily averages: red - *TMP* [mBar]; black - temperature [°C]; blue - permeate flow [L/h]; gray area - membrane airflow [m^3/h]. 117
4.19 Chemical cleaning periods. Plotted values are daily averages: red - *TMP* [mBar]; black - temperature [°C]; green - total suspended solids in the membrane tank [g/L]; yellow - wasteflow rate [L/d] 117

4.20 An exponential behavior in the *TMP* (data from one month) can be observed. 118
4.21 Influent of permeate flow over the *TMP*. 118
4.22 Influence of longer relaxation time on the *TMP*. 119
4.23 The oscillations of the *TMP* and temperature are approximately in the opposition phase. 119
4.24 Influence of injected air temperature on bulk temperature. . . 120
4.25 *TMP* short-term behavior. 122
4.26 Short-term validation : blue is the model and green is the real data. 123
4.28 Short-term cross-validation. The blue line symbolizes real data and the red line the predicted values 124
4.27 Long-term validation: the blue line represents real data, the green line is the identified model and the red line symbolizes the predicted values 125
4.29 Long-term cross-validation detail. The blue line represents real data and the red line predicted values 126

5.1 NMPC-Scheme 135
5.2 The NMPC acting on the descriptive process. 137
5.3 Blue is the sludge cake influence on *TMP* and green is the irreversible resistance on *TMP*. 138
5.4 Linearizing control structure 139
5.5 Quadratic Lyapunov Controller. The set-point (m^*) value in black. 146

6.1 Three different control-Lyapunov functions comparison 150

A.1 Chemostat process representation. 167
A.2 Area where the initial conditions will result in a positive control law (blue zone) or where the control law has negative values (light green zone) 168
A.3 Quadratic Lyapunov Functions with $\lambda_1 = 1$. 170
A.4 Each point means initial conditions, where abscissas are the substrate concentration (S) and the ordinate are the biomass concentrations(X). Blue: positive dilution rate in all trajectory. Green: at least one point of negative dilution rate. 171

List of Tables

1.1 General Characteristics of Membrane 37

2.1 Classification of the sMBR studies 56
2.2 Relation between process variables and fouling formation . . 62

3.1 Parameters of Li and Wang (2006) model, GPS-X and proposed model 83
3.2 Parameters with their standard deviation. 91
3.3 Correlation matrix of the parameters 92
3.4 Minimized Cost Function values with its standard deviation. Index for number of iterations of the full procedure 94

4.1 Identified Parameters 110
4.2 Short-term: Identified Parameters 122
4.3 Long-term: Identified Parameters 123
4.4 Identified Parameters from GPS-X, RAS-sMBR and WWTP-sMBR. 129

5.1 Input concentrations of the sMBR and physical model parameters 135
5.2 Parameter Calibration 136

Chapter 1

MBR Fundamentals

Generally, water treatment plants are integrated with reactors that have physical and biological units. These reactors are equipped with actuators and sensors to develop environmental conditions for the microorganisms to grow, which are responsible for the biological degradation of organic matter. In water treatment plants, effluent quality is directly linked to the soluble and non-soluble matter concentrations. The objective of water treatment processes is to reach very low concentration of both constituents at the output. Additionally, these processes should adopt a policy of a minimum quantity of reagents and energy consumption that increase the process maintenance challenge. New process hydraulic designs, instrumentation and process control strategies have been studied and developed in a continuous fashion. One of these new technologies are the Membrane Bioreactors (MBRs) that are responsible for physical separation of the treated water from solid particles. This separation process physically comprises retention of the solid matter, in order to obtain an effluent high quality with respect to solid particle concentrations, thus transforming various forms of wastewater into high-quality effluent that is suitable for discharge into the environment, and increasingly turning it into a reusable product (Atkinson, 2006).

1.1 The History of Membranes in Water Treatment Processes

The utilization of membranes to separate liquids with different concentrations was reported for the first time in 1748 by Nollet, a French physicist. He was the first to report the process in which semi-permeable membranes are

implemented to disassociate liquids with different concentrations of contaminants until osmotic equilibrium is reached (Atasi et al, 2006).

The use of membranes started to be seen as a new technology in the second part of XIX century and was especially influenced by Fick's law of diffusion, Van't Hoff's osmotic pressure equation and Graham's work in gas separation (Judd and Judd, 2011).

During this period, some experiments demonstrated that when energy (in the form of pressure or a vacuum) was applied to the liquid solution with contaminants, the liquid could still move though the membrane but left contaminants behind and discharged clean water. This simple and powerful idea is the nest of MBR processes where water is forced to pass through a filter with narrow pore sizes capable of removing even tiny particles such as salts, viruses, pesticides and most organic compounds (Atasi et al, 2006). The first documented "ultrafiltration" (UF) experiment was carried out by Schimidt in 1856, where he used bovine heart membranes (the pore dimension being $1 - 50$ *nm*) to separate soluble *A*cacia. This concept has been the core of many studies that resulted in a first synthetic UF membrane prepared by Bechhold in 1907, which he named "ultrafilter".

Inspired by this new technology, Zsigmondy at the University of Goettingen started to think about commercially producing a membrane, and thus did this with Bachmman between 1918 and 1922. They developed a method to produce porous collodion membrane in an industrial scale. *S*artorius Werke GmbH was the first membrane supplier established in Goettingen in 1925 (Judd and Judd, 2011).

One of the first applications with membranes was in the treatment of drinking water, followed by wastewater treatment (Atasi et al, 2006). This combination of a physical separation and the biological treatment has proven successful in the field of wastewater treatment, resulting in a process with a higher concentration of activated sludge retained in the reactor, higher sludge retention time (SRT) and lower F/M ratio (Acharya et al, 2006; Lu et al, 2001).

Throughout the years many combinations of membrane types and applications have been designed, with each membrane property differing according to the process. This will be seen in more details in Section 1.1.1.1 where the pore size refers to the membrane properties, for example: the *Ultrafiltration* removes viruses and is useful for large molecule recovery making water recycling in industry more economic; the *Microfiltration* removes protozoan parasites and decreases turbidity and it is the core of membrane bioreactor treatment plants for effluents; the *Nanofiltration* is applied to surface water

removes, color and large ions, gives a higher flux than reverse osmosis, adds value or recovers value from wastes; and the *Reverse Osmoses* is used for portable use and industrial reuse removal of small ions (Howell, 2004). A summary can be seen in Figure 1.1.

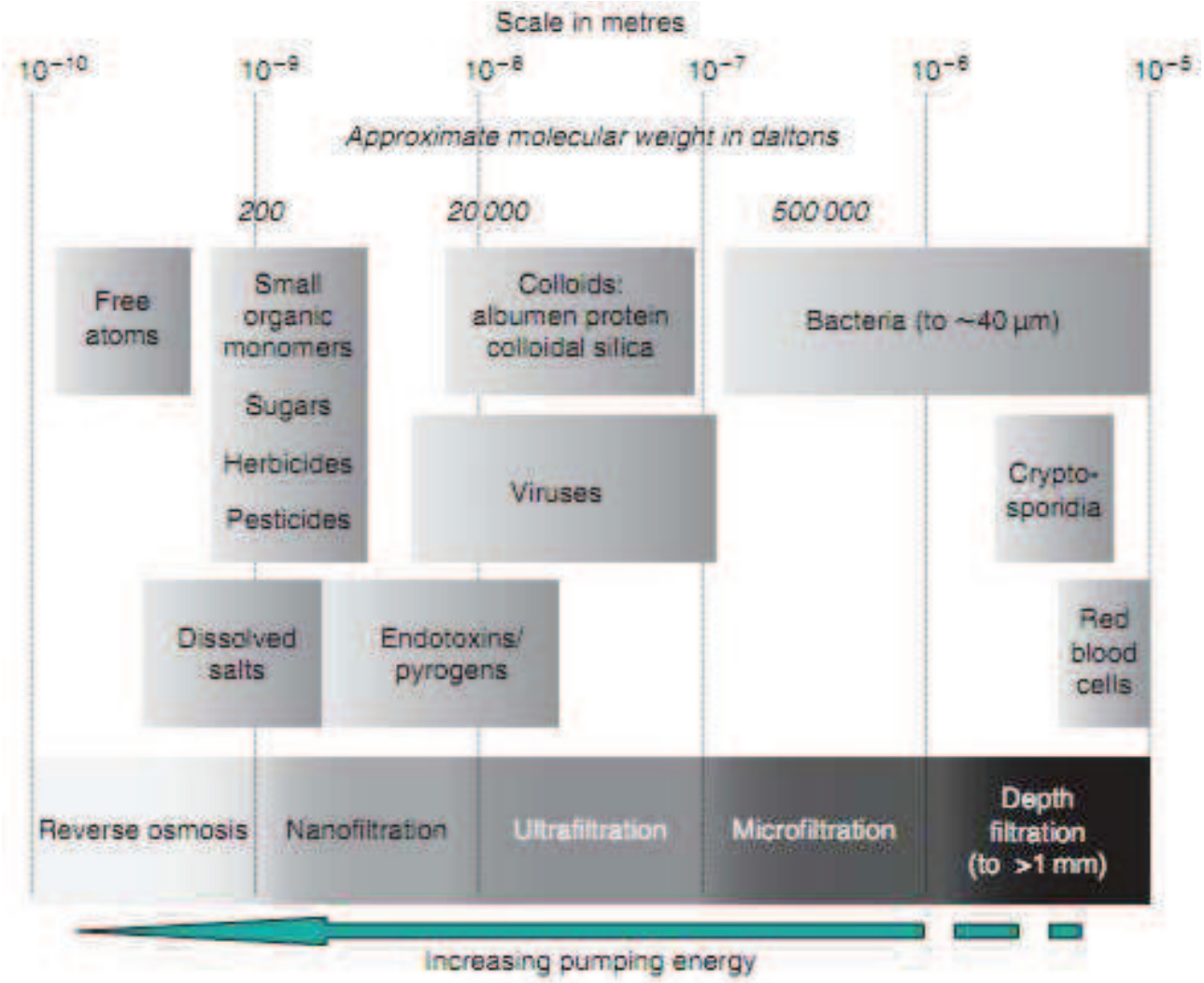


Figure 1.1: Membrane Classification based on the pore size (Judd and Judd, 2011).

1.1.1 Definitions and Descriptions

The term 'membrane bioreactor' (MBR) has been applied to all water and wastewater treatment processes integrating a perm−selective membrane with

a biological process. In Figure 1.2 the generic submerged membrane bioreactor (sMBR) processes scheme is represented .

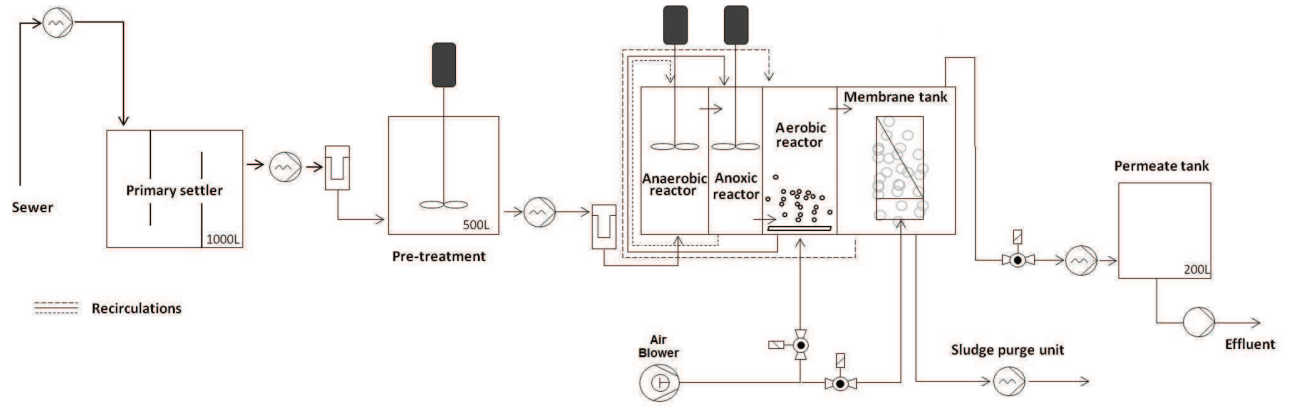


Figure 1.2: Generic application of submerged MBR representation (figure edited from Pimentel et al (2015a)).

Normally, an MBR is integrated with micro or ultrafiltration membrane technology (with pore sizes ranging from 0.05 to 0.4 μm), resulting in complete physical retention of bacterial flocks, as aforementioned, and virtually all suspended solids within the bioreactor.

1.1.1.1 The Membrane Classification

Membrane materials are selected based on the kind of process and application. The most important characteristics in the membrane selection are the membrane pore size, the applied pressure, the Molecular Weight Cutoff (MWCO) and some material characteristics such as hydrophobicity, process temperature and pH, which helps in this selection. Nowadays, membranes can be constituted by three main types of materials: (i) polymeric, the most implemented in industrial MBR processes; (ii) ceramic, with the largest range of utilization and (iii) metallic, which is not used for MBR processes.

The desired effluent quality and removal mechanisms of pollutants may be chosen by selecting the class of membrane. An useful table (Table 1.1) has been proposed by Atasi et al (2006) and summarize these properties. To remove impurities by size exclusion, Microfiltration (MF) and Ultrafiltration (UF) are normally used. If the process requires a removal by diffusion and charges (electrostatic) exclusion as well as size exclusion, the most used are the Nanofiltration (NF) and Reverse osmosis (RO) filters.

Table 1.1: General Characteristics of Membranes (Atasi et al, 2006)

Membrane Operation	Driving Force	Mechanism or Separation	Weight Cutoff Range (DA)	Pore Size Range, Microns	Operating Pressure, psi
MF	Pressure or vacuum	Sieve	>100 000	0.1 - 10	1 - 30
UF	Pressure	Sieve	>2000-100 000	0.01-0.1	3-80
NF/low pressure RO	Pressure	Sieve+ Solution/diffusion+ exclusion	300-1000	0.001-0.01	70-220
RO	Pressure	Solution/diffusion+ exclusion	100-200	<0.001	800-1200

Followed by the material properties, pore size and MWCO, the geometric shape of the membrane has a great impact in the filtration efficiency and in the choice for its application. The following items proposed by Judd and Judd (2011) may be used as a guide for selecting the most reasonable filter for a desired application.

1. pleated filter cartridge (FC) - extremely poor turbulence promotion, no possibility of backwash and applicable in dead-end membrane filtration and used in processes with low total suspended solid concentration;

2. plate-and-frame/flat sheet (FS) - fair turbulence promotion, no possibility of backwash and applicable in electrodialysis, ultrafiltration and reverse osmosis;

3. spiral-wound (SW) - poor turbulence promotion, no possibility of backwash and applicable in reverse osmosis/nanofiltration and ultrafiltration and reverse;

4. (multi)tubular (MT) - extremely good turbulence promotion, no possibility of backwash and applicable in cross-flow membrane filtration/ ultrafiltration and nanofiltration, and used in process with high total suspended solid concentrations;

5. capillary tube (CT) - fair turbulence promotion, possibility of backwash and applicable in ultrafiltration;

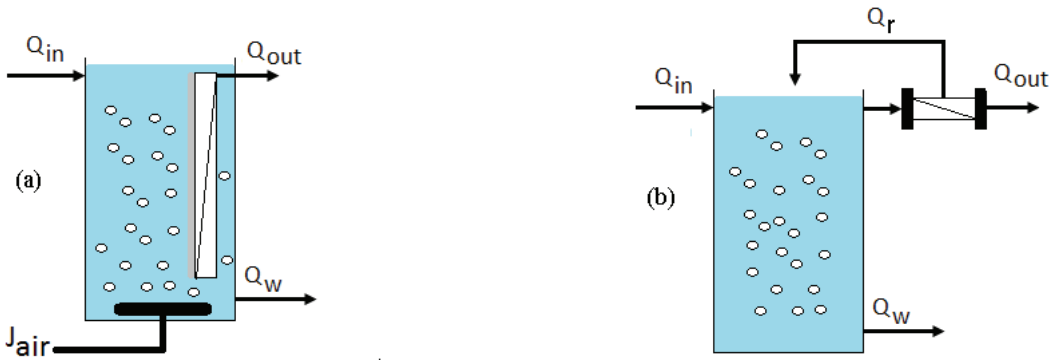


Figure 1.3: The left shows submerged membrane configuration while right side shows the side-stream membrane.

6. hollow fiber (HF) - extremely poor to fair turbulence promotion, possibility of backwash and applicable in microfiltration/ultrafiltration and reverse osmosis;

1.1.2 Membrane Process Configurations

Judd and Judd (2011) stress that the process configuration needs to be designed considering the application, the type and the classification of the membrane. The membrane should be configured so as to have a:

- high membrane area to module-bulk-volume ratio,
- high degree of turbulence for mass transfer promotion on the feed side,
- low energy expenditure per unit of product water volume,
- low cost per unit membrane area,
- design that facilitates cleaning,
- design that permits modularization.

There are two main membrane process configurations: the submerged membrane and side-stream membrane (Figure 1.3).

- The submerged membrane bioreactor (sMBR) is composed by a filter submerged inside a tank (the bioreactor). This tank is equipped with air blowers in the bottom part which have the property to air shear the

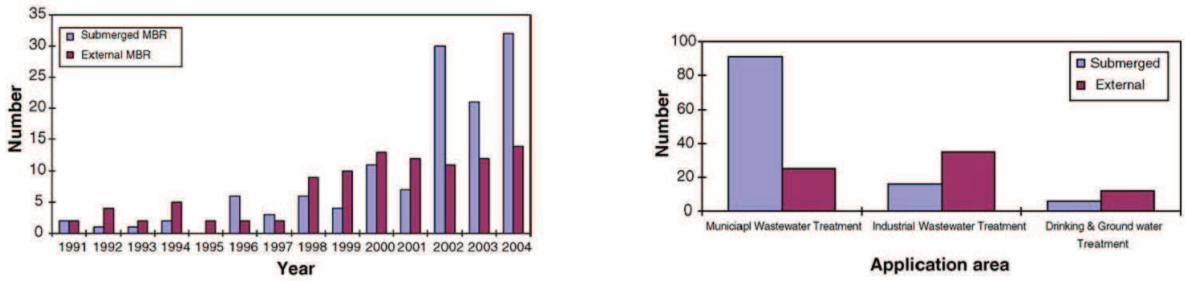


Figure 1.4: A study carried out by Yang et al (2006) on the utilization of side-stream MBR or submerged MBR in North America.

membrane surface preventing it from depositing solid particles, named *fouling* (this will be explained in more detail in Section 1.4). This configuration is increasingly used for domestic wastewater treatment, and there is a growing need to provide valuable modeling tools for sMBR design and operation (Naessens et al, 2012a). In its simplest form, a submerged membrane bioreactor system can combine the functions of an activated sludge aeration system, secondary clarifiers, and tertiary filtrations in a single tank (Atasi et al, 2006). The submerged membrane units features rather low trans-membrane pressure (TMP), requiring less energy consumption and is more cost effective (Wintgens et al, 2003). The aeration provides the main operating cost component, as it is required for both mixing and oxygen transfer. On the other hand, the lower flow under which the submerged system operates implies a higher membrane area and thus a higher associated initial capital cost (Gander et al, 2000). Normally, hollow-fiber and flat-sheet membranes are used in this configuration.

- The side-stream membrane consists of a tank and a separate membrane, with a recirculation, which influent is injected in the membrane compartment forcing the water to pass through the membrane pores. The side-stream MBR is more prevalent in industrial systems where waste characteristics, such high temperatures and pressure, require the use of ceramic membranes (Atasi et al, 2006). This configuration has a higher total energy cost, by up to two orders of magnitude, compared with the submerged system due to the recycled component (Gander et al, 2000).

Figure 1.4 presents some numbers on side-stream and submerged membranes and their application.

1.2 MBR Market

The MBR global market has had continuous growth rates between 10 and 15% in the last decade and continue to vary regionally according to the state of economic development and infrastructure (IWA Group, 2014; Judd, 2014). The report produced by Sartorius et al (2013) shows that China and the United States are the main suppliers and consumers, followed by countries with water shortage such as South Korea and Australia. Figure 1.5 shows the market trends in the last decade.

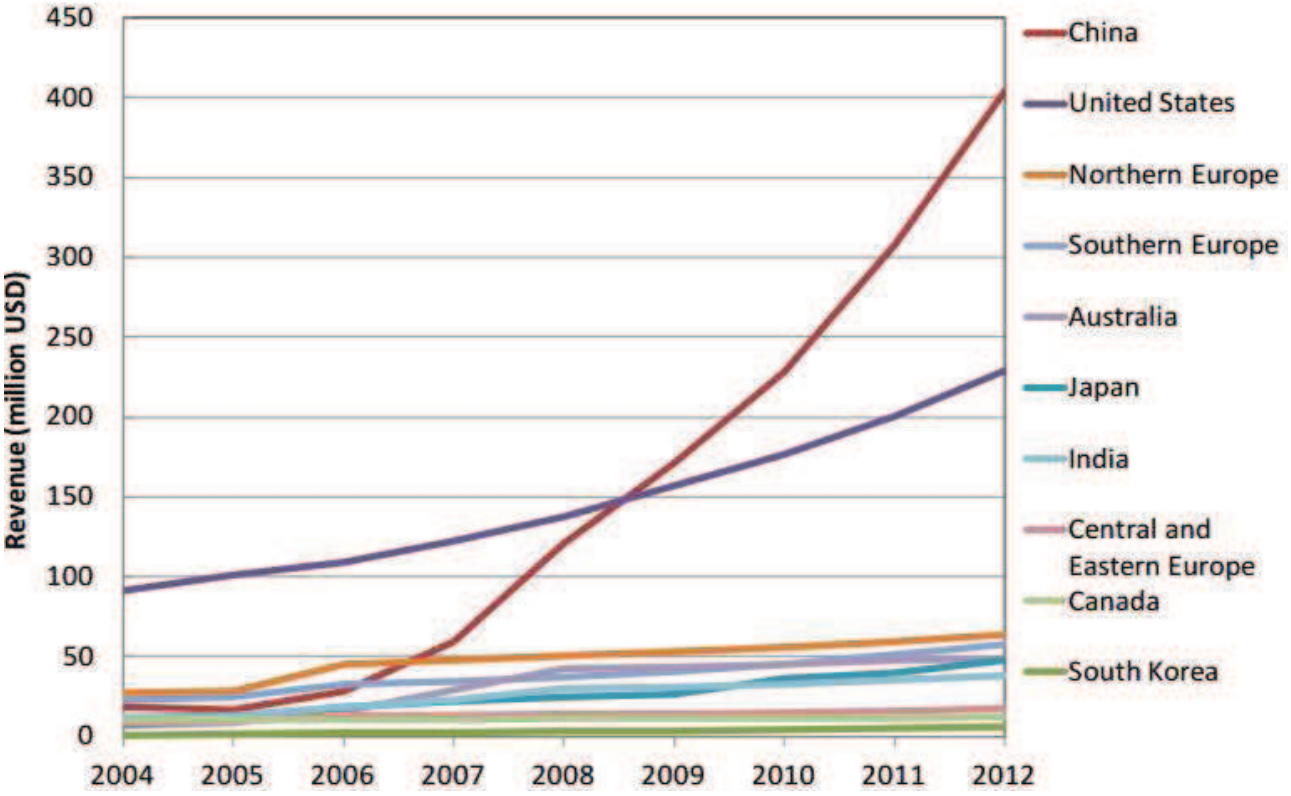


Figure 1.5: Global Market trends (Sartorius et al, 2013).

Recently, processes with limited footprint and high product water quality, especially for reuse, are fitted with MBR instead of conventional treatment plants (IWA Group, 2014). The MBR applicability is very diversified as can be seen in the pie chart in Figure 1.6.

These great quantities of varied applications give us room for academic studies on MBR modeling with a focus on process optimization regarding energy and material consumption.

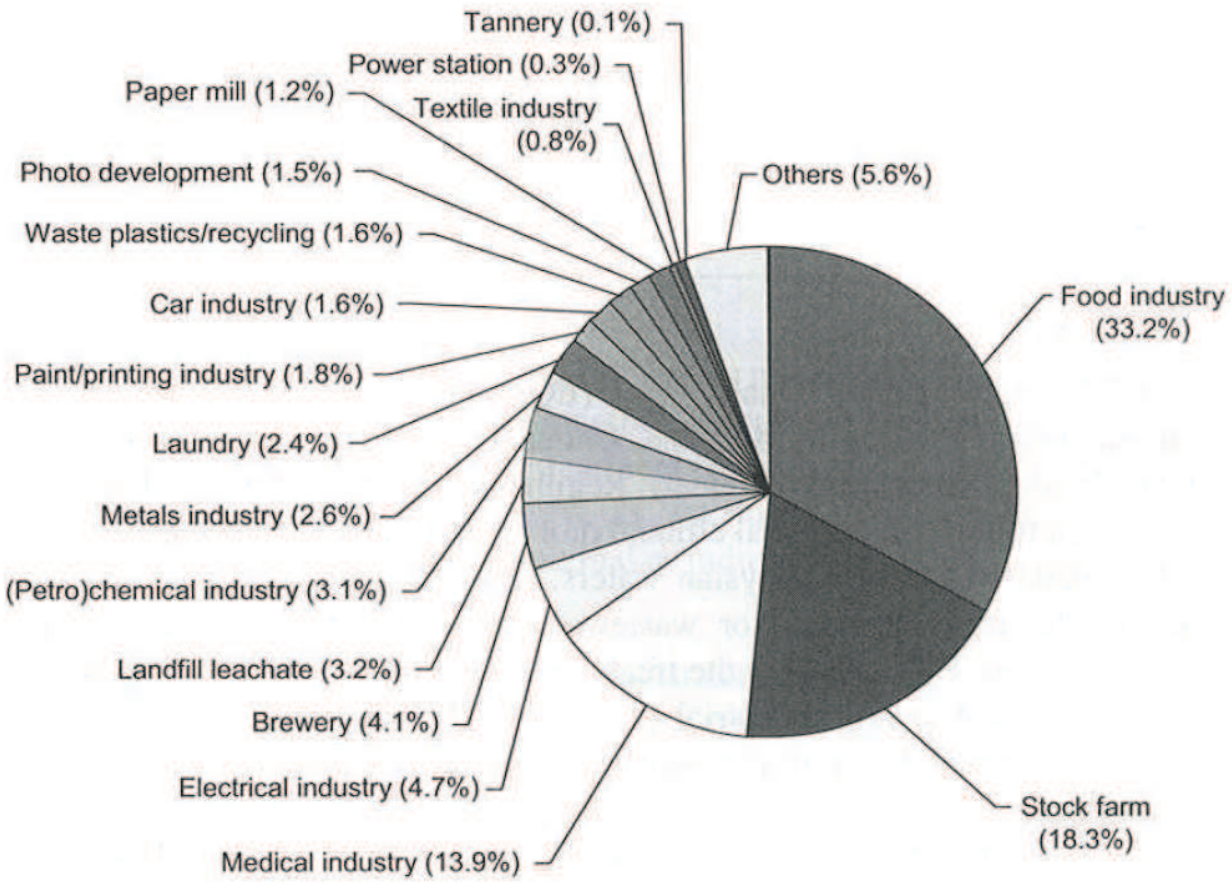


Figure 1.6: Industrial process water treatment in Japan (2009): percentage of MBR installation by industry (Judd and Judd, 2011).

1.3 Conventional Activated Sludge vs. sMBR

Conventional Activated Sludge (CAS) is usually composed by anoxic and aerobic zones with recirculation set for biological degradation in order to reach convenient effluent concentrations (see the top of Figure 1.7 that is based on the configuration of Benchmark Simulation Model no. 1 proposed by Alex et al (2008)). Out of many different processes employed, this one has been proven to be the most popular (Tchobanoglous et al, 2003). Before clean water discharged, a separation step is needed in order to segregate the sludge from the treated water, a clarifier is designed with non-turbulent flux intended to settle the solid particles. To incorporate the sMBR in an activated sludge process, the settler and the last aerobic tank are normally interchanged by a tank with a filter, the submerged membrane bioreactor (Figure 1.7, bottom part, which its configuration is based on the Benchmark

Simlation Model for MBRs presented by Maere et al (2011)).

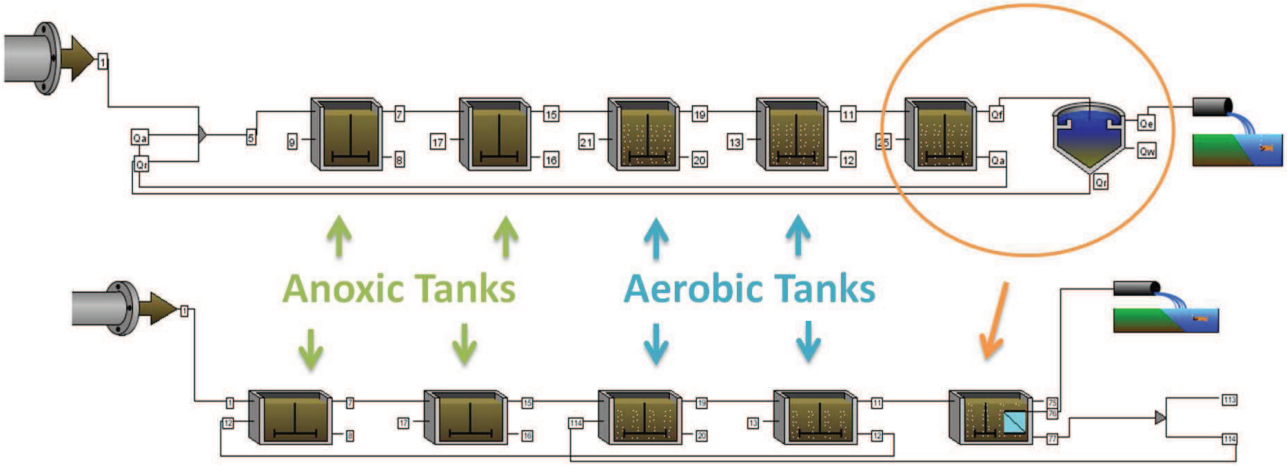


Figure 1.7: Conventional Activated Sludge *versus sMBR*.

1.3.1 sMBR Advantages

A process comprising an sMBR has several benefits if compared to a conventional activated sludge (CAS) process. Adopting an sMBR, the process can be designed with very high sludge ages and concentration (wide range of SRTs), resulting in increased flexibility and more options for system optimizations (Cicek, 2003). A system with long solid retention times can be designed with a smaller footprint reaching the same sludge production of a bigger CAS plant. Related to the high SRT, the system is robust enough to handle elevated mixed liquor suspended solid (MLSS) concentrations for short periods of time, allowing for flexible solids wasting schedules (Atasi et al, 2006; Di Bella et al, 2008; Judd and Judd, 2011; Sarioglu et al, 2009).

Another advantage is that the plant footprint area may be reduced by substituting the secondary clarifier and the settler by sMBR. The sMBR treatment can even be classified as a tertiary treatment (Lapolli et al, 1998). The process has many advantages with respect to complete removal of solids and a high quality of the effluent is reached. Two main causes provoke this high pattern of effluent quality: the biomass is completely retained, resulting in consistently high-quality final effluent and, compared to CAS, the quality depends less on the MLSS concentration and sludge settling properties (Atasi et al, 2006; Sarioglu et al, 2009). In situations where biofilm or granule formation is severely affected by the process, membrane assisted physical separations can be used to achieve the essential sludge retention (Jeison, 2007).

One important feature is the pore sizes that result in a significant physical disinfection capability, low-turbidity effluent, superior organic nutrient removals, higher volumetric loading and less sludge production (see Figure 1.1) (Atasi et al, 2006; Di Bella et al, 2008; Judd and Judd, 2011; Sarioglu et al, 2009; Wintgens et al, 2003). As a result, the sMBR process becomes an increasingly attractive option for the treatment and reuse of industrial and municipal wastewater, as evidenced by their constantly rising number and capacity (Atkinson, 2006).

1.3.2 sMBR Drawbacks

The sMBR filtration performance inevitably decreases with filtration time. This is due to the deposition of soluble and particulate materials onto and into the membrane, named fouling process, attributed to the interactions between activated sludge components and the membrane. This major drawback and process limitation has been under investigation since the early sMBRs, and remains one of the most challenging issues facing further MBR development (Le-Clech et al, 2006; Peiris et al, 2010). Thus, membrane fouling is the most disadvantageous process out of all the processes involved (Di Bella et al, 2008; Zarragoita-González et al, 2008). Like most membrane filtration processes, membrane fouling and its control are a major issue for an economically feasible MBR system due to high energy costs on the need of high necessary pressure gradients when large amounts of fouling are produced from the process(Cicek, 2003; Lee et al, 2002).

In addition, the sMBR plants have a hydraulic limitation of effluent production regarding membrane efficiency. Hence, it is a necessary redundancy of the system parts that shows a limited peaking ability of the MBR process. In contrast to CAS plants, which flow above the design capacity, typically results in a in incomplete treatment (Atasi et al, 2006).

While investment costs are already lower than those of conventional wastewater treatment plants with secondary clarification, operating costs are still higher due to membrane replacement cost and *high-energy demand for aeration* (Cicek, 2003; Jang et al, 2006; Wintgens et al, 2003), as seen in Figure1.8.

As MBRs are a relatively new technology, there is limited amount of data available to verify long-term performances. The operating conditions in the sMBR systems often favor the formation of foam, high membrane price, chemical membrane cleaning causing the process to stop and restart,

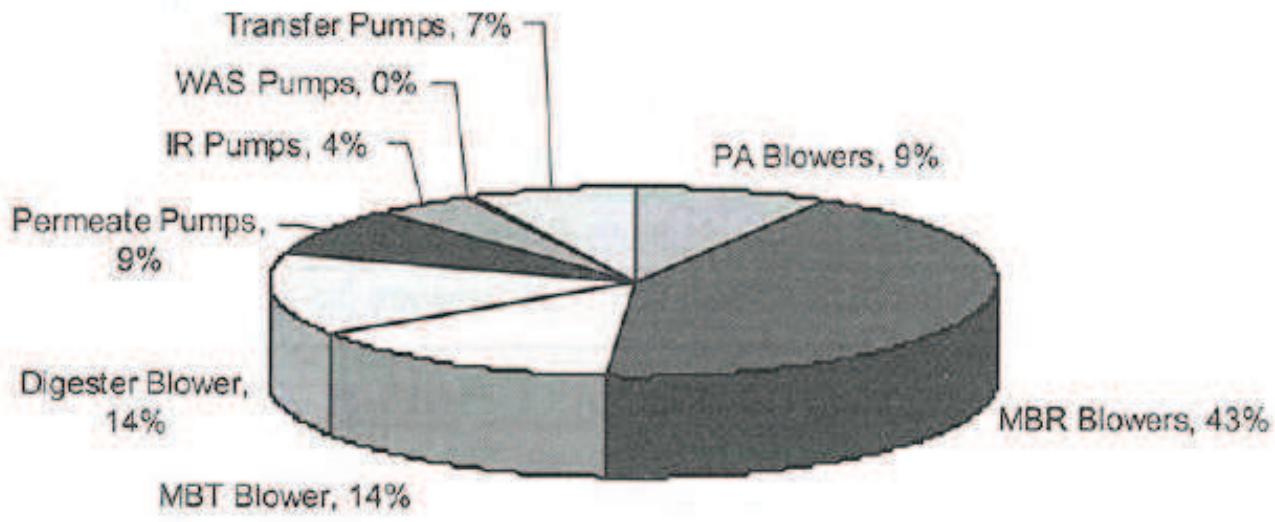


Figure 1.8: Energy demand distribution (Judd and Judd, 2011).

more energy consumption (air scour blower, biological process blower and recycled pumps) and must be closely monitored to detect changes in flux rates and permeability before they escalate.

1.4 Fouling Formation

One of the most important open subjects in the field of membrane bioreactors is how fouling forms itself and evolves over time. This incorporates biochemical and physical properties of fouling that destabilize the filtration process and hampers the efficiency of the process.

In short, the fouling mechanism is linked to the increased deposition of solid material onto the membrane surface and within the membrane structure (pore restriction or pore plugging/constriction) (Henze et al, 2011). This should be distinguished from clogging, which is the filling of the membrane channels with solids.

Permeate back flushing, chemical cleaning, maintaining turbulent conditions, operating at sub-critical flux and selecting a suitable fouling-resistant membrane material are standard procedures applied to minimize the fouling effect and stabilize overall permeability of the membrane systems, but result in loss of net filtration efficiency and possible damage to the membrane due to cleaning agents (Gander et al, 2000). Neither the evolution of membrane permeability under certain operating conditions nor the effect of cleaning

measures can nowadays be predicted. These uncertainties cause considerable difficulties in plant layout, design and operation (Wintgens et al, 2003).

The fouling characterization adversity and its interaction with role process delays the development of a general law for fouling. The nature and the extent of fouling are strongly affected by physical and chemical interactions between the membrane and the mixed liquor. In particular, the mixed liquor composition defines fouling characteristics and various factors affect membrane fouling in the sMBR (Di Bella et al, 2008). These can be classified in relation to the membrane, biomass characteristics and operating conditions (Jang et al, 2006).

In Section 2.4.2, this subject is discussed in more detail and its dynamics are modeled with different rates of complexity.

However, the flux reduction phenomenon is usually analyzed in terms of filtration resistances. The flux through the membrane is a function of trans-membrane pressure(TMP), permeate apparent viscosity (η) and the total membrane resistance ($R_{total,Busch}$)

$$J = \frac{TMP}{\eta R_{total,Busch}} \tag{1.1}$$

in which J represents the applied flux. The total membrane resistance can be divided in several partial resistances (Busch et al, 2007b):

$$R_{total,Busch} = R_m + R_c + R_p + R_b + R_{cp} + R_{sc} \tag{1.2}$$

where R_m is the membrane intrinsic resistance and most of the time is represented by a constant value provided by the membrane factory; R_c is the resistance due to cake layer formation onto the membrane (Figure 1.9); R_p is the resistance due to membrane fouling linked to pore blocking (Figure 1.10, which shows a summary of different types of pore blocking); as soon as microorganisms attach to a surface, biofilm formation begins to yields biofilm resistance R_b. R_{cp} is the resistance originated from the formation of the condensation polarization layer. Figure 1.11 shows the layer due to the cross flow air) and R_{sc} is the scaling resistance, related to coating, incrustation, bulk or surface crystallization. Information on the total resistance distribution in all its partial components is greatly beneficial for strategies on the flux decline mitigation, that can only be effective if the causes of flux reduction can be determined (Jeison, 2007).

Since the fouling mechanism is not completely understood, its control

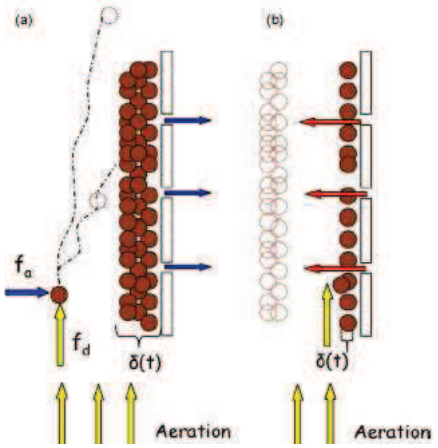


Figure 1.9: Cake formation and particle trajectory: (a) air cross-flow ; (b) backwash (Di Bella et al, 2008).

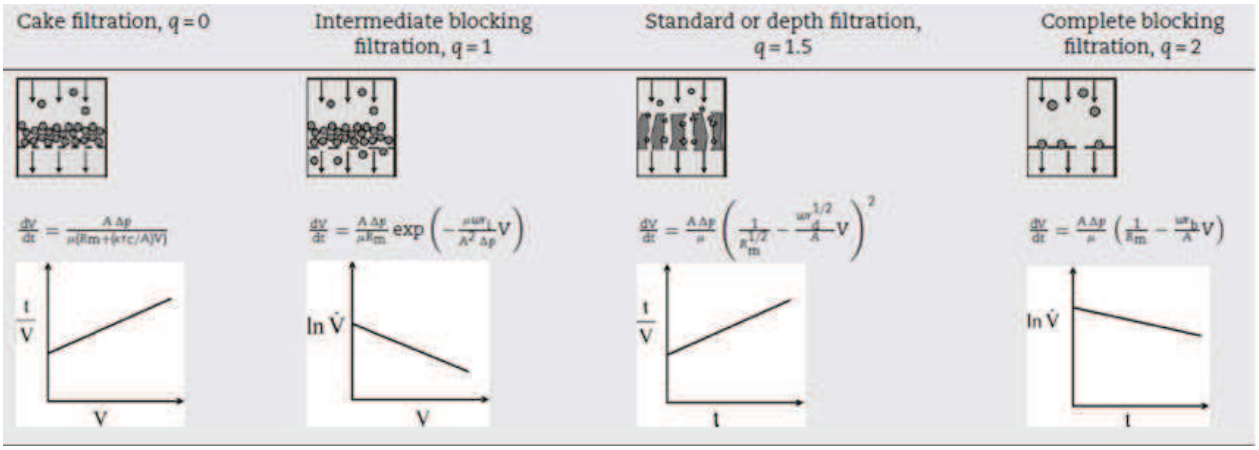


Figure 1.10: Filtration mechanisms with their schemas, equation and linear representation (Fernández et al, 2011).

strategy is an onerous task to accomplish, the subject of which is discussed further in Section 5. Nonetheless, acquiring knowledge on process operation introduces us to some practical techniques to mitigate the fouling build-up.

1.4.1 Backwash, Relaxation and Chemical Cleaning

The concept of backwash is an inversion of the liquid flow, the goal of which is to dissipate the cake formation onto an into the membrane surface. Several studies show that it is possible to optimize the backwash sequence until the period between two chemical cleaning procedure is increased (Judd and

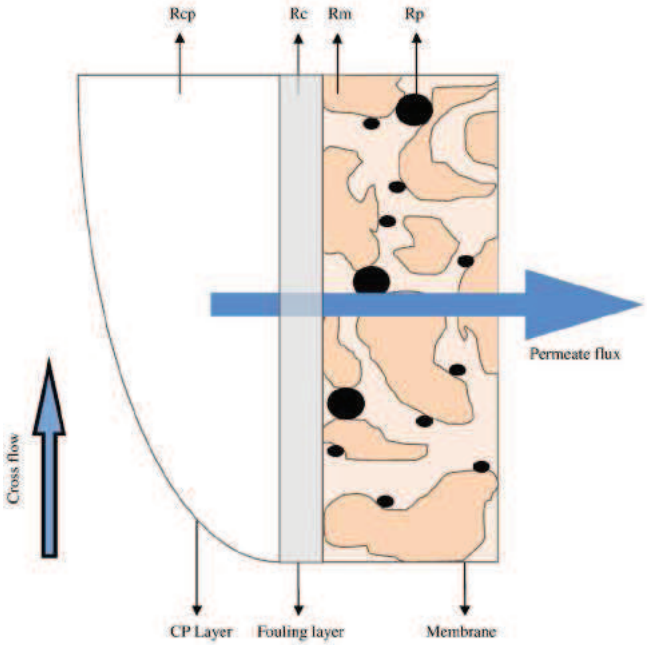


Figure 1.11: Concentration Polarization Layer (CP Layer) (Shirazi et al, 2010).

Judd, 2011). One impasse is in order to optimize the backwash sequence, it is necessary to predict the fouling formation onto the membrane.

In MBRs, physical cleaning is normally achieved either by backwash or relaxation, which is simply stopping permeation while continuing to scour the membrane with air cross-flow. These two techniques may be used together while backwashing may be enhanced by combining it with air (Braak et al, 2011).

In connection to that, chemical cleaning is carried out with mineral or organic acids, caustic soda or, more usually in MBRs, sodium hypochlorite, and can be performed either in situ ("cleaning in place" or CIP) or ex situ. Alternatively, a low concentration of chemical cleaning agent can be added to the backwash water to produce a "chemically enhanced backwash" (CEB) (Judd and Judd, 2011).

The main impact of the operating flux lies in the period between cleanings, which may be either by physical or chemical means (Figure 1.12). Generally, the backwash cycles are fixed, the permeate cycles are measured in minutes and the backwash in seconds. The backwash is periodically implemented, as seen in Figure 1.13. The cycles are repeated until the maximum pressure is reached and chemical cleaning is executed. However, to predict the interval between two chemical cleaning depends on the variables of the system which

include MLSS, influent concentration, fouling deposition, solid retention time and F/M ratio that makes this prediction not so trivial.

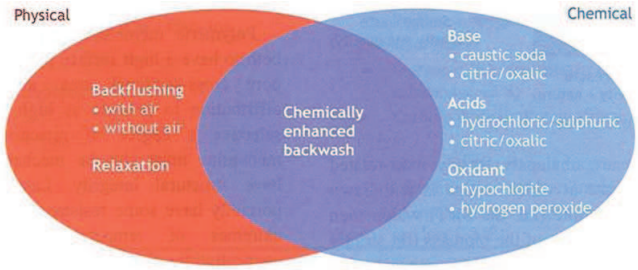


Figure 1.12: Physical and Chemical Cleaning Methods (Judd and Judd, 2011).

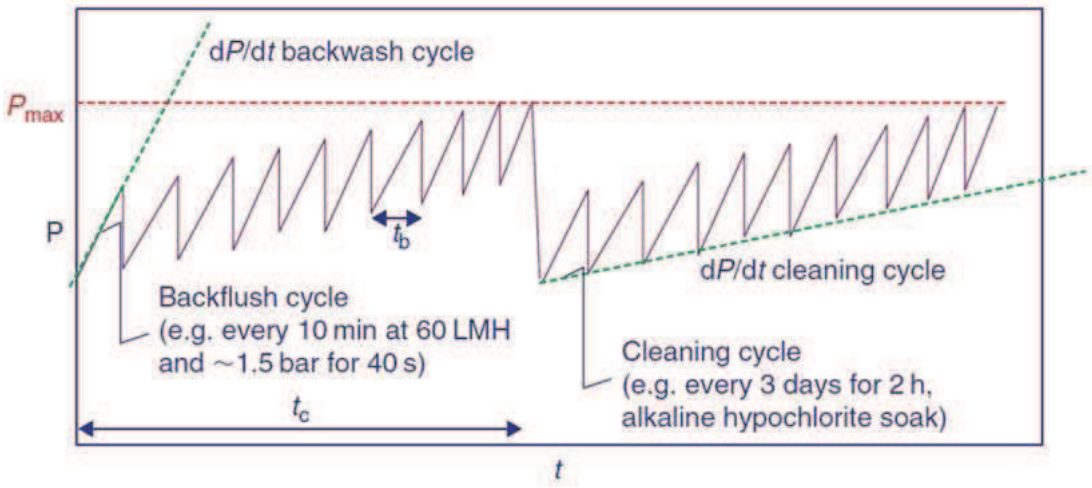


Figure 1.13: Pressure transient for constant flux operation of a dead-end filter (Judd and Judd, 2011).

The different configurations and types of sMBR, presented in this chapter, reflect the possible large range of implementations of MBRs. Despite this, the main challenges remain in the prevention of the fouling process by the continuous development of new materials, MBR configuration, process modeling and/or process control strategies.

Chapter 2

Modeling sMBR

2.1 Mathematical Modeling of Biological Systems

In recent years, the field of biology has borrowed mathematical tools to model and understand the complex phenomena of biology (Jones and Sleeman, 2003).

Murray (2002) defined mathematical modeling of biological systems as a *fast-growing, well-recognized, albeit not clearly defined, subject and is the most exciting modern application of mathematics*. The development of this area is linked with the fact that biology becomes more quantitative and the interdisciplinary involvement is essential. The development of simple dynamic equations gives room for many insights and discoveries in biotechnological complex processes. Modeling has become a fundamental tool for many areas of knowledge such as: mechanics, heat transfer and diffusion, traffic flow, electrical networks, communication and coding, economics, music, sports and biology (Klamkin, 1995).

The interconnection between mathematics and biology is based on some principles, including a prior understanding of biological problems; a realistic mathematical representation of important biological phenomena, and mathematical tools to find useful solutions and translate these into beneficial biological processes (Murray, 2002).

It is not evident to follow these simple rules, but when this stage is accomplished the combination of biology and mathematics creates a powerful tool to study complex biological systems.

The biological processes have an intricate nature and, normally, assumptions to simplify the studied process are needed. For example, different

environments and organisms can differ in rate of biological activities. This turns finding the definition of the system boundaries into a delicate task, and most of the time process analysis into smaller sub-processes without substantially altering the dynamic phenomena becomes unfeasible (Van Impe et al, 1998). Another adversity is the biological process coupled between dynamics, in which, generally, variations of scale and time-constants are small, blurring the selection of appropriate level of cognition for simplifications.

Additionally, biotechnological systems show low accessibility to its dynamics behavior as a consequence of processes being difficult to separate and measurement techniques being inadequate and/or very expensive (Van Impe et al, 1998).

For these reasons, the use of models can result in a fast process cognition, prediction and potential system optimization. Regarding this, virtual experiments (or simulations) are used, combining biology, mathematics and computational powers, allowing the performance of many virtual experiments in a short time frame. This is clearly advantageous over tedious lab experiments, especially for slow processes like bioprocesses (Naessens et al, 2012a). Note that for realistic process simulations, many biological experiments may be carried out before, in order to achieve a large quantity of information on the process for model calibration.

The assumptions imposed to the models, abovementioned , give only the simplification of reality and, with this, many sources of existing uncertainty are added to the model. The uncertainties are composed by, for example, model structures, model parameters and experimental data measurements, which will propagate through the model and constitute the model output uncertainty (Naessens et al, 2012a). The level of the complexity that reflects the reality and the omission of some dynamics may provoke a large difference between the modeled dynamic and the real one. With this compromise in mind, complexity and error are the art of modeling (Van Impe et al, 1998).

The main task of *modeling* is the continuous research for models with simple standard sub-models, with primitive laws, that are able to emulate a larger-scale process. As a consequence, techniques and insight are required to infer the unknown in framework and structure from the available information sources.

The modeling of a biotechnological process can be achieved following some simple but important rules. Firstly, the objectives of the model are chosen, in which the model structure, degree of complexity and functional behavior are established. These three main aspects help on the choice of type

of model, static or dynamic. For this purposed mathematical tools are needed and a possible interconnection with internal behaviors must be studied. In this step, characteristic features and properties of modeling methods have to be compared and evaluated with respect to the actual modeling task and previous knowledge concerned with fundamental laws and previous modeling efforts. The on-line and off-line assembled measurements providing direct information on the specific system must be carried out (Van Impe et al, 1998). Having the basis of the model in hand, numerical analysis can be executed followed by model coding into computer languages for simulations. The simulations phase is extremely important for the first validation between numerical analysis and simulation results. At this moment, the "virtual" process can be stressed to validate the assumption made in the first step. Finally, the model output should be compared with the real process measurements and a sensitivity analysis is carried out with the purpose of diagnosing which process or operational parameters impact output variables of interest.

2.2 Mathematical Model Types

A mathematical model can be designed with different approaches taking into account the quantitative description of a biotechnological process. These approaches are divided into three main model methodologies.

2.2.1 Black-box Models

Black-box modeling is useful when the primary interest is focused on fitting the data regardless of a particular mathematical structure of the model. The models are built based on the study of the input and output behaviors and internal relations are not taken into account.

These models describe the dependency of the system output y at time t_k on past and present inputs $u(t_i)$. An example of such a model is:

$$y(t_k) = \frac{B(s)}{A(s)} u(t_k) \tag{2.1}$$

where $A(s)$ and $B(s)$ are polynomial in the backward shift operator s, i.e.,

$$s^{-j}(y(t_i)) = y(t_{i-j}) \tag{2.2}$$

$$A(s) = 1 + a_1 s^{-1} + a_2 s^{-2} + \cdots + a_n s^{-n} \tag{2.3}$$

$$B(s) = b_0 + b_1 s^{-1} + b_2 s^{-2} + \cdots + b_m s^{-m} \tag{2.4}$$

To determine the a_i and b_i and the order of the polynomials n and m, the process input is excited and the output is measured. Therefore, the relation between input-output is established. On one hand, the essential feature of black-box models is that they have no physical or internal relationship between the system's inputs and outputs. On the other hand, the inputs should produce observable responses in the output (Sjöberg et al, 1995).

2.2.2 White-box Models

The white-box or mechanistic models use the process knowledge and physical law to design models with parameters that have physical or biological meaning. This type of model is preferred in the bioprocesses domain, due to the possibility to understand the process interconnections and behaviors only analyzing the model parameters and dynamics.

As most of the biological process dynamics involve nonlinear relations, a nonlinear model may be built such as:

$$\frac{d\mathbf{x}}{dt} = \mathbf{f}(\mathbf{x}, \mathbf{u}, \theta) \tag{2.5}$$

$$\mathbf{y} = \mathbf{h}(\mathbf{x}, \theta) \tag{2.6}$$

where the nonlinear relations $\mathbf{f}$ and $\mathbf{h}$ between the state variables, inputs and outputs, and the model parameters θ are represented.

Depending on the level of the description needed, the nonlinear models can be linearized in a desired region and described using the following state-space model:

$$\frac{d\mathbf{x}}{dt} = A\mathbf{x} + B\mathbf{u} \tag{2.7}$$

and the output observations $\mathbf{y}$ are given by

$$\mathbf{y} = C\mathbf{x} \tag{2.8}$$

Note that here the vector of system inputs $\mathbf{u}$ and output vector $\mathbf{y}$ are described by the internal dynamics represented by the state vector $\mathbf{x}$, which contains

variables such as the biomass, substrate, oxygen and nitrate. The matrices A, B and C contain the characteristic (possibly time varying) parameters of the system, which must represent be positive variables in the case of the biological systems.

2.2.3 Gray-box Models

The fusion of models composed by one structural part or parameters with biological and physical aspects and another with black-box description are considered gray-box models. These models merge the advantage of both the abovementioned structures, simplifying model analysis studies and parameter identifications.

2.3 Motivation for Modeling sMBRs

The submerged membrane bioreactors cannot be considered a fully-known process. Studies of sMBRs date more than 20 years and some problems still have no solution. Modeling biological behavior in the presence of a membrane has become a well-studied branch and its main objective is to understand fouling formation and its composition in more depth. Thus, the main drawback of a membrane bioreactor could be mitigated. Another branch of research focuses on the modeling of fouling formation onto the membrane surface, which is normally related to the understanding of physical sludge cake formation (reversible resistance), pore blocking (irreversible resistance) and a decrease in the efficiency on the membrane outflow. Finally, studies interconnecting both models couple biological and physical behaviors. Fluid and cross air dynamics inside the tanks is the computational fluid dynamics (CFD) study, a third branch which could be addressed and which if of great importance in order to understand fouling attaching and detaching on the membrane surface.

A common element in all the studies mentioned is the descriptive and cognitive objective of the models. The expertise on sMBR processes has been the main ambition of, many of the “modelers” in this domain. Based on literature, it has been noticed that there is a lack of integrated models designed to process control. As mention in Section 2.1, the objective of the model determines the validity domain to which this model could be applied. Therefore, a model based on process control must have simple sub-models

and interconnects the physical and biological behaviors. The compilation and understanding of many models and literature results should thus be summarized and well-understood as seen in the following sections.

2.4 sMBR Model Types

Typically, research on sMBR modeling is classified into three categories: biomass kinetic models, membrane fouling models and integrated models. Extremely few models tailored especially for control purposes have been found as supported by Busch et al (2007b) who present a very simple black-box model where a batch-to-batch parameter identification and control strategy are implemented for a real application.

2.4.1 sMBR Biological Modeling

Biological kinetic models are based mainly on Activated Sludge Models (ASMs) (Henze et al, 2000) which could be suitably adapted or not to model sMBR processes (Fenu et al, 2010). In particular, the ASMs have been modified to take into account the formation and degradation of the soluble microbial products (SMPs) in the MBRs. In technical literature on kinetic models, the hybrid models, which are basically a coupling of the ASMs and the SMP formation process, are also defined. The hybrid models, conversely to the kinetic ones, describe the influences of SMPs in the biological processes and effluent quality (Benyahia et al, 2011; Henze et al, 2000; Jang et al, 2006; Zarragoita-González et al, 2008).

In a nitrogen removal process, the most used model is the Activated Sludge Model No.1 (ASM1), proposed by the Task Group (Henze et al, 1987), which gathers the most important process reactions. These models consist of 13 components and eight reactions, which take into account heterotroph and autotroph microorganisms, their decay, ammonification of soluble organic nitrogen, and hydrolysis of entrapped organics and entrapped organic nitrogen. The model has been exhaustively validated by several experiments (Fenu et al, 2010; Maere et al, 2011; Ng and Kim, 2007; Sarioglu et al, 2009; Spérandio and Espinosa, 2008).

This model exemplifies the complex interconnection of components, represented in Figure 2.1, for a biodegradation process. The ASM1 subdivides

the organic matter in wastewater into a number of categories, normally indirectly measured by the chemical oxygen demand (COD) test: the non-biodegradable organic matter is biologically inert and passes through an activated sludge system unchanged in form; the biodegradable organic matter may be divided into two parts: readily biodegradable and slowly biodegradable; the hydrolysis factor of slowly and readily biodegradable substrate; the heterotrophic biomasses is generated by the growth on readily biodegradable substrate under either aerobic or anoxic conditions, but is assumed to stop under anaerobic conditions; the biomass decay; the non-biodegradable and biodegradable nitrogenous matter and autotrophic biomass.

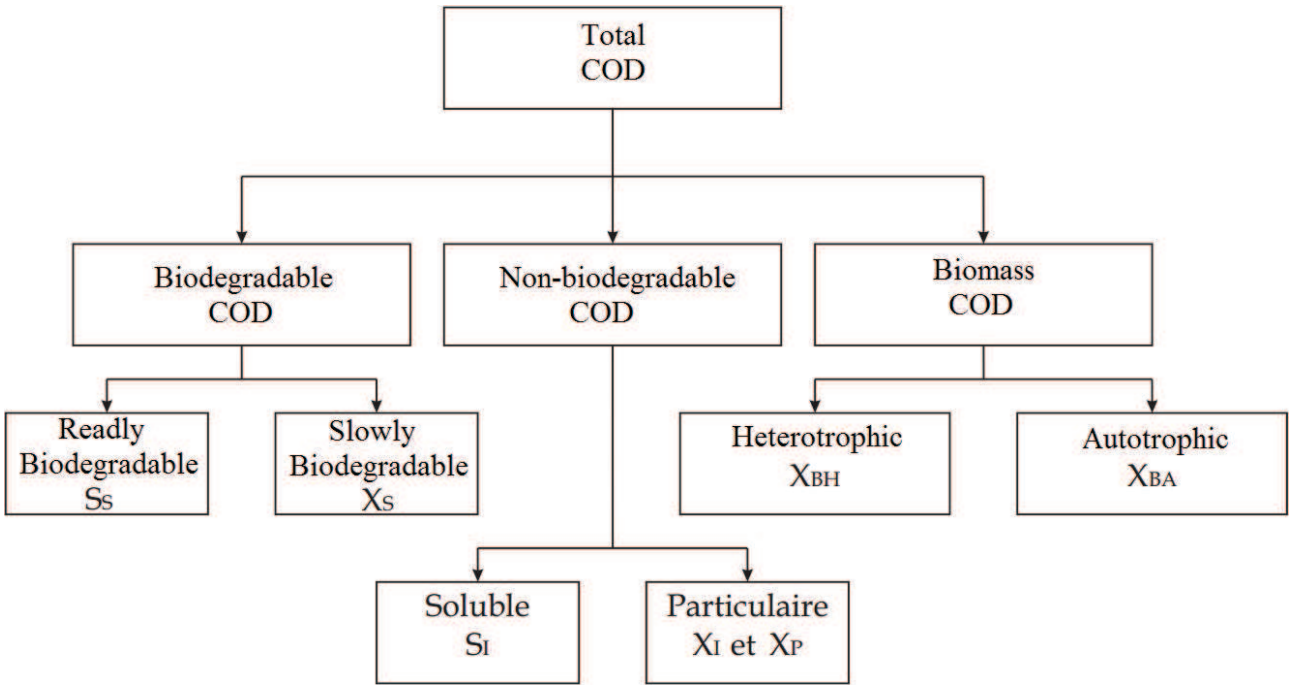


Figure 2.1: ASM1 Scheme. Adapted from David (2008)

The ASM1 is a dynamic model that uses the sum of the products of the process rate (ρ_j) expressed with the simple Monod-Herbert model and the stoichiometric coefficients (ν_{ij}) to compose the reaction term (r_i), and the mass balance for the transport part. The Monod equation announces that the growth of the biomass is proportional to biomass concentration in a first manner and to substrate concentration in a mixed order manner. The Herbert expression states that biomass decay comes first with respect to biomass concentration. Therefore, the system reaction term (r_i) is obtained by adding together the products of the stoichiometric coefficients (υ_{ij}) and the process

Models describing biomass kinetics in an MBR
ASM1(Henze et al, 2000)
ASM3 (Wintgens et al, 2003)
SMP model (Lu et al, 2001)
ASM1 - SMP hybrid Model (Chen et al, 2012; Lu et al, 2001)
ASM1 - ASM3 long range SRT (Spérandio and Espinosa, 2008)

Table 2.1: Classification of the sMBR studies. Adapted from Judd and Judd (2011)

rate expression, as shown in the following equation:

$$r_{S_S} = \frac{1}{Y}\mu\frac{S}{S+K_S}X \quad r_{X_B} = \mu\frac{S}{S+K_S}X_B - bX_B \tag{2.9}$$

where S and X are the substrate and the biomass concentrations, μ is the maximum specific growth rate, K_S is the half saturation constant and b is the specific decay rate. The mass balance is composed by input and output variation plus the values of the reaction results.

This model can be considered as a descriptive model since it has been developed mainly to understand the interconnections of the nitrogen removal process and process prediction (Henze et al, 2000). The activated sludge system has previously been widely studied, leading to "complete" kinetic knowledge for modeling the main heterotrophic and autotrophic biological processes (Spérandio and Espinosa, 2008).

Some studies have been carried out to understand the connection between ASM1 and sMBR; some of them are listed in Table 2.1.

A normal practice which entails large dynamic descriptive models is model reduction. Based on several hypotheses, the main objective of this is to reduce the model by restricting the model generalization properties. One example is the simplified model proposed by David (2008). This model was proposed for the Conventional Activated Sludge (CAS) process and the reduction was based on the biological and chemical arguments and singular perturbation methods. The CAS differs from the sMBR mostly by the physical structure and all advantages and drawbacks reported in section 1.3.1 and 1.3.2.

2.4.2 sMBR Physical Modeling

The sMBR physical aspect is associated with the deposition of solid matter onto and into the membrane surface, named the fouling mechanism. Many of mathematical modeling approaches have been considered to simulate the descriptive model reversible fouling phenomenon such as: the sludge cake formation (Busch et al, 2007b; Gehlert et al, 2005; Polyakov, 2006; Shirazi et al, 2010; Tien and Ramarao, 2011; Wu et al, 2012); the entire fouling process itself (Charfi et al, 2012; Li and Wang, 2006; Robles et al, 2013a,b); the pore blocking mechanism (Broeckmann et al, 2006; Fernández et al, 2011); the influence of particle size (Ho and Zydney, 2000); the cake compression factor (Jan Kincl and Cakl, 2009; Jørgensena et al, 2012); the cake filtration phenomenon (Kuberkar and Davis, 2000). Few models take into account the empirical (Khan et al, 2009) and artificial neural network model (Choi et al, 2012). Some of them are simply based on solid-liquid separation, hydrodynamics (CFD) and simulated filtration processes as an ideal settler with unitary efficiency (Braak et al, 2011; Tchobanoglous et al, 2003).

Several studies of different viewpoints have been published to understand this mechanism, showing the high complexity of the fouling process, in which a variety of physical, chemical and biological phenomena take place on different time-scales. The interaction of the biological and the filtration system is complex and has a decisive impact on modeling (Busch et al, 2007a). Some important references for a better understanding of the physical process is presented in the following list:

- Busch et al (2007b) proposed a filtration resistance model that incorporates pore blocking, cake layer formation, polydispersed particles, biofilm formation and bulk concentration polarization. This model is a descriptive complex model, which presents a large quantity of parameters to model the fouling formation;

- Wintgens et al (2003) presented a semi-empirical model with sludge cake formation, concentration polarization and irreversible resistance. The fouling model is validated using full-scale municipal wastewater treatment plant data, but for the biological aspect, only a steady-state system behavior is presented;

- Polyakov (2006) showed that the hollow fiber membrane in series process can be described using the depth filtration theory, but only simulation results are presented in this study;

- Gehlert et al (2005) detailed UF cassette module modeling for the separation of activated sludge in a side stream MBR. A resistance-in-series approach is used to describe mass transfer for both forward filtration and backflushing. Reliable results presented in the experimental validation section shows that a filtration model with a reasonable quantity of parameters (less than 10) is sufficient for a good approximation of *TMP* behavior;

- Chellam (2005) is a purely empirical approach, using artificial neural networks to describe the microfiltration of polydispersed suspension with hollow-fiber membranes. The model comprises a black-box that allows the gains to be interpreted as mechanical behavior;

- Geissler et al (2005) demonstrated a semi-empirical model with a data-driven approach for a hollow fiber membrane with validation based on a real process. The semi-empirical model has a small number, but the long term study is validated with permeability mean values, which could hide important process behaviors as the water temperature influences membrane permeability;

- Marriott and Sørensen (2003) proposed a general modeling approach for hollow fiber and spiral wound based on: mass, momentum, energy balances for generic separation application. This model, if used for modeling sMBRs, lacks interconnection with biological aspects, but its general framework shows the possibility of many other applications;

- Mangold et al (2004) modeled a software library comprising modular components from which generic membrane models can be synthesized. Studies with this tool are important for first results in order to study the viability of implementation of a membrane bioreactor in a new process;

- Zarragoita-González et al (2008) deduced a link regarding membrane fouling, filtration pressure, aeration bubbles size, resulting in an interesting connection between the ASM+SMP and cake formation. This general model has a large quantity of parameters that could make the design of a more advanced controller, i.e. optimal and robust controllers, more difficult.

The above list shows that mainly the physical models are extremely linked to the type of membrane and in most of time tries to describe in detail

the fouling process and models focused in fouling main dynamics are very scarce. This lack of simple models motivated the study of main dynamics in a submerged membrane bioreactor.

2.4.3 sMBR Integrated Modeling

Many dedicated single process models have been developed for sMBR processes. The biological aspects are normally based on an ASM framework (Henze et al, 2000). Regarding membrane fouling dynamics, plenty of models have been designed in order to understand the process. However, these processes are strongly linked and an integrated model is needed (Mannina et al, 2011). The process is dependent on the total amount of fouling material and this in turn depends upon both the thickness of the interface, the feed-water composition (and specifically its foulant content) and the flux through the membrane. The feed water composition and the process operating conditions thus largely determine process performance (Judd and Judd, 2011).

Naessens et al (2012b) point out the importance of developing an integrated model and the risk of using these separate models for optimizing the entire system, since optimal conditions for one process may not be optimal for another (e.g. optimizing the air cross flow can modify biomass properties resulting in a faster/slower degradation of the substrate).

The importance of an integrated sMBR model has been captured and its theory applied for the first time by Lee et al (2002) and Wintgens et al (2003). The former presented an ASM1-SMP model (activated sludge model No.1 with soluble microbial products, which are free in mixed liquor) and the latter an ASM3-EPS model (activated sludge model No.3 with extra-cellular polymeric substances that are biopolymers attached on the microorganisms). Many other models followed the same path as Li and Wang (2006), Zarragoita-González et al (2008), Di Bella et al (2008) and Zuthi et al (2012) developing many different models with different properties. Most of the time, these models have a large number of parameters, as evidenced by the model proposed by Mannina et al (2011) comprising 45 parameters. Despite this large quantity of parameters, in this same study, a sensitivity analysis study showed that only around 30% of the parameters are crucial to process dynamics emulation. These studies led us to another viewpoint on the entire sMBR modeling process. Instead of having a model that describes the process and that is used for its gain of insight, a simplified integrated model regarding the process

control is proposed.

2.5 Proposed Simple Integrated sMBR Model

One of the greatest challenges for water treatment process is the development of an integrated model (comprising biological phenomena and a filtration mechanism). Additionally, those models include many parameters which can be difficult to estimate from experimental data and are, in general, too complex for control purposes, for instance. As a general rule, it is always necessary to make a trade-off between model complexity and dynamic predictive capability. For control purposes, a model should not be more detailed than required by a specific control task (Kokotović et al, 1986). In this context, there are only a few proposals of sMBR models based on empirical approaches (Khan et al, 2009), artificial neural network models (Choi et al, 2012) or black-box model to estimate filtration performance (Dalmau et al, 2013).

The proposed model design is proceeded based on the following rules:

- study the basic principles of sMBR dynamics;
- study basic physical/biological phenomena;
- compile the main model references;
- select a few mathematical models;
- consider the description of a few selected models to build the desired one.

The modeling of the fouling process is selected as the starting point. The results of the literature inspection for the fouling formation process are shown in the Table 2.2, which shows the relation between the process variables and the sludge cake formation, for instance. Figure 2.2 describes the fouling evolution over time.

Fouling sludge cake evolution can be split into two parts. The left side (t_0) of the Figure 2.2 demonstrates when the permeate pump is off and there is no fouling attached to the membrane. The center (t^+) reveals the moment when the permeate pump is turned on and the solid particles in the neighborhood of the membrane are attracted by the flow toward the membrane surface,

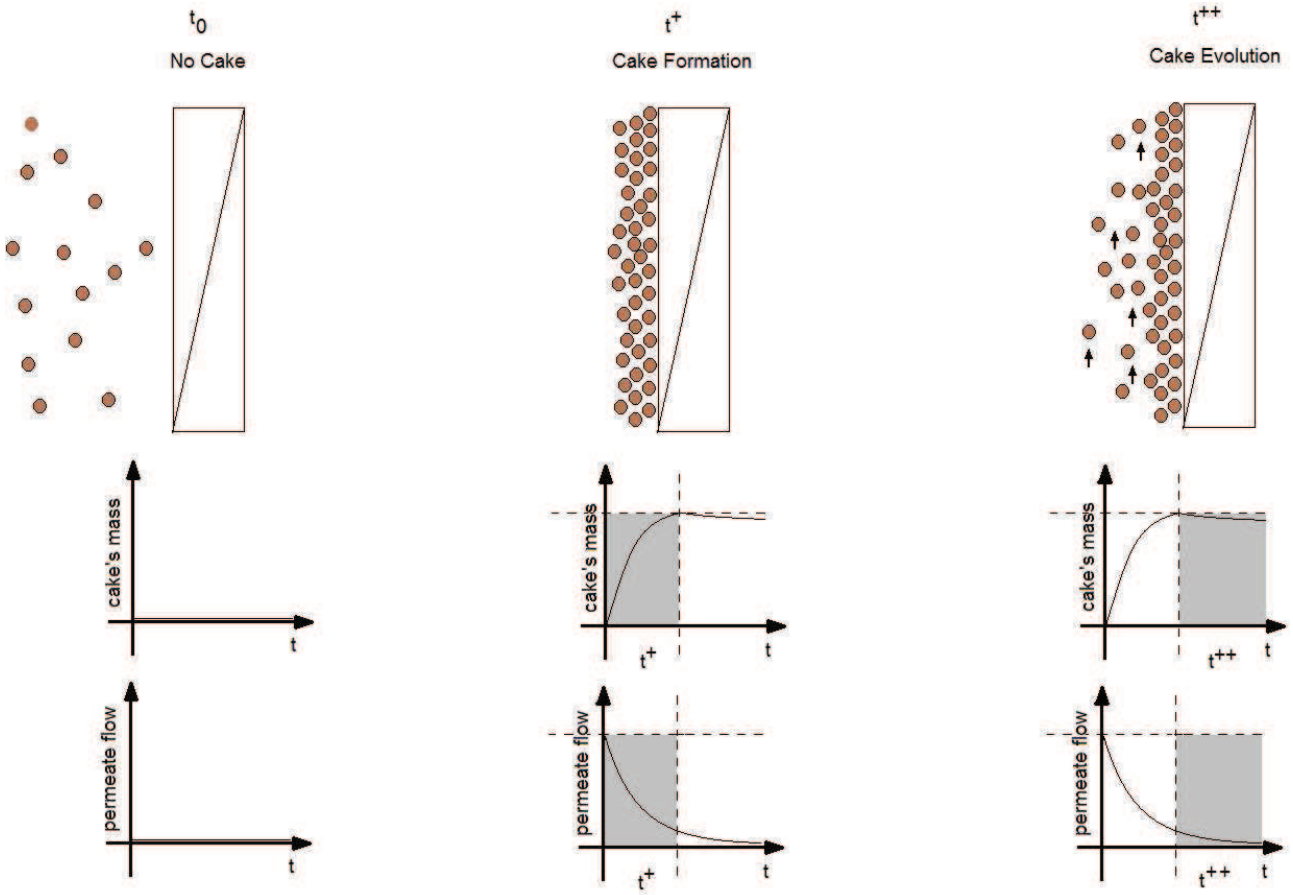


Figure 2.2: Time evolution of cake mass and effluent flow: at t_0, $Q_{out} = 0$; at t^+, the cake is formed; the time interval up to t^{++} shows the further cake evolution

Table 2.2: Relation between process variables and fouling formation.

Effect	fouling formation
↑ Cycle Permeate	↑
↑ Cycle Backwash	↓
↑ Cycle Idle	↓
↑ TSS	↑
↑ Air Cross-Flow	↓
↑ Q_{out}	↑
↑ Pressure	↕
↑ BckWsh Efficiency	↓
↑ Cake Compression	↑
↑ Area	↑

resulting in the fouling formation. The right side (t^{++}), depends on the long-term fouling evolution. The transition between t^{+} and t^{++} is considered when the first layer of fouling mass is formed. Considering a process with constant trans-membrane pressure and air cross-flow, the effluent flow decreases with time, due to the fouling build-up on the membrane surface.

This study considers that particle deposition creates a resistance to the flow through the membrane. According to literature, several descriptions of the total fouling resistance can be found (Busch et al, 2007b; E.Remigi, 2008; Lee et al, 2002; Sarioglu et al, 2012). The total fouling resistance (R_{total} $[m^{-1}]$) is represented by equation (2.10). Lee et al (2002) and Khan et al (2009) claim that the sludge reversible resistance(or sludge cake resistance), R_{rev} $[m^{-1}]$, can be considered as the most important aspect for total fouling resistance. R_m $[m^{-1}]$ is the intrinsic resistance, R_{irrev} is the irreversible resistance, which can only be removed by chemical cleaning while R_{rev} denotes the reversible resistance that is affected by the air cross-flow and δ_R is used to represent total resistance disturbance, resulting from biofilm, concentration polarization and scaling resistances.

$$R_{total} = R_m + R_{rev} + R_{irrev} + \delta_R \tag{2.10}$$

The process has two possible modes os operation: (1) the effluent flow rate is given by $Q_{out}(m) = TMP\ A/\eta R_{total}$, where TMP $[mbar]$ is the trans-membrane pressure and η $[mbar \cdot d]$ is the water apparent viscosity and A is

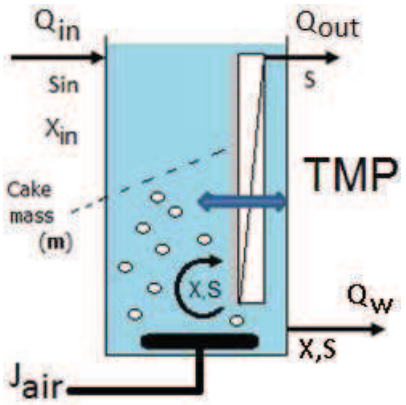


Figure 2.3: sMBR process sketch.

the membrane area, Figure 2.3.Note that when the TMP is constant the Q_{out} is in function of m, i.e. $Q_{out}(m)$;(2) the trans-membrane pressure is given by $TMP(m) = \frac{Q_{out}}{A}\eta R_{total}$, where the Q_{out} is constant and TMP is in function of m. The (m) will be suppressed in order to improve the readability of the text and will be added when needed.

The reversible sludge cake resistance is ruled by

$$R_{rev} = \rho_{rev}\frac{m + m0}{A} \tag{2.11}$$

where ρ_{rev} $[m.g^{-1}]$ is the specific sludge cake resistance, m_0 $[g]$ is the initial sludge cake mass and m $[g]$ is the current sludge cake mass. The latter can be described by dynamic equation (2.12).

$$\frac{dm}{dt} = Q_{out}X - J_{air}\mu_{air}(m)m, \text{ with } \mu_{air}(m) = \beta\frac{m}{K_{air} + m} \tag{2.12}$$

The right hand side of equation (2.12) has two terms. The first term represents the attachment of total suspended solids on the membrane surface which depends on the effluent rate Q_{out} $[m^3/d]$ and its concentration X $[g/m^3]$. The time-scale is represented in Figure 2.2 by t^+, showing that the particles in suspension near the membrane walls are rapidly forced against the filter. The second term of equation (2.12) represents the sludge cake detachment proportional to air cross-flow. The parameter β $[m^{-1}]$ is linked to the resistance of the sludge cake to detachment. This latter mechanism is of course influenced initially by $J_{air}[m^3/m^2d]$, but also by the mass of the cake. With an increasing attached mass, detachment becomes more likely and is represented by a

'Monod law'-like equation, i.e. a monotone law with saturation (saturation occurrence being adjusted by the half-saturation coefficient K_{air}). This model structure guarantees that the cake mass will never reach negative values, which is indeed physically impossible. This time-scale dynamic compared to the other dynamics of the process can be understood as an instantaneous behavior (see Section 3.2.1 for further explanation).

The irreversible resistance R_{irrev} $[m^{-1}]$ is proportional to the amount of total permeate produced between two chemical cleaning procedures and is computed through specific irreversible fouling resistance in terms of the filtrate volume (ρ_{irrev} $[m^{-2}]$), proposed by Di Bella et al (2008).

$$R_{irrev} = \rho_{irrev} \sum \frac{Q_{out}}{A} t_f \tag{2.13}$$

where t_f $[d]$ is the duration of the filtration period.

Having proposed a membrane filtration model, the biological activity is described using a simple chemostat model (Smith and Waltman, 1995), involving one biomass growing on a limiting substrate, equation (2.14). It is important to highlight that this simple biological model structure can be easily extended to more than one biological reaction, see for instance Dochain and Vanrolleghem (2001). However, adding details and complexity will make model calibration more delicate and reduce model suitability to control purposes.

$$\begin{cases} \dfrac{dS}{dt} = -\dfrac{1}{Y}\mu(S)X + \dfrac{Q_{in}}{V}(S_{in} - S) & \text{(2.14a)} \\ \dfrac{dX}{dt} = \left(\mu(S) - \dfrac{Q_w}{V}\right)X + \dfrac{Q_{in}}{V}X_{in} - \dfrac{Q_{out}}{V}X + \dfrac{J_{air}}{V}\mu_{air}(m)m & \text{(2.14b)} \end{cases}$$

Equation (2.14a) represents the consumption of the substrate by the free biomass, ruled by a Monod-law $\mu(S) = \mu_{S,max}\frac{S}{K_S+S}$, and the transportation of incoming and outgoing substrate through the tank. Note that the substrate is not affected by the membrane, knowing that only solid matter is retained.

Equation (2.14b) shows that there is an interaction between the suspended solid and cake build-up. The first part of the equation represents the growth of the free biomass that consumes the substrate. Material transportation involves the cake attachment by $\frac{-Q_{out}X}{V}$ and detachment and the instantaneous "conversion" in suspended solids by the air cross-flow $+\frac{J_{air}}{V}\mu_{air}(m)m$. The free particle matter is transformed in sludge cake and vice-versa depending on the

process input values. The waste flow is represented by Q_w and the influent is defined as $Q_{in} = Q_w + Q_{out}$. The biological time-scale is governed by the consumption rate of substrate and, consequently, the growth of biomass. This rate is represented by a Monod-law equation ($\mu(S)$) and is normally measured in days.

The water treatment processes are normally operated in a continuous mode, thus the long-term evolution of the cake is observed and can be modeled by

$$\frac{d\beta}{dt} = \gamma\beta \tag{2.15}$$

The parameter β $[m^{-1}]$ represents the ease (or difficulty) of detaching the sludge cake from the membrane using an air cross-flow. In a process with constant trans-membrane pressure, the permeate flow decreases with time, hence β increases and $\gamma[d^{-1}]$ is positive, thus signifying the efficiency of J_{air} increases as a consequence of the loss of the drag force of the membrane to the particle deposition. In contrast, if the process has constant permeate flow, the capacity of J_{air} to detach the cake decreases, β decreases, thus γ has a negative value. This phenomenon can also be related to the cake compression coefficient proposed by Li and Wang (2006). It is important to highlight that this phenomenon has a long-term behavior, which is observed on a time-scale depending on the following process cycles: permeate cycle (Q_{out} is considered as a positive and constant value), relaxation cycle (where the air cross-flow is maintained constant and the permeate flow is zero, resulting in a zero trans-membrane pressure), and backwash cycle (Q_{out} flow is reversed to force the particles detachment). This evolution is normally measured in weeks or months (Merlo et al, 2000).

Regrouping the previous equations, the integrated model is represented by equation (2.16), where β, S, X and m are always positive and bounded (properties that are linked to the biological and physical phenomena that rule the process).

$$\begin{cases} \dfrac{d\beta}{dt} = \gamma\beta & \text{(2.16a)} \\ \dfrac{dS}{dt} = -\dfrac{1}{Y}\mu(S)X + \dfrac{Q_{in}}{V}(S_{in} - S) & \text{(2.16b)} \\ \dfrac{dX}{dt} = \left(\mu(S) - \dfrac{Q_w}{V}\right)X + \dfrac{Q_{in}}{V}X_{in} - \dfrac{Q_{out}}{V}X + \dfrac{J_{air}}{V}\mu_{air}(m)m & \text{(2.16c)} \\ \dfrac{dm}{dt} = Q_{out}X - J_{air}\mu_{air}(m)m & \text{(2.16d)} \end{cases}$$

$$\text{with } \mu(S) = \mu_{S,max}\frac{S}{K_S + S}\ , \quad \mu_{air}(m) = \beta\frac{m}{K_{air} + m}$$

Note that the model can be extended for process with more species and substrate without great effort.

The model (2.16) may be extended to other process cycles such as idle/relaxation and backwash cycles. The cycles can differ by the trans-membrane pressure values. The permeate cycle is considered when TMP is negative (suction); the idle cycle is considered when it is zero, and the backwash cycle when it is positive.

A simplified sMBR model including a model of the cake formation, and a simple biological model based on the growth of a single biomass on a limiting substrate, has been proposed. In the next chapter, model properties are studied and comparison with more detailed models and experimental data are carried out in order to show that a model with few parameter is sufficient to model the may dynamics of an sMBR process.

Chapter 3

Analysis, Parameter Identification & Simulation

3.1 Introduction

In order to better understand a water treatment plant behavior and its interconnections, many different procedures, such as bench tests and long laboratories tests, should be performed. This is time consuming due to the process slow behavior, and some experiments may turn into a risky procedure as result of the biological washout from the bioreactor. In Section 2.5, a general model has been proposed to mimic the water treatment process. To extract the potential knowledge intrinsically designed in the model, an analytical analysis is carried out followed by parameter identification and model simulations designed to process cognition. These insights will be applied to experimental data in Chapter 4.

3.2 Full Model Analysis

The developed model has been designed in order to have a low complex structure and to maintain the physical and biological aspects of the parameters. These advantages are straightforward when the dynamic model (equation (3.1)) is analyzed. The first conduct is addressed to study the process time-scales by a fast and slow dynamics method.

$$\begin{cases} \dfrac{d\beta}{dt} = \gamma\beta & \text{(3.1a)} \\ \dfrac{dS}{dt} = -\dfrac{1}{Y}\mu(S)X + \dfrac{Q_{in}}{V}(S_{in} - S) & \text{(3.1b)} \\ \dfrac{dX}{dt} = \left(\mu(S) - \dfrac{Q_w}{V}\right)X + \dfrac{Q_{in}}{V}X_{in} - \dfrac{Q_{out}}{V}X + \dfrac{J_{air}}{V}\mu_{air}(m)m & \text{(3.1c)} \\ \dfrac{dm}{dt} = Q_{out}X - J_{air}\mu_{air}(m)m & \text{(3.1d)} \end{cases}$$

$$\text{with } \mu(S) = \mu_{S,max}\frac{S}{K_S + S}\ , \quad \mu_{air}(m) = \beta\frac{m}{K_{air} + m}$$

3.2.1 Fast and Slow Dynamics

In Section 2.5, the sMBR model has been characterized and the three different time-scales have been deduced from the process behavior: the sludge cake attachment and detachment, the biology and the cake long-term evolution.

To take advantage of this hypothesis, the singular perturbation approach is used. The presence of a small parameter in the description of the dynamic model that can (regular perturbation) or cannot (singular perturbation) be approximated by putting the small parameter to zero, reveals the possibility of model reduction in smaller dimension (Kokotović et al, 1986; Saksena et al, 1984). The simultaneous occurrence of fast and slow phenomena contribute to complex dynamics, stiffness of the model and computational effort for simulation. Detecting the different time-scales results in reduced models, where the slowest phenomenon is the dominant dynamic. This can be understood as an inner and outer process loop. The fast dynamic, also named a boundary layer, represents the deviation from the predicted slow behavior. This approach is considered in more detail in the framework of singular perturbations.

3.2.1.1 Singular Perturbations

The mathematical tool used to deal with the different time-scales is Tikhonov's theorem which allows reducing the complexity of the system through suitable approximations (Khalil, 2002). A fast-slow system is in singular perturbation form when it can be expressed using suitable coordinates, so as to distinguish two subsystems with a small positive parameter ϵ.

$$\begin{cases} \dot{x} = f(t, x, z, \epsilon) \\ \epsilon \dot{z} = g(t, x, z, \epsilon) \end{cases} \tag{3.2}$$

The function f and g are continuously differentiable in their arguments for $(t, x, z, \epsilon) \in [0, t_1] \times D_x \times D_z \times [0, \epsilon_0]$, where $D_x \subset \mathbb{R}^n$ and $D_z \subset \mathbb{R}^m$ are open connected sets. Considering $\epsilon = 0$ in (3.2), the dimension of the state equation reduces from $n+m$ to n because the differential equation degenerates into the algebraic equation.

$$0 = g(t, x, z, 0) \tag{3.3}$$

It is assumed that (3.3) admits $k \geq 1$ isolated real roots

$$z = h_i(t, x), \ i = 1, 2, ..., k \tag{3.4}$$

defined by $(t, x) \in [0, t_1] \times D_x$. This assumption ensures that a well-defined $n-$dimensional reduced model will correspond to each root of (3.3). To obtain the i^{th} reduced model, equation (3.4) has to be substituted into (3.2), at $\epsilon = 0$, to obtain

$$\dot{x} = f(t, x, h_i(t, x), 0) \tag{3.5}$$

It will be clear from the context which root of (3.3) is used. This model is sometimes called a *quasi-steady-state model*, because z, whose velocity $\dot{z} = g/\epsilon$ can be large when ϵ is small and $g \neq 0$, may rapidly converge to a root of (3.3), which is the equilibrium of (3.2). Equation (3.5) is called the slow dynamics of the model (Sari, 2005).

3.2.1.2 Three-time-scale Singular Perturbation

In the previous subsection, fast and slow theory is recalled considering two time-scales. In the sMBR model, three time-scales can be identified: the sludge cake attachment is considered as the ultrafast time-scale, the free biomass growth and substrate consumption as the fast time-scale, and the evolution of the sludge cake as the slow time-scale resulting in the following generic representation:

$$\begin{cases} \frac{d\beta}{dt} = \gamma\beta & \longrightarrow \dot{x}_{sl} \\ \frac{dS}{dt} = -\frac{1}{Y}\mu(S)X + \frac{Q_{in}}{V}(S_{in} - S) & \longrightarrow \dot{y_1} \\ \frac{dX}{dt} = (\mu(S) - \frac{Q_w}{V})X + \frac{Q_{in}}{V}X_{in} - \frac{Q_{out}}{V}X + \beta\frac{J_{air}}{V}\frac{m^2}{K_{air}+m} & \longrightarrow \dot{y_2} \\ \frac{dm}{dt} = Q_{out}X - \beta J_{air}\frac{m^2}{K_{air}+m} & \longrightarrow \dot{z} \end{cases} \tag{3.6}$$

where x_{sl} is the slow state variable, y the fast state variable, and z the ultrafast state variable. The small parameters are assumed to be $\epsilon_1 = |\gamma|$ and $\epsilon_2 = \frac{1}{V}$.

Hypothesis 3.2.1. *γ is small.*

Hypothesis 3.2.2. *The volume V is large, with $V < \frac{1}{|\gamma|}$.*

The application of the procedure introduced in the previous subsection therefore yields:

First: The stretched time-scale $\tau_1 = \epsilon_1 t \longrightarrow \frac{1}{dt} = \frac{\epsilon_1}{d\tau_1}$

$$\frac{dx_{sl}}{d\tau_1} = sign(\gamma)x_{sl} \qquad (Slow)$$

$$\epsilon_1\frac{dy_1}{d\tau_1} = g_1(y_1, y_2) = -\frac{1}{Y}\mu(y_1)y_2 + \frac{Q_{in}}{V}(S_{in} - y_1) \qquad (Fast)$$

$$\epsilon_1\frac{dy_2}{d\tau_1} = g_2(x_{sl}, y_1, y_2, z) = \mu(y_1)y_2 + \frac{Q_{in}}{V}X_{in} - \frac{Q_{in}}{V}y_2 + x_{sl}\frac{J_{air}}{V}\frac{z^2}{K_{air}+z} \qquad (Fast)$$

$$\epsilon_1\frac{dz}{d\tau_1} = h(x_{sl}, y_2, z) = Q_{out}y_2 - x_{sl}J_{air}\frac{z^2}{K_{air}+z} \qquad (Fast)$$

$$0 = g_1(y_1, y_2) \tag{3.7}$$

$$0 = g_2(x_{sl}, y_1, y_2, z) \tag{3.8}$$

Based on the three fast equations, the solution of y_1 and y_2 are computed as if x_{sl} is constant (quasi-state approximation of the first equation).

$$\begin{cases} \mu(y_1)y_2 = Y\frac{Q_{in}}{V}(S_{in} - y_1) & \text{(3.9a)} \\ \mu(y_1)y_2 = \frac{Q_{in}}{V}(y_2 - X_{in}) - \frac{x_{sl}J_{air}z^2}{V(K_{air}+z)} & \text{(3.9b)} \\ \frac{x_{sl}J_{air}z^2}{V(K_{air}+z)} = Q_{out}y_2 & \text{(3.9c)} \end{cases}$$

Applying equation (3.9a) and (3.9c) into equation (3.9b)

$$\frac{Q_{in}}{V}(y_2 - X_{in}) - \frac{Q_{out}y_2}{V} = \Upsilon\frac{Q_{in}}{V}(S_{in} - y_1) \tag{3.10}$$

The solution of y_2 can be computed as follows:

$$y_2 = \frac{Q_{in}(\Upsilon S_{in} + X_{in} - \Upsilon y_1)}{Q_{in} - Q_{out}} \tag{3.11}$$

Applying equation (3.11) to (3.9a), considering $Q_w = Q_{in} - Q_{out}$ and letting $\bar{S}_{in} = S_{in} + \frac{X_{in}}{\Upsilon} > S_{in}$ the following equation can be written:

$$\mu(y_1) = \frac{\Upsilon Q_w(S_{in} - y_1)}{V(\Upsilon S_{in} + X_{in} - \Upsilon y_1)}, \tag{3.12}$$

or equivalently

$$\mu(y_1) = g(y_1) = \frac{Q_w}{V}\frac{S_{in} - y_1}{\bar{S}_{in} - y_1} \tag{3.13}$$

The uniqueness of y_1 and y_2 can be prove as follows: considering $\bar{S}_{in} > S_{in}$, $g(\cdot)$ is a decreasing concave function defined on $]0, \bar{S}_{in}[$ and on $]\bar{S}_{in}, +\infty[$, $g(\cdot)$ is equal to zero for $y_1 = S_{in}$ and is positive for $S \notin (S_{in}, \bar{S}_{in})$. Furthermore, it has $\lim_{y_1 \to \bar{S}_{in}^-} g(y_1) = -\infty$ and $\lim_{y_1 \to \bar{S}_{in}^+} g(y_1) = +\infty$. The sketch of function $g(\cdot)$ is represented in Figure 3.1.

The following cases occur:

- $\exists!$ solution of $\mu(y_1) = g(y_1)$ on $]0, \bar{S}_{in}[$ (this is such that $y_1 < S_{in}$);
- $\exists$ solution of $\mu(y_1) = g(y_1)$ on $]\bar{S}_{in}, +\infty[$ when $\mu_{S,max} > \frac{Q_w}{V}$; but the solution $y_1 > \bar{S}_{in} \Rightarrow y_2 < 0$ is not physically possible.

Based on these statements it is possible to conclude that there exists necessarily a solution (y_1, y_2) and it is unique on $\mathbb{R}^+ \times \mathbb{R}^+$.

An approximation of y_1 may be obtained, when using the function $\mu(y_1)$ as a Monod function $\mu(y_1) = \mu_{S,max}\frac{y_1}{K_S + y_1}$ and applying (3.12), it results in the following polynomial:

$$y_1^2\left(\Upsilon(Q_w - V\mu_{S,max})\right) + y_1\left((V\mu_{S,max}(\Upsilon S_{in} + X_{in}) - \Upsilon Q_w(S_{in} - K_S))\right) - (\Upsilon Q_w S_{in} K_S) = 0$$

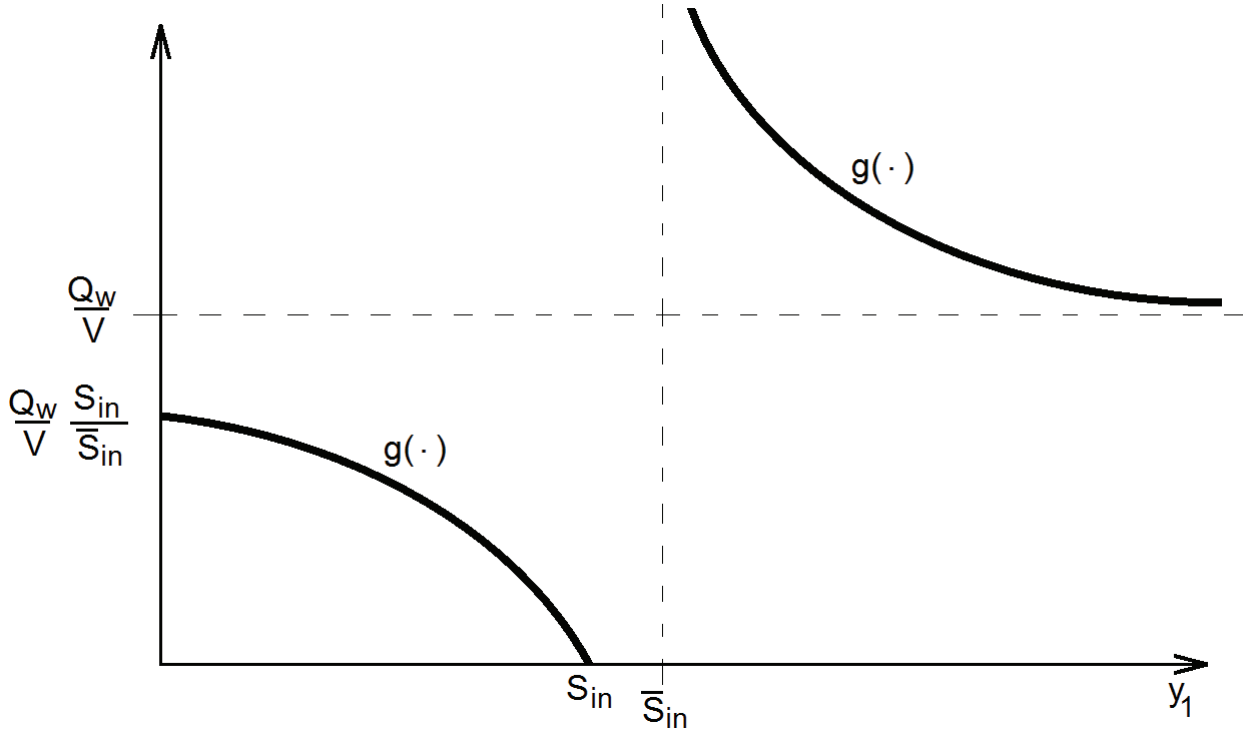


Figure 3.1: Evolution of function g related to y_1.

Considering V as a large value, the solution y_1 of the last polynomial can be approximated by the solution of:

$$y_1^2 \mu_{S,max} - y_1 \mu_{S,max} \bar{S}_{in} + \frac{Q_w S_{in} K_S}{V} = 0$$

that belongs to $]0, S_{in}[$ which is:

$$y_1 = \frac{\mu_{S,max}\bar{S}_{in} - \sqrt{\mu_{S,max}^2 \bar{S}_{in}^2 - \frac{4Q_w S_{in} K_S}{V}}}{2\mu_{S,max}} \tag{3.14}$$

$$= \frac{\bar{S}_{in}}{2}\left(1 - \sqrt{1 - \frac{4Q_w S_{in} K_S}{V \bar{S}_{in}^2 \mu_{S,max}}}\right) \tag{3.15}$$

$$\sim \frac{\bar{S}_{in}}{2}\left(\frac{2Q_w S_{in} K_S}{V \bar{S}_{in}^2 \mu_{S,max}}\right) \tag{3.16}$$

$$\sim \frac{Q_w S_{in} K_S}{V \bar{S}_{in} \mu_{S,max}} \tag{3.17}$$

When V is large y_2 can be approximated by $y_2 \simeq \frac{Q_{in}}{Q_w} Y \bar{S}_{in}$ from equation (3.11).

Second: The stretched time-scale $\tau_2 = \epsilon_2 \tau_1 = \epsilon_2 \epsilon_1 t \longrightarrow \frac{1}{d\tau_1} = \frac{\epsilon_2}{d\tau_2}$ and x_{sl} is constant.

$$\epsilon_1 \frac{dy_1}{d\tau_2} = -\frac{1}{Y\epsilon_2}\mu(y_1)y_2 + Q_{in}(S_{in} - y_1) \qquad (Fast)$$

$$\epsilon_1 \frac{dy_2}{d\tau_2} = \left(\frac{\mu(y_1)}{\epsilon_2} - Q_w\right) y_2 + Q_{in}X_{in} - Q_{out}y_2 + x_{sl}J_{air}\frac{z^2}{K_{air}+z} \qquad (Fast)$$

$$\epsilon_2\epsilon_1 \frac{dz}{d\tau_2} = h(x_{sl}, y_2, z) = Q_{out}y_2 - x_{sl}J_{air}\frac{z^2}{K_{air}+z} \qquad (Ultrafast)$$

$$0 = h(x_{sl}, y_2, z) \longrightarrow z \simeq \frac{\frac{Q_{out}Q_{in}Y\bar{S}_{in}}{Q_w} + \sqrt{Q_{out}^2\left(\frac{Q_{in}Y\bar{S}_{in}}{Q_w}\right)^2 + 4\frac{Q_{out}Y\bar{S}_{in}K_{air}J_{air}x_{sl}Q_{in}}{Q_w}}}{2x_{sl}J_{air}} \qquad (3.18)$$

Note that these approximations show that y_1 and y_2 do not depend on x_{sl}, while z do depend. The analytical analysis points out the three time-scales of the process and this characteristic is used to model analysis and for the parameter identification procedure, and is finally validated by experimental data from two different processes in Chapter 4.

3.2.2 Asymptotic Analysis

The filtration process is an unstable process by nature, since solid matter continuously accumulates in an irreversible manner (see the dynamic of β in equation (3.1)), but it is possible to analyze it on a short time span t, where the process could be considered non evolving. Analyzing the process in this period, the long-term evolution of the cake is neglected (i.e. it is considered constant). Based on a fast and slow dynamics study, the coupling of the system is simplified and thus when the equilibrium points of S and X are computed, m is considered constant, and reversely, when m is computed, S and X are considered constant. This helps in determining the biomass and reversible layer equilibrium points that are strongly coupled.

3.2.3 Study of the Linearized Dynamics - Short-term

In this section relations of the process actuators are presented and a short-term analysis is presented. A particular case where $X_{in} = 0$ and the trans-membrane pressure is constant, the effluent flow is computed as follows:

$$Q_{out}(m) = A\frac{TMP}{\eta\left(R_m + \rho_{rev}\frac{m+m_0}{A}\right)}. \qquad (3.19)$$

The dynamic model of this particular case is expressed in equation (3.20).

$$\begin{cases} \dfrac{dS}{dt} = -\dfrac{1}{Y}\mu(S)X + \dfrac{Q_{in}}{V}S_{in} - \dfrac{Q_w}{V}S - \dfrac{Q_{out}(m)}{V}S & \text{(3.20a)} \\ \dfrac{dX}{dt} = \left(\mu(S) - \dfrac{Q_w}{V}\right)X - \dfrac{Q_{out}(m)}{V}X + \dfrac{J_{air}}{V}\mu_{air}(m)m & \text{(3.20b)} \\ \dfrac{dm}{dt} = Q_{out}(m)X - J_{air}\mu_{air}(m)m & \text{(3.20c)} \end{cases}$$

$$\text{with } \mu(S) = \mu_{S,max}\frac{S}{K_S + S}\ , \quad \mu_{air}(m) = \beta\frac{m}{K_{air} + m}$$

The positive equilibrium point is given by $\bar{S} = \frac{Q_w K_S}{V\mu_{S,max} - Q_w}$, $\bar{X} = \frac{J_{air}\mu_{air}(\bar{m})\bar{m}}{Q_{out}(\bar{m})}$ and $\bar{m}$ is the solution of $Q_w\bar{X} = Y(Q_{in}S_{in} - Q_w\bar{S} - Q_{out}(m)\bar{S})$. Considering $Q_{out}(\bar{m}) = A\frac{TMP}{\eta\left(R_m + \rho_{rev}\frac{\bar{m}+m_0}{A}\right)}$ and $Q'_{out}(\bar{m}) = A\frac{TMP}{\left(\frac{\eta\rho_{rev}}{A}\right)^2}$, the Jacobian matrix is given by the following expression:

$$\begin{bmatrix} -\frac{1}{Y}\mu'(\bar{S})\bar{X} - \frac{Q_w}{V} - \frac{Q_{out}(\bar{m})}{V} & -\frac{1}{Y}\mu(\bar{S}) & -\frac{Q'_{out}(\bar{m})}{V}\bar{S} \\ \mu'(\bar{S})\bar{X} & -\frac{Q_w}{V} - \frac{Q_{out}(\bar{m})}{V} & -\frac{Q'_{out}(\bar{m})}{V}\bar{X} + \beta\frac{J_{air}}{V}\left(\frac{2\bar{m}(K_{air}+\bar{m}) - \bar{m}^2}{(K_{air}+\bar{m})^2}\right) \\ 0 & Q_{out}(\bar{m}) & Q'_{out}(\bar{m})\bar{X} - \beta J_{air}\left(\frac{2\bar{m}(K_{air}+\bar{m}) - \bar{m}^2}{(K_{air}+\bar{m})^2}\right) \end{bmatrix}$$

Its eigenvalues have been computed numerically to check that this matrix is Hurwitz for the positive equilibrium and unstable for the washout equilibrium.

This strategy is empirically used by the sMBR operators that change permeate flux (i.e. directly changing sludge cake mass (m) attachment (see equation (3.1d)) and air cross-flow set-points to reach an equilibrium point resulting in a constant cake mass. The Jacobian matrix computation is only valid on a short-term basis, when the long-term cake evolution phenomenon can be neglected.

Figure 3.2 shows the variation of sludge cake formation m and the permeate flow $Q_{out}(m)$ for different trans-membrane pressure values. If the trans-membrane pressure increases the cake formation increases, but permeate flow decreases. The same behavior is observed in Di Bella et al (2008) and Sarioglu et al (2012).

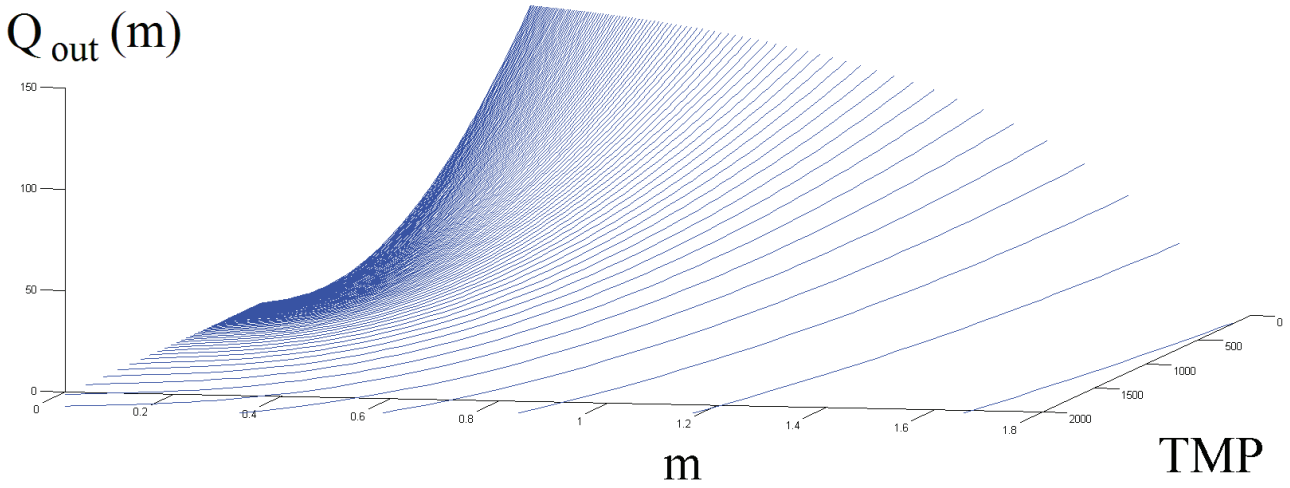


Figure 3.2: Relation between fouling, trans-membrane pressure and ϕ.

3.2.4 Observability

The sMBR model observability study based on the Strictly Linked Lower Hessenberg System method is carried out taking the substrate S measurements into account.

The *Strictly Linked Lower Hessenberg System* method is introduced by letting $\mathcal{U}$ be an open set of $\mathbb{R}^n$ and $\mathcal{U}$ the set of admissible control. The set of admissible controls $\mathcal{U}$ is a subset of the space of measurable bounded functions $u : [0, T_u[\rightarrow U$ (Bernard et al, 1998).

A differential system (Σ) is defined on a domain $\Omega \subset \mathbb{R}^n$

$$(\Sigma) = \begin{cases} \dot{x}(t) &= F(x(t), u(t)) \\ y(t) &= h(x(t)) \\ x(0) &= x_0, u \in \mathcal{U} \end{cases} \quad \text{where } F \text{ is a smooth function } \mathbb{R}^n \times \mathbb{R}^m \rightarrow \mathbb{R}^n$$

and h the observation function is also supposed to be smooth $\mathbb{R}^n \rightarrow \mathbb{R}^p$

Definition 3.2.1. *(Lower Hessenberg System): Considering* (Σ) *as a Lower Hessenberg (LH) system, for any* $(x, u) \in \Omega \times U$*, and for any indexes* (i, j) *with* $j > (i + 1)$

$$\frac{\partial F_i}{\partial x_j}(x, u) = 0. \tag{3.21}$$

Remark 1. *This definition simply determines that the Jacobian of* F*,* $\frac{\partial F}{\partial x}$ *is a Lower Hessenberg Matrix for any input* u *(considered as a constant input).*

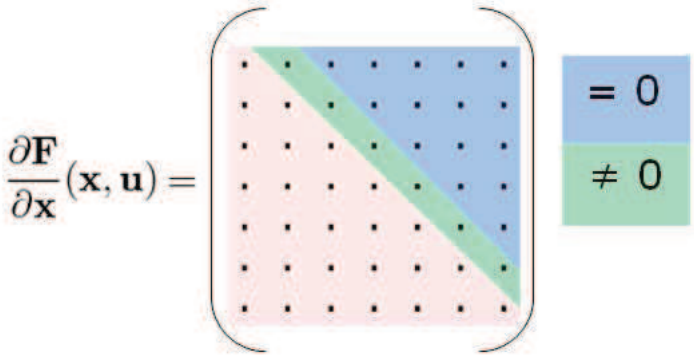


Figure 3.3: Strictly Linked Lower Hessenberg System (SL_2H). Adapted from Mailier et al (2010)

.

Definition 3.2.2. *(Strictly Linked Lower Hessenberg): A system* (Σ) *is a Strictly Linked Lower Hessenberg* (SL_2H) *if it is LH and for any* $(x, u) \in \Omega \times U$ *and for any index* i

$$\frac{\partial F_i}{\partial x_{i+1}}(x, u) \neq 0. \tag{3.22}$$

Definition 3.2.3. *(U M S* L_2H *System): An* SL_2H *system* $(\sum)$ *is called Upper Measured (U M S* L_2H*) if any* $x \in \Omega$ *has* $h(x) = h(x_1)$*, with* $\partial h/\partial x_1 \neq 0$.

Figure 3.3 summarizes the definitions.

Proposition 3.2.1. *Any (U M S* L_2H *System) is observable on* Ω *for any input* $u(\cdot) \in \mathcal{U}$.

3.2.4.1 SL_2H applied to sMBR Model

In order to test process observability, it is considered that the substrate concentration (S) is measured and the model is rewritten considering ($x_1 = S$, $x_2 = X$ and $x_3 = m$).

$$\begin{cases} \dot{x}_1 = -\frac{1}{Y}\mu(x_1)x_2 + \frac{Q_{in}}{V}(S_{in} - x_1) \\ \dot{x}_2 = \left(\mu(x_1) - \frac{Q_w}{V}\right)x_2 + \frac{Q_{in}}{V}X_{in} - \frac{Q_{out}}{V}x_2 + \frac{J_{air}}{V}\mu_{air}(x_3)x_3 \\ \dot{x}_3 = Q_{out}x_2 - J_{air}\mu_{air}(x_3)x_3 \\ h(t) = x_1 \end{cases} \tag{3.23}$$

Equations (3.23) represent the states of the system:

$$\begin{cases} \dot{x}_1(t) = f_1(x_1, x_2) \\ \dot{x}_2(t) = f_2(x_1, x_2, x_3) \\ \dot{x}_3(t) = f_3(x_2, x_3) \\ h(t) = x_1(t) \end{cases} \tag{3.24}$$

The three partial computed derivatives must have the following structure:

$$\frac{\partial f_1}{\partial x_2} \neq 0 \tag{3.25}$$

(3.26)

$$\frac{\partial f_1}{\partial x_3} = 0 \tag{3.27}$$

(3.28)

$$\frac{\partial f_2}{\partial x_3} \neq 0 \tag{3.29}$$

Applying it to equation (3.23)

$$\frac{\partial f_1}{\partial x_2} = -\frac{\mu_{S,max}}{Y}\frac{x_1}{(x_1+K_S)} \tag{3.30}$$

$$\frac{\partial f_1}{\partial x_3} = 0 \tag{3.31}$$

$$\frac{\partial f_2}{\partial x_3} = \left(\frac{2J_{air}\beta x_3}{V(K_{air}+x_3)}\right) - \left(\frac{J_{air}\beta x_3^2}{V(K_{air}+x_3)^2}\right) \tag{3.32}$$

This shows that the system is observable by measuring $x_1(t)$.

3.2.5 Controllability

The study of controllability is important in order to understand in which way the process behavior can be influenced through certain inputs. According to Slotine and Li (1991), one of the most used mathematical tools for nonlinear systems is the *Lie Brackets*, represented as follows:

Assuming Q_{out} and J_{air} are the manipulated variables and rewriting system (3.1) in the following form

$$\dot{\mathbf{x}} = \mathbf{f}(\mathbf{x}) + \mathbf{g}(\mathbf{x})u \tag{3.33}$$

Definition 3.2.4. *Let* $\mathbf{f}$ *and* $\mathbf{g}$ *be two vector fields on* $\mathbb{R}^n$. *The* Lie Brackets *of* $\mathbf{f}$ *and* $\mathbf{g}$ *is a third vector field defined by*

$$[\mathbf{f},\ \mathbf{g}] = \nabla\mathbf{g}\ \mathbf{f} - \nabla\mathbf{f}\ \mathbf{g} \tag{3.34}$$

It can be defined as $(ad^1_{\mathbf{f}}) \equiv [\mathbf{f}, \mathbf{g}]$ where "*ad*" means "*adjoint*".

Theorem 1. *The system defined by:*

$$\dot{\mathbf{x}} = \mathbf{f}(\mathbf{x}) + \sum_{i=1}^{m} \mathbf{g}_i(\mathbf{x})u_i \tag{3.35}$$

is locally accessible at about x_0 *if the accessibility distribution* C *spans an* n *space, where* n *is the rank of* $\mathbf{x}$ *and* C *is defined as follows:*

$$C = \left[g_1, g_2, \ldots, g_m, [g_i, g_j], \ldots, [ad^k_{g_i}, g_j], \ldots, [f, g_i], \ldots, [ad^k_f, g_i], \ldots\right]$$

The system is therefore controllable.

3.2.5.1 *Lie Brackets* Applied to sMBR Model

Considering the long-term fouling evolution null, the proposed model (equation (3.1)) can be rewritten as follows:

$$\dot{\mathbf{x}} = \underbrace{\begin{bmatrix} -\frac{1}{Y}\mu(S) + \frac{Q_{in}}{V}(S_{in} - S) \\ (\mu(S) - \frac{Q_w}{V})X + \frac{Q_{in}}{V}X_{in} \\ 0 \end{bmatrix}}_{\mathbf{f}(\mathbf{x})} + \underbrace{\begin{bmatrix} \frac{(S_{in}-S)}{V} \\ -\frac{X}{V} \\ X \end{bmatrix}}_{\mathbf{g}_1(\mathbf{x})} Q_{out} + \underbrace{\begin{bmatrix} 0 \\ \frac{\mu_{air}(m)m}{V} \\ -\mu_{air}(m)m \end{bmatrix}}_{\mathbf{g}_2(\mathbf{x})} J_{air}, \tag{3.36}$$

$$[ad_f, g_1] = \begin{bmatrix} \left(\frac{-2X\mu(S)}{VY}\right) \\ -\frac{X\left(Q_{out} + J_{air}V\mu_{air}(m)\right)}{V^2} \\ X\left(\mu(S) + J_{air}\mu_{air}(m)\right) + \frac{Q_{in}}{V}X \end{bmatrix} \text{ and} \tag{3.37}$$

$$[ad_f, g_2] = \begin{bmatrix} \frac{m\mu_{air}(m)\mu(S)}{VY} \\ \frac{\mu_{air}(m)mQ_{in} - Vm\mu_{air}(m)(\mu(S) - J_{air}\mu_{air}(m)}{V^2} \\ \frac{-m\mu_{air}(m)(Q_{out} + J_{air}V\mu_{air}(m))}{V} \end{bmatrix}. \tag{3.38}$$

Applying Theorem 1, results in

$$\mathbf{C} = \begin{bmatrix} g_1 & g_2 & [ad_f, g_2] & [ad_f, g_2] \end{bmatrix}.$$

The **C** matrix has full rank which results in a controllable system for Q_{out} and J_{air} as process actuators.

3.3 Biological Aspect Simulations and Analysis

3.3.1 Global Stability Study

In the previous section the local stability of the system is presented. In this section, the biological global stability of the process is studied using the Poincarè-Bendixson Theorem and assuming the ideal behavior of the membrane. The ideal membrane retains all the solids inside the tank with no pressure limitation, where the fouling formation is not taken into account. Bearing this in mind, the sMBR model is simplified as represented in Figure 3.4. To maintain a constant volume in the tank the Q_w and Q_{out} should be related to the inflow rate. Thus $Q_w = \alpha Q_{in}$ and $Q_{out} = \phi Q_{in}$, where $\alpha + \phi = 1$. In order to simplify the study, the volume of the tank is 1 m^3.

$$\begin{aligned} \frac{dS}{dt} &= -\frac{1}{Y}\mu(S) + \frac{Q_{in}}{V}(S_{in} - (\alpha + \phi)S) \\ \frac{dX}{dt} &= (\mu(S) - \alpha\frac{Q_{in}}{V})X \end{aligned}$$

ϕ is the permeate flux factor and α is the withdrawal factor see Figure 3.4.

Figure 3.5 shows the system *nullclines* and the vector fields. The sMBR model, as the classical chemostat model, comprises two equilibrium points. One for the system washout ($X = 0$) and the other is *nullcline* intersections.

The arrows in Figure 3.5 show the trajectory of the system until it reaches stability. Both equilibrium points are stable and do not have *limit cycles* as

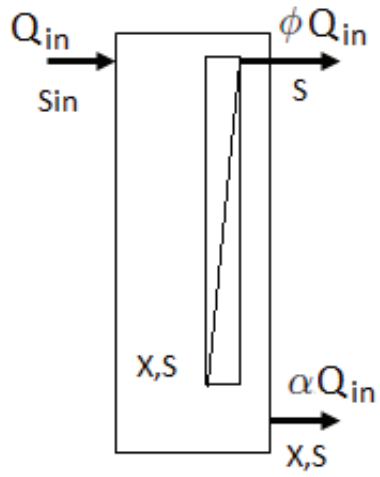


Figure 3.4: Bioreactor with membrane, ϕ is the permeate flux factor and α is the withdrawal of the biomass factor.

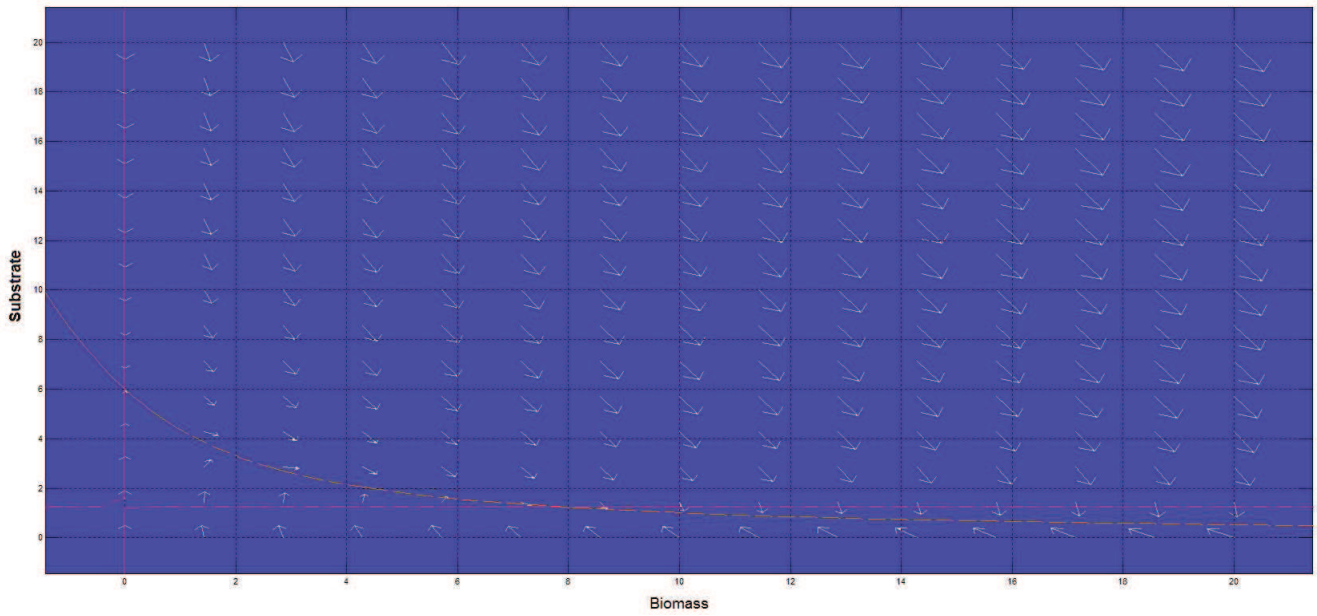


Figure 3.5: Nullcline Arrows PPlane. $Q_{in} = 1.1$, $S_{in} = 6$, $\alpha = 0.4$, $\phi = 0.6$, $K_S = 10$, $Y = 0.67$ and $\mu_{S,max} = 4$. The nullcline orange is the substrate and the violet is the biomass

confirmed when applying the Poincarè-Bendixson Theorems 2 and 3. Thus, it is possible to conclude that the process is globally asymptotically stable.

Theorem 2. *(Poincarè-Bendixson Theorem)(Perko, 1991)*
Variation 1: *If region $\mathcal{D}$ is bounded in the plane that contains a single repelling steady-state (unstable equilibrium) and into which flow enters but from which it does not exit, then the system possesses a periodic solution (represented by a closed orbit lying entirely inside $\mathcal{D}$)*

Theorem 3. *(Poincarè-Bendixson Theorem)(Perko, 1991)*
Variation 2: *If there is a bounded region that contains a single repelling steady-state, and within which all trajectories are trapped (i.e. cannot flow out), then the system contains limit cycles.*

3.4 Physical Aspect Simulation and Analysis

The physical part of the proposed model is analyzed using two well known models. The simulations have the trans-membrane pressure TMP constant with the value of 96 $mBar$. The first is based on the GPS-X software which was validated in practice by Sarioglu et al (2012). This model is represented by the equation (3.39), which uses the equation (3.40) to compute the sludge cake resistance.

$$\frac{dm_{GPS-X}}{dt} = q_{perm}x_{liq}f_{cap} - q_{bw}x_{cake}f_{bw} - \frac{q_{cross}}{A}\frac{x_{cake}}{x_{cake} + K_{S,cake}}f_{cross} \tag{3.39}$$

$$R_{cake,GPS-X} = \frac{180(1-\epsilon_p)m_{GPS-X}}{d_p^2\epsilon_p^3 A\rho_p} \tag{3.40}$$

The simulations are executed with a membrane surface area of $0.35m^2$ and a bioreactor size of 0.05 m^3. The inflow characteristics are the same for all models. The influent concentrations of the sMBR are identical to the Benchmark Simulation Model no.1 (BSM1) (S_i = 30 mg/L, S_s = 69.5 mg/L, X_i = 51.2mg/L, X_s = 202.32 mg/L, X_{bh} = 28.7 mg/L, X_{ba}, X_p, S_o, S_{no} = 0 mg/L, S_{nh} = 31.56 mg/L, S_{nd} = 6.95 mg/L, X_{nd} = 10.59 mg/L and S_{alk} = 7 mg/L), proposed by Alex et al (2008). Figure 3.6 shows the diagram block of GPS-X and Matlab/Simulink.

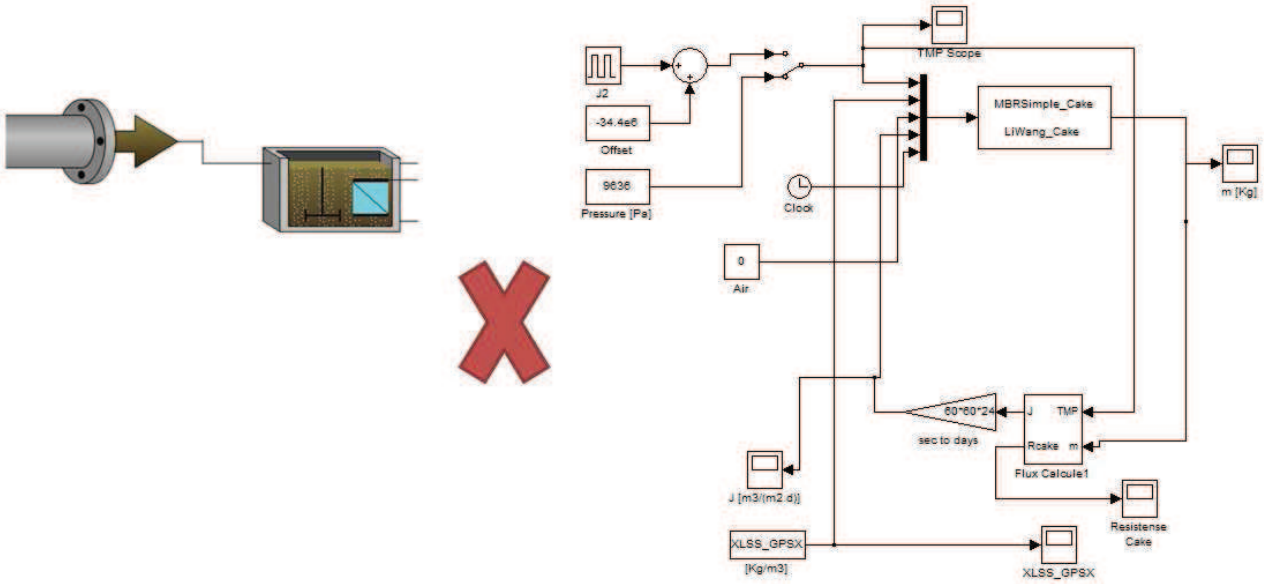


Figure 3.6: Comparison: left - GPS-X blocks. Right - proposed model and Li and Wang (2006) model.

The second model proposed by Li and Wang (2006) covers reversible and irreversible cake layer formation, pore blocking and the influence of the feed side hydrodynamics. A particular case of the model where only the sludge cake dynamic, equation (3.42) with sludge cake resistance (3.41) is taken into account.

$$R_{cake,LiWang} = R_{sc} + R_{dc} \tag{3.41}$$

where $R_{sc} = r_{sc} \cdot M_{sc}$ and $R_{dc} = r_{dc} \cdot M_{dc}$.

These expressions include M_{sc} $[kg/m^2]$ that denotes the stable sludge cake mass and M_{dc} $[kg/m^2]$ the dynamic sludge cake mass onto membrane surface.

$$\begin{cases} \dfrac{dM_{sc}}{dt} = \dfrac{24C_{ss}J^2}{24J + C_d d_p G} - \dfrac{\beta_b(1-\alpha_b)GM_{sc}^2}{\gamma_b V_f t + M_{sc}} & \text{(3.42a)} \\ \dfrac{dM_{dc}}{dt} = \dfrac{-\beta_b(1-\alpha_b)GM_{dc}^2}{0.1\gamma_b V_f t + M_{dc}} & \text{(3.42b)} \end{cases}$$

where C_{ss} $[kg/m^3]$ is the sludge concentration, C_d is the coefficient of the drag and lift force, $d_p[m]$ is the particle size, β_b is the erosion rate coefficient of the dynamic sludge film, α_b is the stickiness of the biomass particle, γ_b $[kg/m^3 s]$ is the compression coefficient for the dynamic sludge film, V_f is water production within a filtration period of an operation cycle, t $[d]$ is time and G $[s^{-1}]$ is

Table 3.1: Parameters of Li and Wang (2006) model, GPS-X and proposed model

Li & Wang	**GPS-X**	**Proposed Model**
$r_{sc} = 1.0 \times 10^{15}[m/kg]$	f_{cross} = default	$\beta_0 = 40000[m^{-1}]$
$\mu_w = 0.001[Pa\ s]$	$K_{S,cake}$ = default	$K_{air} = 50[g]$
$\gamma_b = 2.5 \times 10^{-5}[kg/(m^3\ s)]$	$\epsilon_p = 0.15[-]$	$m_0 = 0[g]$
$\beta_b = 3.5 \times 10^{-4}[-]$	$d_p = 1.0 \times 10^{-6}[m]$	$\rho_{rev} = 4.4 \times 10^{+13}[m/g]$
$\alpha_b = 0.5[-]$	$\rho_p = 1020[kg/m^3]$	
$d_p = 1 \times 10^{-6}[m]$		
$C_d = 1[-]$		
$K_1 = 4 \times 10^{-6}[-]$		
$\rho_w = 1000[kg/m^3]$		
$g = 9.81[m/s^2]$		

the shear intensity

$$G = \left(\frac{\rho_w g q_a}{1.05 \mu_w e^{0.08 C_{ss}}} \right)^{1/2} \tag{3.43}$$

where ρ_w and μ_w are the density and viscosity, respectively, of the sludge mixture, q_a is the air cross-flow and g is the gravitational constant.

The model proposed by Li and Wang (2006) and the GPS-X sMBR model are compared in a short time period with the proposed sludge cake fouling dynamic model

$$\frac{dm}{dt} = Q_{out} X - J_{air} \mu_{air}(m) m \tag{3.44}$$

with $R_{rev} = \rho_{rev} \frac{m+m_0}{A}$.

The parameters of each model are presented in Table 3.1.

Figure 3.7 reveals that the three dynamics are very similar when there is no air cross-flow.

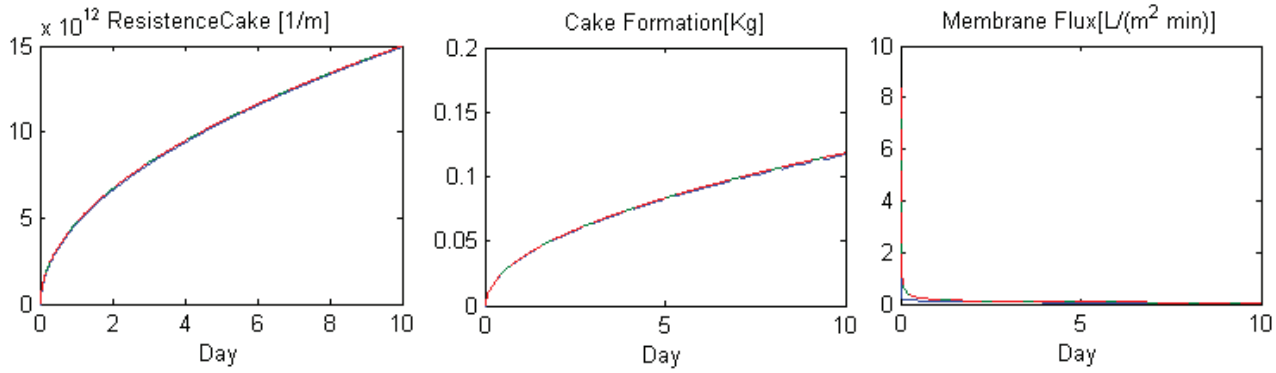


Figure 3.7: Comparision between the models. Blue: Li Model, Red: GPS-X model and Green:Proposed Model.

The same study taking the air cross-flow into account is proceeded. The simulations are divided into cycles with and without air cross-flow. Figure 3.8 shows the dynamics without air cross-flow until day seven; after that the air cross-flow is set, the resistance and cake formation decrease and the membrane flux increases. The simulation results are very similar.

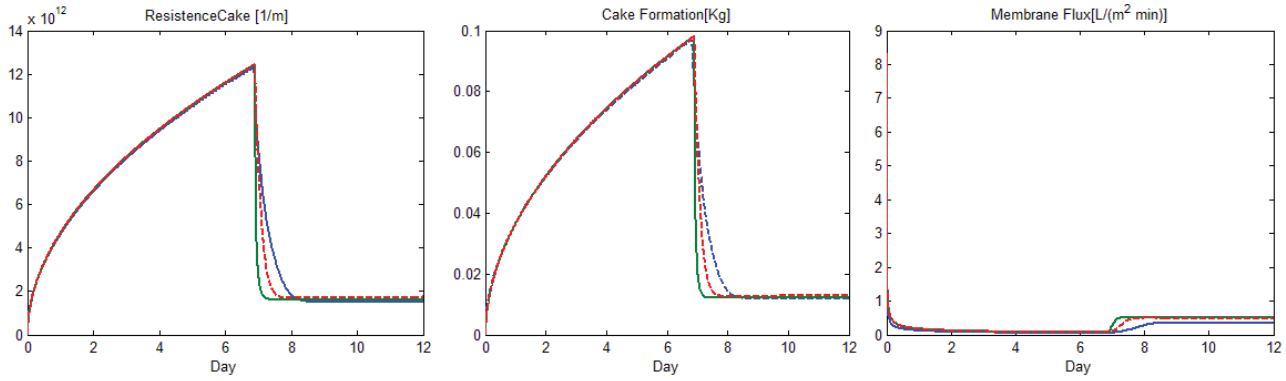


Figure 3.8: Comparision between the models with air cross-flow. Blue: Li Model, Red: GPS-X model and Green:Proposed Model.

Figure 3.9 shows the behavior of the states with and without air. The main difference is that without air, the cake (m) goes to infinity, contrary to the system with air where the cake mass stabilizes in a certain value, thus stabilizing the systems.

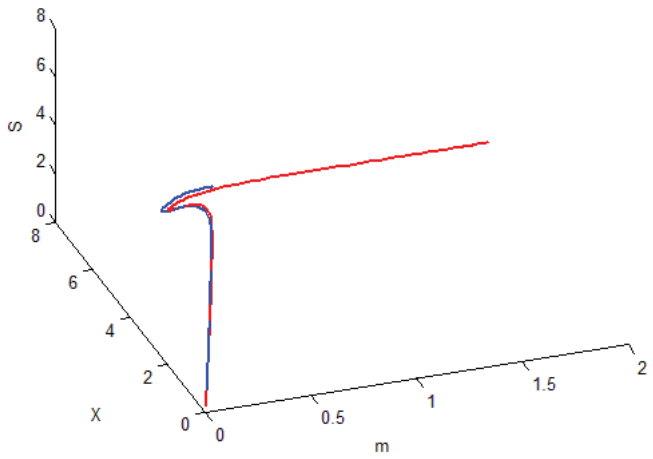


Figure 3.9: The blue dynamic is with air and the red dynamic without air.

3.5 Model Simulation and Parameter Identification

In this section, the well-established GPS-X simulator (Hydromantis - Environmental Software Solution, Inc, 2012) is exploited so as to generate realistic biological and filtration simulation data, which can be used as a database for the estimation of the parameters of the proposed simplified model. The objective is to show that the simplified model is able to reproduce the behavior of a more detailed process representation, implemented in a recognized software environment.

The nitrification process of the recirculating aquaculture system with sMBR pilot plant that will be detailed in Section 4.1.2 is used as an application example.

Figure 2.3 shows the sketch of the nitrification compartment with membrane bioreactor. This illustration is a simplified representation of the two tanks inside the dashed square in Figure 4.1. The advantage of lumping both reactors is to model only the dynamics that are the most important for process control, without considering all the internal variables and parameters of the process. This leads to a simplified input-output black-box model with a "biologically inspired" structure, but with much less variables and parameters.

The considered process, which is taken as an application example, has a

membrane permeate flow of 18.75 $L/(m^2h)$, resulting in an influent flow of 0.16284 m^3/d. The nitrification process is composed of two aerobic tanks; the first tank has a volume of 0.09 m^3 and the second, which includes the membrane, has a volume of 0.045 m^3. The sludge retention time of the plant is 25 *days*, and the hydraulic retention time 0.5 *days*. The total area of the membrane is 0.35 m^2. The total suspended solids concentration in the membrane compartment ranges from 5 to 15 g/L. The influent characteristics are extracted from Viadero Jr. et al (2005) with total suspended solids of 10.9 g/m^3, BOD of 2.4 g/m^3 and total ammonia nitrogen of 1.5 g/m^3.

At this stage, the simulator makes use of specific GPS-X modules (and not of our proposed model) with ASM1 as the biological model and the cake formation with equation (3.39). Standard conditions of 20 °C, at sea-level with a barometric pressure of one *atm* are set. The GPS-X dynamic sludge cake model is represented by equation (3.39) and the sludge cake resistance by equation (3.40). The ASM1 parameters are the GPS-X default values.

To illustrate the previous discussion, the process trajectory is computed over a period of 150 days: the first 100 days with an air cross-flow of 2.86 m/d and the next 50 days with a reduced flow of 1.43 m/d. Figure 3.10 clearly shows the existence of at least three time-scales (ultrafast, fast and slow) thus confirming our observation in the previous section. The ultrafast behavior of the cake mass is clear when the air-flow is changed. A fast time-scale is then observed which corresponds to the transient of the substrate and free biomass. Finally, a slow evolution of the fouling is apparent (the evolution of the fouling has been reported by Merlo et al (2000) with a fouling rate constant of 0.001 d^{-1}).

In Figure 3.11, a phase plane plot of three GPS-X simulations with different initial conditions are presented. Note that the system rapidly converges to the equilibrium point, which confirms our analysis of a fast evolution of the suspended solids to the cake.

The proposed model has been solved using *ode45* (an explicit variable-step Runge-Kutta method) and *ode15s* (an implicit solver for stiff ODEs based on numerical differentiation formulas) as implemented in Matlab, using an Intel Celeron 2.20*GHz* processor, and with simulation times 211.65 seconds and 3.08 seconds respectively, demonstrating the process stiffness.

In order to fit the response of the simplified model to the experimental data collected from the GPS-X simulator, the weighted least-squares cost function

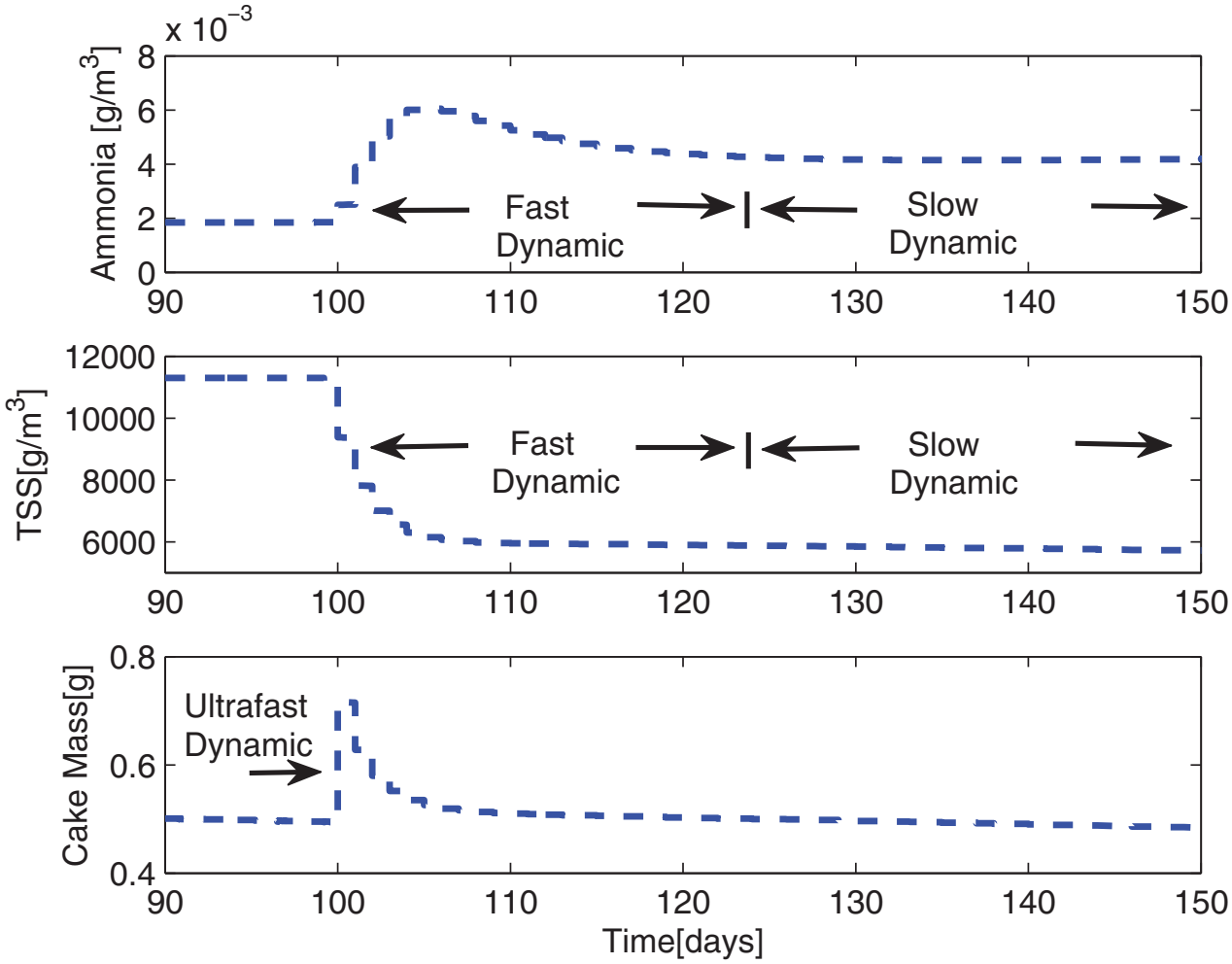


Figure 3.10: GPS-X simulation: Time Simulation with cake evolution.

$$f_{cost}(\theta) = \sum_{i=1}^{n_t} \left(\xi_{sim}(i) - \xi_{GPS-X}(i)\right)^T \Omega^{-1} \left(\xi_{sim}(i) - \xi_{GPS-X}(i)\right) \tag{3.45}$$

is minimized, where $\xi_{GPS-X} = [S\ X\ m]$, $\xi_{sim} = [S_{sim}\ X_{sim}\ m_{sim}]$, $\theta = [\beta_0\ K_{air}\ Y\ \mu_{S,max}\ \gamma]$, n_t is the number of measurements and Ω is defined as a scaling matrix that is selected as a diagonal matrix of the square of the maximum values corresponding to each state. The optimization is performed in this study using a *Nelder Mead* algorithm as implemented in *fminsearch* in *Matlab*.

A lower bound on the covariance matrix $\hat{P}$ of the parameter estimates is obtained by the inverse of the Fisher Information Matrix (FIM):

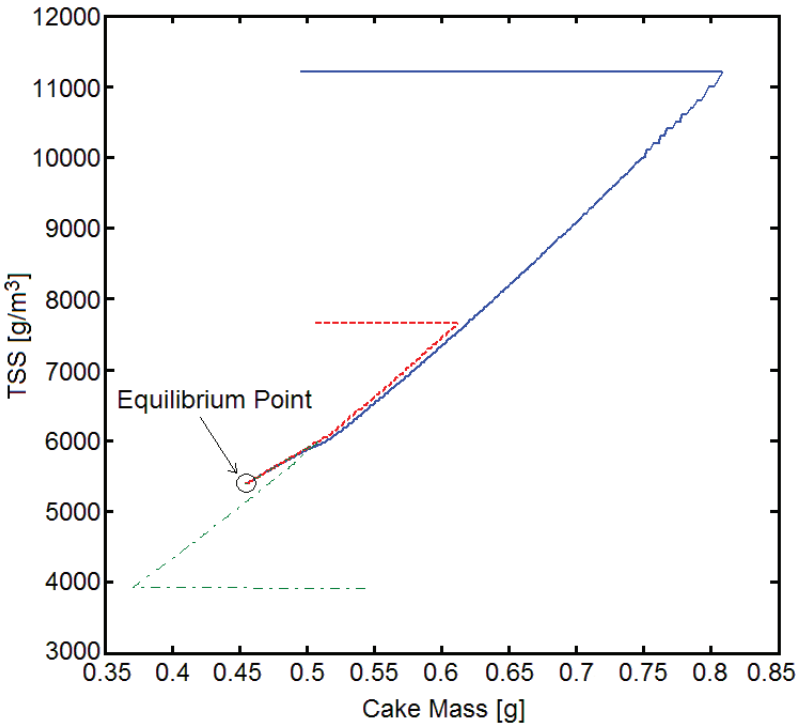


Figure 3.11: GPS-X simulation: Phase plane plot. Trajectories from three different initial conditions.

$$\hat{P} = F^{-1}(\hat{\theta}) \tag{3.46}$$

The FIM is computed by:

$$F(\hat{\theta}) = \sum_{i=1}^{n_t} \left[\frac{\partial Y_m}{\partial \theta}\right]^T_{(t_i,\hat{\theta})} \Sigma^{-1} \left[\frac{\partial Y_m}{\partial \theta}\right] \tag{3.47}$$

where Y_m is the vector of the process outputs, Σ is the estimated covariance matrix

$$\Sigma = \frac{f_{cost}(\hat{\theta})}{(n_t - p)} I \tag{3.48}$$

and p is the number of parameters to be estimated.

The square root σ_j of the j^{th} diagonal element of $\hat{P}$ is an estimate of the standard deviation of $\hat{\theta}$, which is used to obtain the parameters confidence intervals of 1.96 σ corresponding to a probability of 95%.

Based on the fast and slow dynamics analysis, parameter identification can be organized in three steps corresponding to the three time-scales. Indeed, a

direct identification of all the parameters at the same time is delicate and leads to the occurrence of several local minima. A divide-and-conquer approach is therefore used, where subsets of parameters are estimated first, and the full set of parameters is then re-estimated starting from the previous estimates, which are then much closer to the optimum and severely decrease the computational efforts.

Figure 3.12 shows simulation results corresponding to step-changes in the membrane aeration at days 100 and 140 with values of 1.43 m/d and 2 m/d, respectively. The ultrafast (orange), fast (green) and slow (blue) time windows are shown. The parameters related to ultrafast dynamics β_0, which is considered constant, and K_{air} are first estimated using the data collected on a period of 0.02 days, while all the other parameters are fixed (to some initial values that can be randomly chosen in the parameter space using the latin hypercube strategy - explained further). The biological parameters linked to the fast dynamics (Y and $\mu_{S,max}$) are then estimated from data collected over a period of six days (all the other parameters remain fixed) and finally, the remaining slow dynamics parameter (γ) is estimated from data over a period of 33 days (again, all the other parameters are fixed to their last estimated values). The three successive parameter identification steps are followed by an identification of all parameters at the same time, starting from the current parameter estimates and using the full data set. The resulting vector of parameters θ is the starting point for a new sequence of ultrafast, fast and slow partial identification and identification of all parameters. This process can be iterated as necessary, but for this application it is observed that after two iterations the minimization algorithm converges to one single point.

The identification procedure is summarized in Figure 3.13. The columns represent the identification procedure and the lines represent the parameters to be identified, i.e. the fast procedure uses the parameters identified in the ultra-fast dynamic identification procedure and the initial guess values for the slow parameters. Once fast parameter identified, they are used for the slow dynamic identification procedure.

The identified parameters are shown in Table 3.2.

Following the identification procedure, it is important to test the predictive capability of the model with a set of data that has not been used in the identification procedure, i.e. the so-called model cross-validation. Within this step, it is important to check if the parameters inferred from the experimental data indeed translate the process behavior and not only some specific and restricted operating conditions. In this study, the initial conditions and air

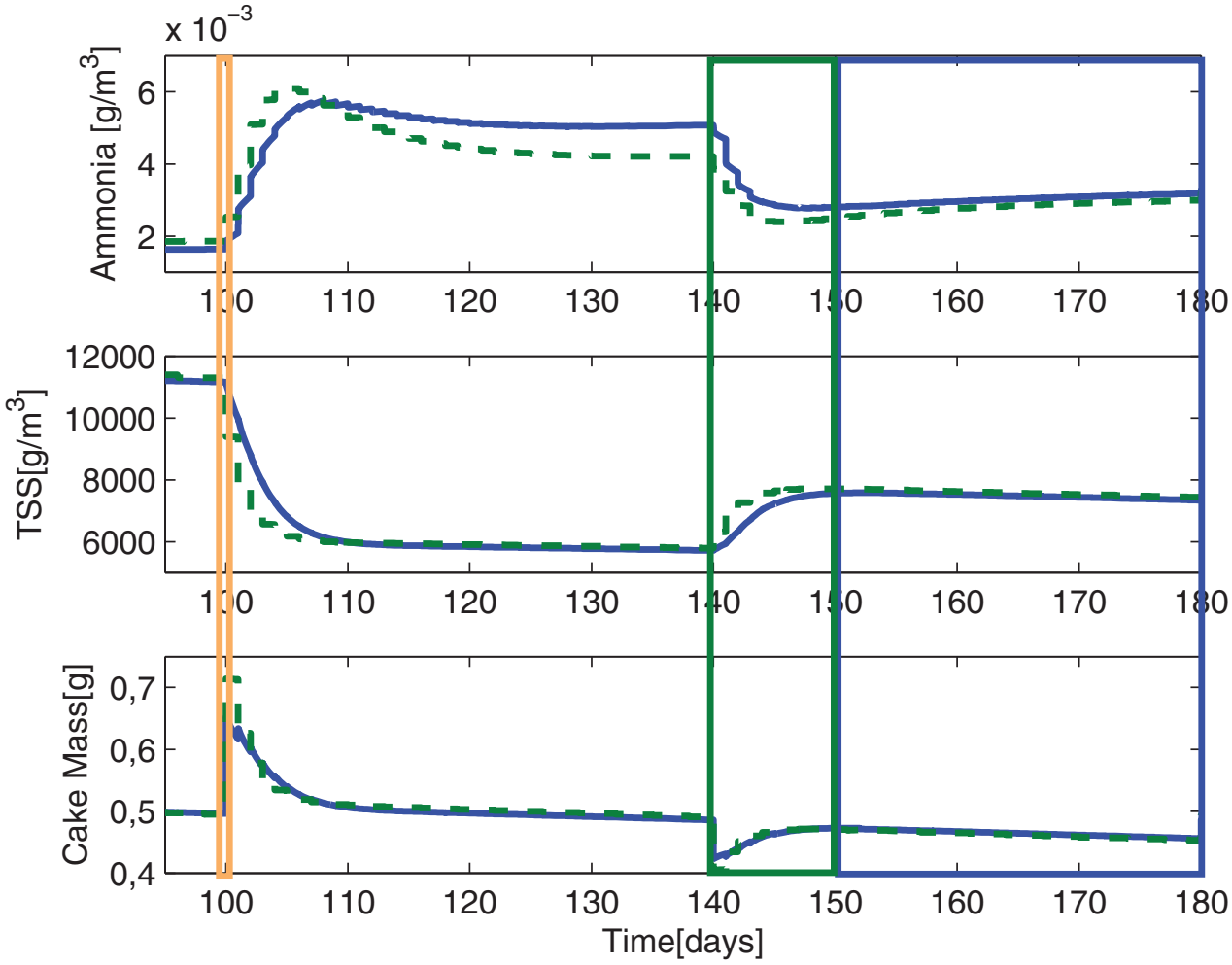


Figure 3.12: Dotted line: GPS-X with full ASM1 model; solid line: proposed simplified model. Orange window - ultrafast; Green window - fast; Blue window - slow.

Table 3.2: Parameters with their standard deviation.

	Ultrafast [0.02 Days]	Fast [6 Days]	Slow [20 Days]	All Parameters
β_0	$(4.819 \pm 0.573) \times 10^4$	fixed value	fixed value	$(5.531 \pm 0.643) \times 10^4$
K_{air}	$(4.773 \pm 0.575) \times 10^1$	fixed value	fixed value	$(4.596 \pm 0.134) \times 10^1$
Y	fixed value	$(8.996 \pm 0.022) \times 10^{-1}$	fixed value	$(8.985 \pm 0.016) \times 10^{-1}$
$\mu_{S,max}$	fixed value	(2.004 ± 0.722)	fixed value	(2.265 ± 0.343)
γ	fixed value	fixed value	(0.001 ± 0.882)	(0.001 ± 0.535)
$min\,(f_{cost}(\theta))$	53.55	0.8592	6.42	22.79

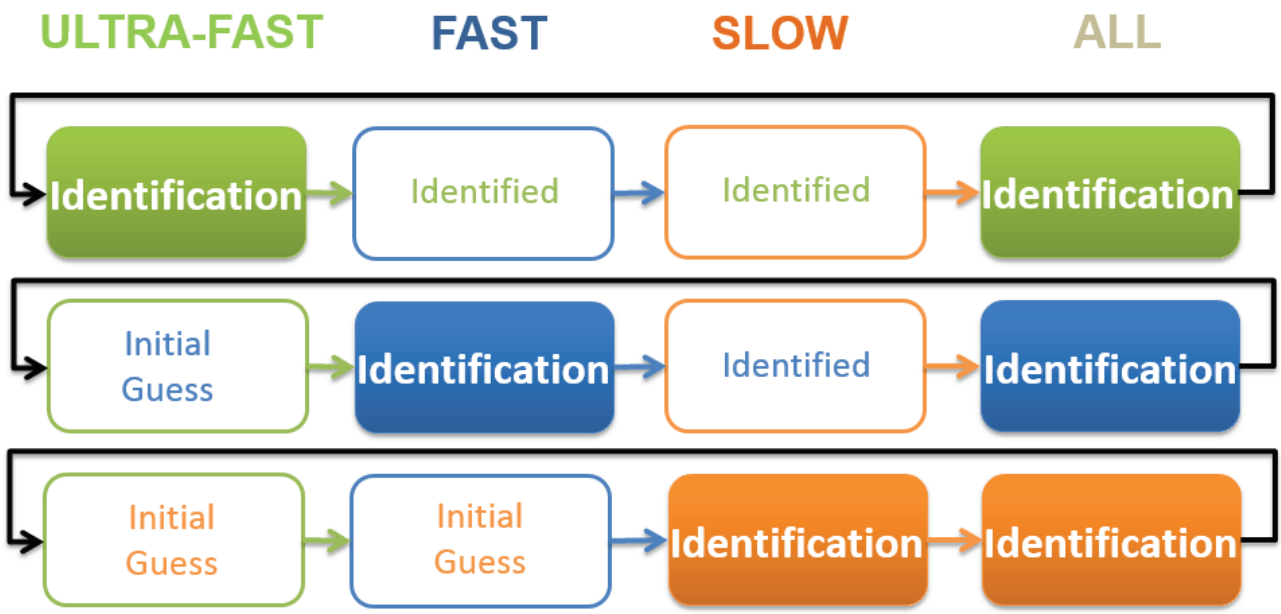


Figure 3.13: Identification Procedure. The columns represent the procedure and the line the parameters to be estimated.

cross-flow are modified, e.g. to 2.29 m^3/d, 2.86 m^3/d, 2 m^3/d and 1.43 m^3/d, at days 100, 120, 160 and 180, respectively. Figure 3.14 shows the satisfactory cross-validation results.

The correlation matrix of the estimated parameters is presented in Table 3.3. It is apparent that β_0 correlates with Y and $\mu_{S,max}$, since the value of β_0 affects biomass and, in turn, the substrate concentration. The pair of parameters Y and $\mu_{S,max}$ strongly correlate, which is often the case in bioprocess identification. Note that K_{air} is the short-term detachment factor and correlates with γ that rules the behavior of the long-term detachment, confirming again the behaviors of the three time-scales.

Table 3.3: Correlation matrix of the parameters

	β_0	K_{air}	Y	$\mu_{S,max}$	γ
β_0	1	−0.52018	0.74435	0.74407	−0.99999
K_{air}		1	−0.52101	−0.52084	0.52322
Y			1	1	−0.74489
$\mu_{S,max}$				1	−0.74489
γ					1

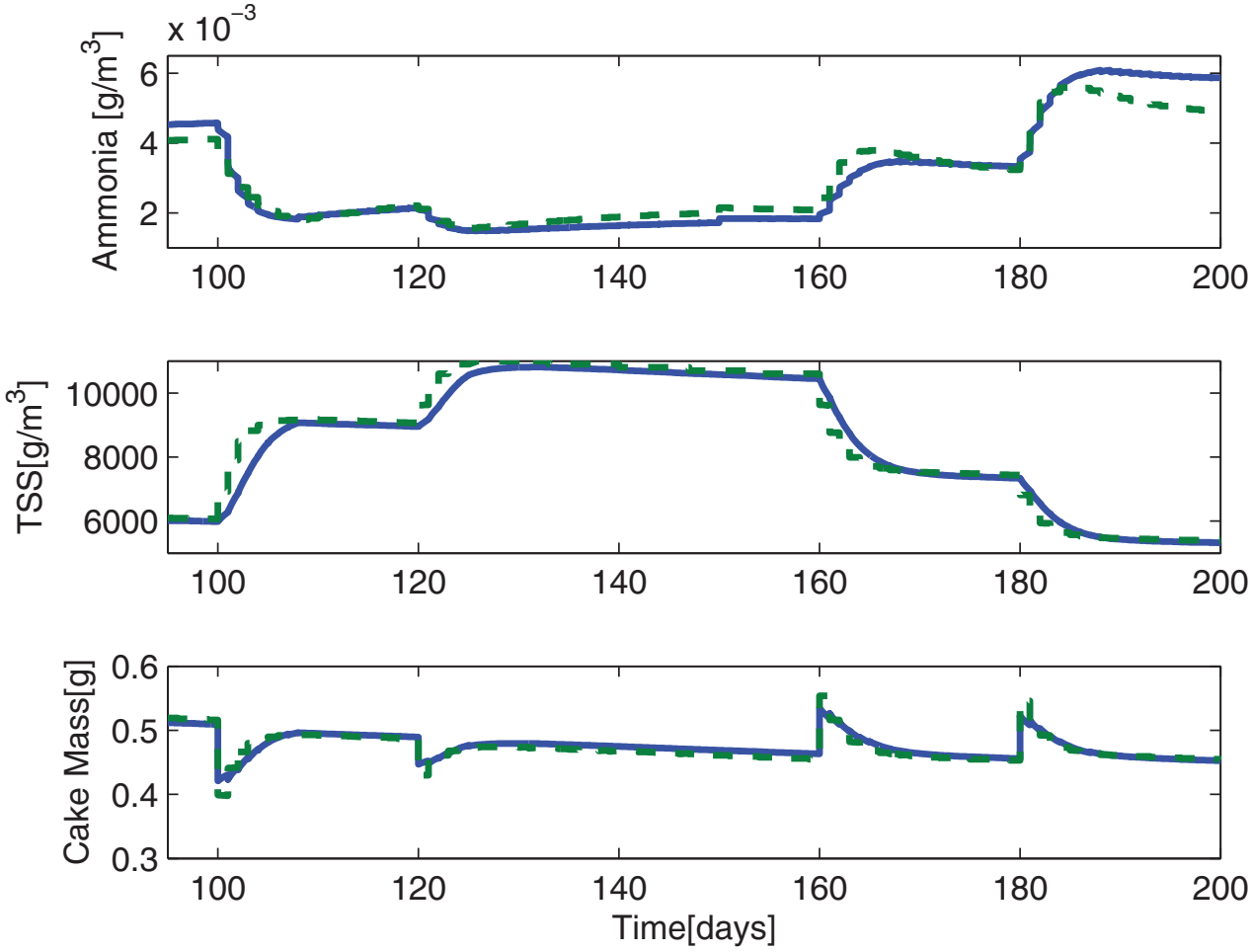


Figure 3.14: Cross-validation with different initial values and set-points. Dotted line: GPS-X with full ASM1 model; solid line: proposed simplified model.

Accurate correlation coefficients (R^2) of 0.98, 0.94 and 0.93 are obtained for the substrate, free suspended solids and cake build-up outputs, respectively. Figure 3.15 represents the L1-norm of the normalized parametric sensitivities (Muñoz Tamayo et al, 2009). The matrix is computed by $\sum_{i=1}^{nt} \left| \frac{\hat{\theta}_j}{y_m(t_i,\hat{\theta})} \left[\frac{\partial y_{m_k}}{\partial \hat{\theta}} \right]_{(t_i,\hat{\theta})} \right|$ and shows the interaction between the identified parameters and states. Note that the brown color denotes that the parameter is more susceptible to the state variation, meaning that this parameter is strongly linked to this state. It is the opposite for parameters represented by the dark blue color.

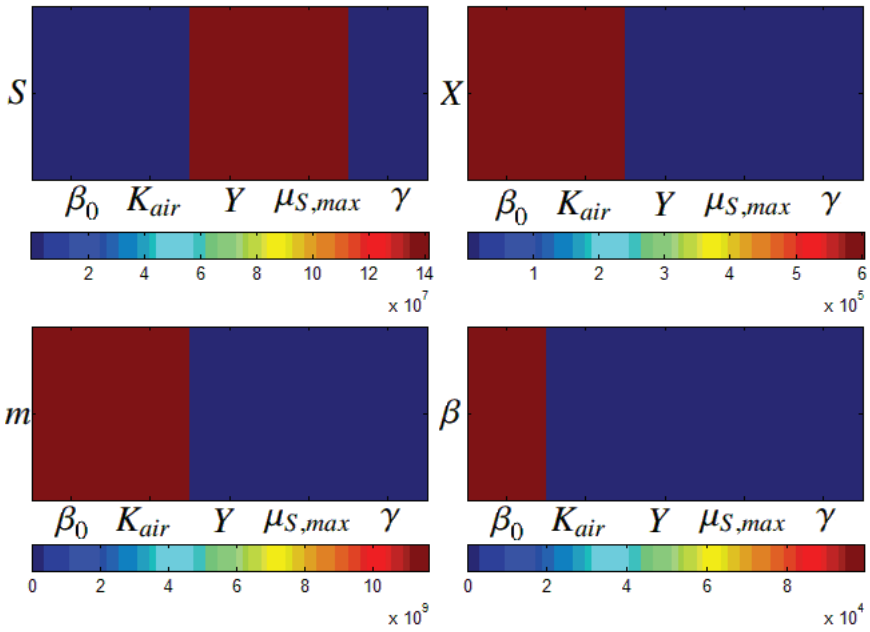


Figure 3.15: L1-norm of parametric sensitivities

In addition, a multi-start strategy using the Latin Hypercube Sampling (LHS) is used (McKay et al, 1979). The LHS method is a form of stratified sampling, which allows a reasonably accurate random distribution to be achieved, while reducing the computational costs associated with Monte Carlo techniques. The parameter bounds defining the exploration space are fixed at plus 50% and minus 50% of the nominal values found after identification in Table 3.2. Parameter estimation is repeated 80 times using LHS. The minimum costs for all trials are summarized in Table 3.4, showing that the minimum found has a relatively large region of attraction.

Table 3.4: Minimized Cost Function values with its standard deviation. Index for number of iterations of the full procedure

	Ultrafast [0.02 Days]	Fast [6 Days]	Slow [20 Days]	Global
$min\,(f_{cost}(\theta))_1$	(77.49 ± 145.3)	(0.8595 ± 0.0014)	(6.58 ± 2.16)	(22.86 ± 1.42)
$min\,(f_{cost}(\theta))_2$	(52.63 ± 2.35)	(0.8592 ± 0.0013)	(6.50 ± 0.36)	(22.79 ± 0.39)

It can be observed that some parameters presented in Table 3.2 do not totally converge with the standard parameters of the ASM1 model (Henze et al, 1987). This is due to the simple fact that the simplified model is used to fit a complex data behavior. Nonetheless, GPS-X uses detailed models,

such as the full ASM1 (Henze et al, 1987) for the biological compartment, and this study demonstrates that under standard operating conditions, a simple model can capture the main dynamics.

Chapter 4

Model Validation with Experimental Data

In previous sections, the proposed model has been compared to well-known sMBR models in research, showing its capability to mimic these models despite its simple structure and small quantity of parameters. Analytical and numerical analyses have been carried out and the results have shown the possibility to implement this model as a reference for process operation and maintenance. In the modeling design procedure, the last and more important step is the model validation with data obtained from experimental processes. In this chapter, the model is validated by two different processes: (i) a recirculating aquaculture system for ammonia removal and (ii) a wastewater treatment plant. It is important to highlight that both processes have different characteristics (i.e. inflow water characteristics, total suspended solids concentration and effluent characteristics); in the same manner, these validations show the relevance of the proposed model. In both experiments in this chapter, the sMBRs mode of operation is based on fixing an effluent flow (Q_{out}) value and letting the trans-membrane pressure TMP evolve over time due to the accumulation of the fouling, i.e. $TMP = \frac{Q_{out}}{A}\eta R_{total}$.

4.1 Recirculating Aquaculture System Fitted with sMBR Pilot Plant Design

The growth of the population and the competition for water, land and other natural resources motivate an intensification of recirculating systems and

their optimization as a greener process in the field of aquaculture (Piedrahita, 2003). As for several other agro-food processes, profits are computed based on the quantity of consumed resources, production yield by process footprint, and environmental impact. Aquaculture has its main economic and ecological impact on the ratio between fresh incoming water and discharge. Moreover, more severe legislation on the allowed discharge concentration results in continuous research for tools and strategies for recirculating process optimization. One extensively used technique is the recirculating aquaculture system (RAS), which can be defined as a process that reuses water and has less than 10% of the total volume replaced per day (Hutchinson et al, 2004). This recirculation, however, causes accumulation of ammonia, nitrate and organic matter that should be removed before reentering the system. Nitrogen removal for RAS normally includes some filtering technologies such as rotating biological disk contactors, trickling filters, bead filters and fluidized sand biofilters (Crab et al, 2007). One of these filtration techniques is the submerged membrane bioreactor (sMBR).

The use of submerged membrane bioreactors (sMBR) in aquaculture systems is a relatively new issue. Studies related to costs, water quality and fish health as well as their benefits, can be found in Viadero Jr. and Noblet (2002). Lab-scale RAS fitted with an sMBR have been developed to investigate the effects of fouling in this particular application. A remarkable reduction in wastewater and residue load could thus be evidenced (Gemende et al, 2008; Pulefou et al, 2008).

As aquaculture fitted sMBR data are very scarce, therefore a RAS pilot plant has been designed, automated and analyzed. These sets of recorded data are used to validate the proposed model.

4.1.1 Process Description

Recirculating aquaculture systems are considered a sustainable fish production in terms of water usage. The water reuse is achievable only if efficient nitrification, denitrification and organic removal is setup. The recirculation rates between aerobic, anoxic, sMBR and fish tank are extremely important for high removal efficiency. The sMBR can be incorporated adding its advantage of high effluent quality to the process. The scheme of the recirculating aquaculture systems fitted with an sMBR is shown in Figure 4.1. This study focuses on the ammonia removal process based on the classes of fish, tilapia and trout that are susceptible to high concentrations of ammonia resultant

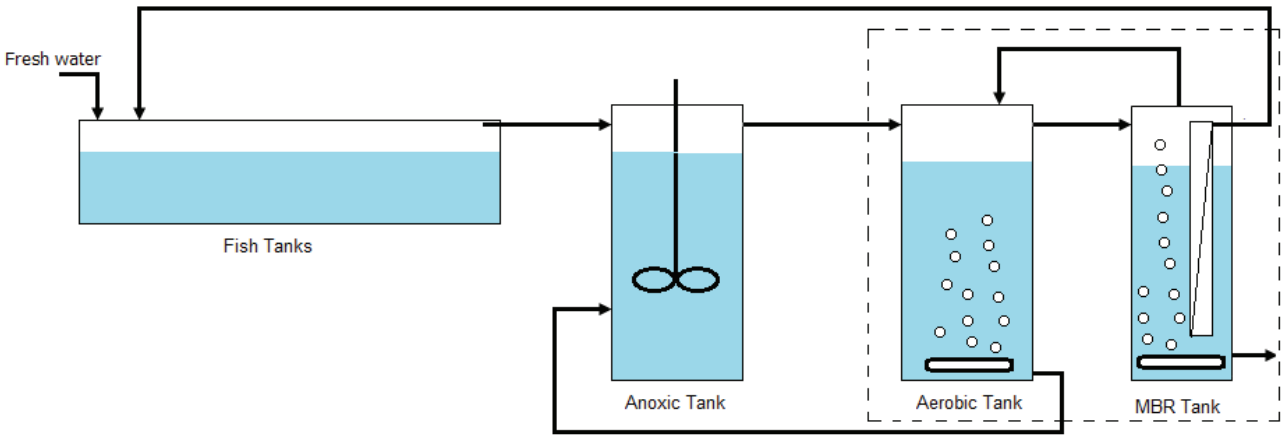


Figure 4.1: The recirculating aquaculture systems scheme fitted with an sMBR.

from fish feces and excretion, but tolerate higher nitrate concentrations (Eding et al, 2006).

4.1.2 Experimental Setup

The experimental RAS-sMBR pilot plant is able to remove nitrogen and solid matter (see Figure 4.2). The influent is composed of a synthetic wastewater to mimic fish excretion with ammonia mass flow of around 19.8 $mgNH_4^+ - N/h$. This value was based on the ammonia excretion values reported by Thomas and Piedrahita (1998) and Gershanovich and Pototskij (1992), a total fish basin volume of $0.05m^3$ and a fish density of 24 kg/m^3.

The bioreactors have a total volume of 0.22 m^3 divided in an anaerobic (41% of the total volume) and an aerobic compartment (41%), a compartment with submerged microfiltration membranes (18%). The recirculation between sMBR and nitrification tank is 0.7 m^3/d and the recirculation between nitrifier tank and denitrifier is 0.7 m^3/d. The total area of the membrane used is $0.35m^2$ (Microdin Nadir), working at $t_{permeate} = 0.0035\ d$ (5 min) filtration and $t_{relax} = 6.94 \times 10^{-4}\ d$ (1 min) relaxation (see Figure 4.3). The permeate production is around 18.71 L/m^2h, and membrane aeration is around 20 m^3/d. The suspended solids concentration in the membrane compartment ranges from $0.05 - 0.6\ g/L$. Online data, including temperature, flows and transmembrane pressure TMP, are gathered every one second. Offline measurements of suspended solids concentration, pH, air-flow rates and ammonium concentration are carried out daily.

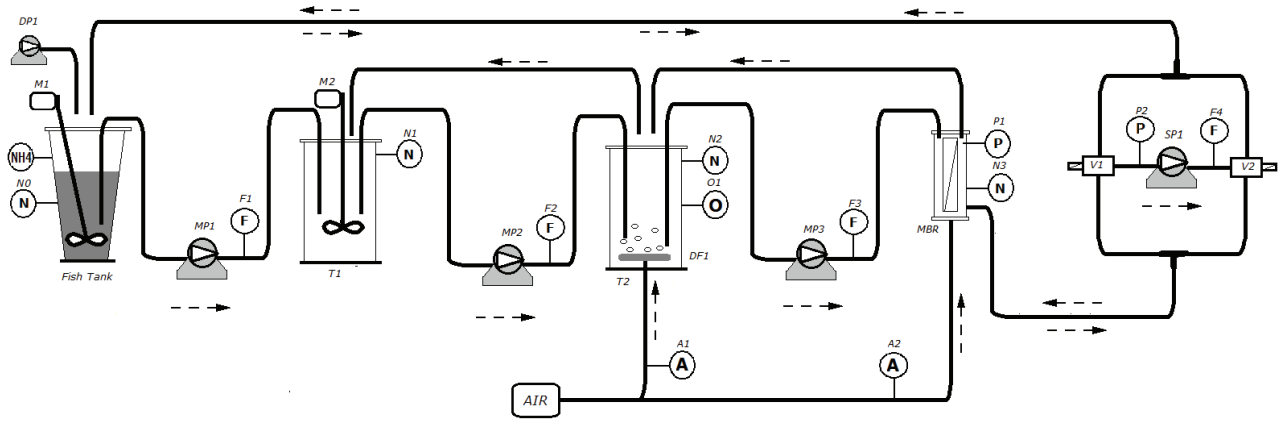


Figure 4.2: Pilot Description. Where, DP is ammonia dosing pump, M are the mixers, NH4 is the point of ammonia measurement, N are the tank level sensors, MP are the magnetic pumps, F are the liquid flow-meter sensors, T are the tanks, DF is the air diffuser, A are the air flow-meters, O is the measuring point for oxygen, P are the pressure sensors, V are the direction valves and SP is the suction pump.

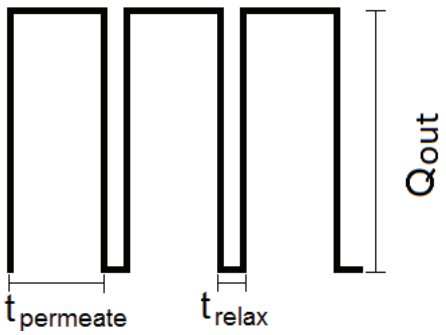


Figure 4.3: Relaxation and permeate cycles, t_{relax} and $t_{permeate}$ minutes.

The pilot plant is equipped with controlled pumps that are responsible for transporting ammonia to the nitrification tank, the nitrate to denitrification tank and the treated water to the fish tank. The system includes five pumps of three different types. The intermediate circulation pumps (MP1, MP2, MP3) are magnetic couple AC pumps (*IWAKI* model MD-6-230GS01), which allow flows up to 8 L/min. The global recirculation and backwash pump is a diaphragm 24 Vdc pump (*SHURflo* model 8000-991-236) with a maximum flowrate of 2 L/min. The last pump is the dosing pump (*ISMATEC* model Reglo Digital MS-2/6-160), here the flow is adjusted to emulate the behavior of the fish excretion injecting ammonia in the system.

The AC pump sources are phase-angle dimmers (NS−80 from FG ELEKTRONIK) that allow the PLC to control the pumps through its analog outputs. The diaphragm pump is a DC pump powered by a DC driver, which allows the PLC to change its flow by a PWM output.

To control the pump flow rates, the level of the tanks and the differential pressure into the membrane tank, the following sensors are used: level sensors, which consist of a simple float switch that prevents the tank from overflowing; flow-meters, ranging from 0.05 to 10 L/min, which allows great versatility of operating conditions; and a pressure sensor that is used for the *TMP* measurement and ranges from −1 to 1.6 *bar* producing an output current of 4 to 20 mA.

Two motorized 3-way valves (V1 and V2) are used to reverse the flow flux from permeate to backwash on the MBR module. The system uses reinforced flexible tubing of 13 mm in diameter.

For the aeration of the nitrification tank, a Roeflex disc diffuser from *Passavant−Geiger Gmbh* is used, which allows good diffusion of air at the bottom of the tank. The air source for the nitrification tank is separated from the MBR air source. For the nitrification tank, an air pump with variable air-flow is used while for the MBR the rate of the flow is constant. Air sensors with manual control have been installed to measure and control the airflow rate, with a range from 0 to 300 NL/h.

The membrane used is a BIO-CEL Lab from *Microdyn-Nadir Gmbh* (Figure 4.4). It has a membrane surface area of $0.35m^2$ installed in a PVC frame with integrated cross-flow aeration via a membrane diffuser. Connections for permeate drainage and air supply are already provided. The PES ultrafiltration membrane (type UP150) is identical to that of the full scale BIO-CEL module, enabling qualitative statements to be made on experimental filtration measurements.

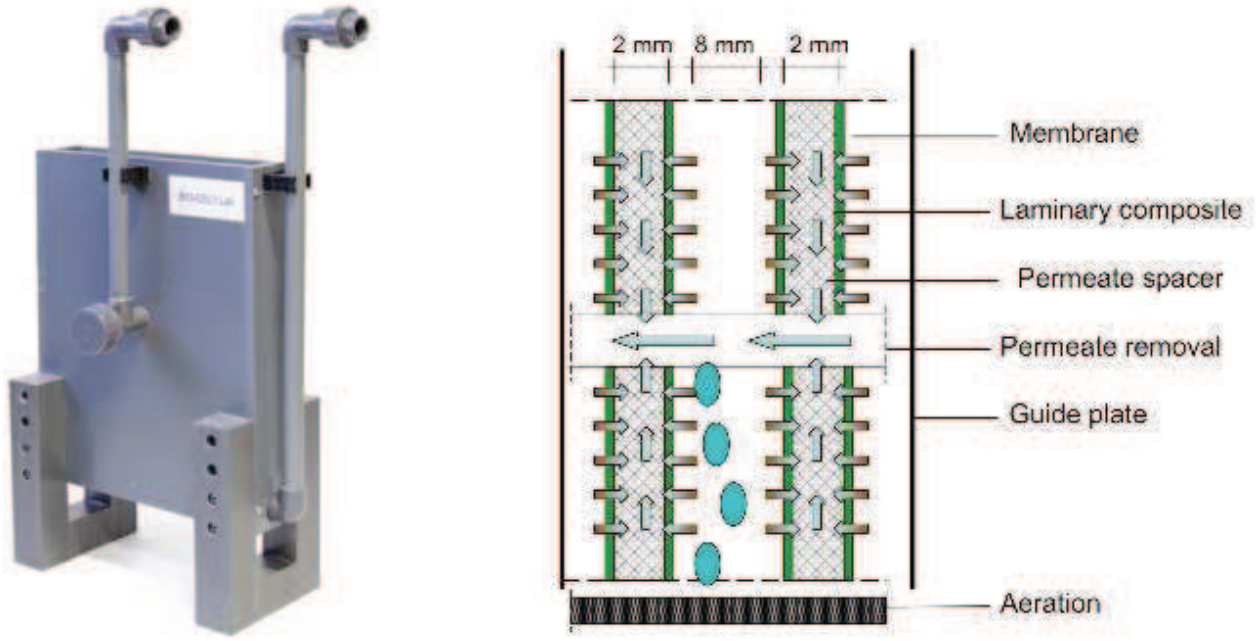


Figure 4.4: Microdyn-Nadir: 0.35 m^2 and 150 $MWCO[kDa]$.

The membrane uses the Nadir membrane: 150 MWCO [1] [kDa], made of Polyethersulfone (PES). The material is hydrophilic with a high chemical resistance (pH from 0 to 14 and max temperature 95 °C). The membrane has been designed for environmental protection, metal processing, textiles, paper, food/dairy, pharma/biotech and chemical processes.

For data acquisition and control, a PLC S7-1200 from *Siemens* has been selected, which has all the inputs and outputs needed for the process monitoring and control. To complete the monitoring part, a PC is used as an OPC-server to ensure the communication between the PLC and LabView. In this configuration, the PLC and *LabView* are the OPC-clients. A *LabView* interface has been designed for human machine interface. It is important to highlight that the usage of *LabView* allows the interaction between the PLC and *Matlab/Simulink* for data validation.

In Figure 4.5, the automation structure of the process is represented. This includes the human-machine interface on the top (Labview), the control part (PLC), sensors, drivers and the actuators at the bottom. With this layout, it is possible to measure, collect data and actuate in the system.

A command board has been designed and assembled to keep the equipments safe, to protect the laboratory's power network and for possible sepa-

[1] Molecular weight cut-off

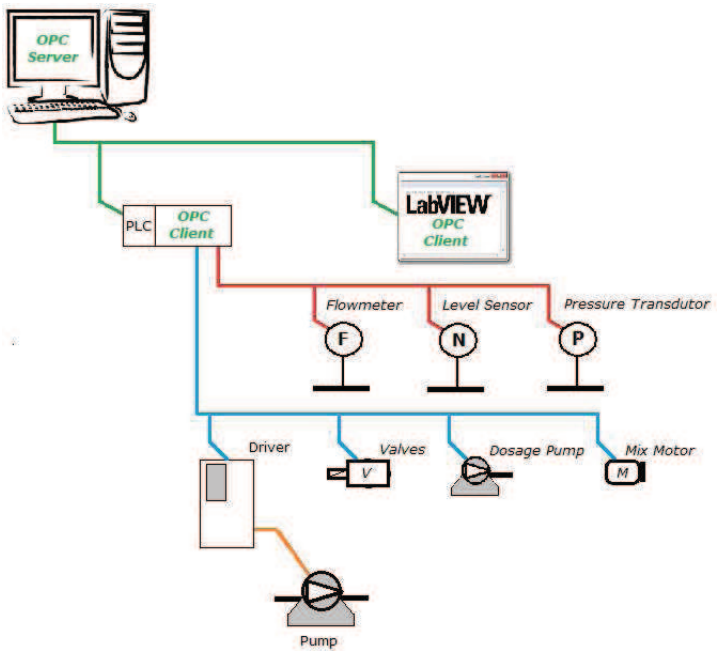


Figure 4.5: Layers of automation.

rate interruption of the reactors.

4.1.3 Data Logging and Instrumentation

The data logging has two structures: (i) OPC connection between Labview and the PLC that records the data from the process every second; (ii) data logging records data every 5 min. The latter can be downloaded accessing the PLC memory via a web-browser using the PLC address in the network which has 15 days of autonomy.

Before any data acquisition and process operation, instrument calibrations should be executed. An optical densitometer is used to indirectly measure the total suspended solids (TSS) concentration. Its calibration was carried out by taking samples from the pipe between denitrification and nitrification tanks, from the nitrification tank and a dilution of 1:2 from the latter. The samples were dried in an oven to weigh the solid particles. The relation between measurements was computed by a linear regression method and is described using the following equation: $X[g/L] = 1.6245 \cdot [CU] - 0.009$ with $R^2 = 0.9996$ where CU is the measurements provided by the optical densitometer.

A PT-100 sensor was added into the sMBR to measure the bulk temperature. The conversion of the PLC values to temperature is $Temp$[°C]



Figure 4.6: Water samples. On the left permeate sample and on the right sMBR tank sample

$= 0.008 \cdot F_{PLC} - 12.3127$ with $R^2 = 0.9993$ where F_{PLC} represents values measured by the PLC.

A PI controller is applied to the low level of the process, which means controlling each pump using the flow-meters.

4.1.4 Recirculating Aquaculture System and sMBR

The advantage of effluent quality is evident, as seen in Figure 4.6. The RAS-sMBR has been operating over one year continuously with the input ammonia mass flow of 19.8 $mgNH_4^+ - N/h$. As a result, the total ammonia concentrations in the process is around $(0.177 \pm 0.098)\ mgNH_4^+/L$. When necessary tap water was added to the system due to evaporation or technical problems.

Figures 4.7 and 4.8 show experimental trials during one month. The fouling build-up in *TMP* plot is evident, and the constant effluent flow (Q_{out}), Temperature (*TEMP*), total suspended solids (X), pH and air cross-flow can be seen in the other plots. Note that, in the plot NH_4^+, fluctuations of the ammonia values are observed. This is due to experiments to extract the dynamics of the biological process, that is explained in Section 4.1.7.2.

In order to understand certain properties of the RAS-sMBR, experiments focusing on the filtration aspect of the plant were carried out. The process

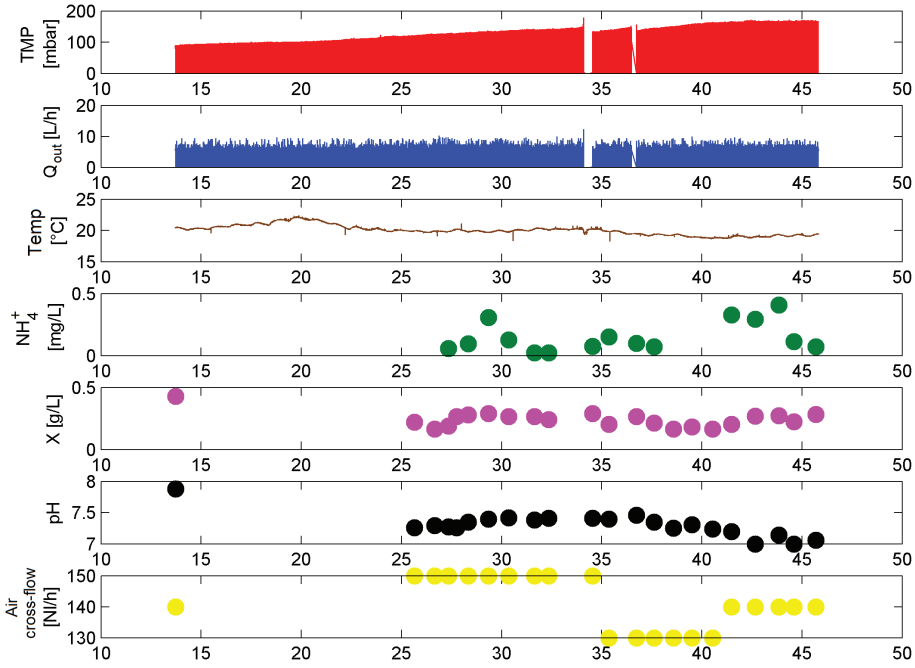


Figure 4.7: Measurements from an experiment in August.

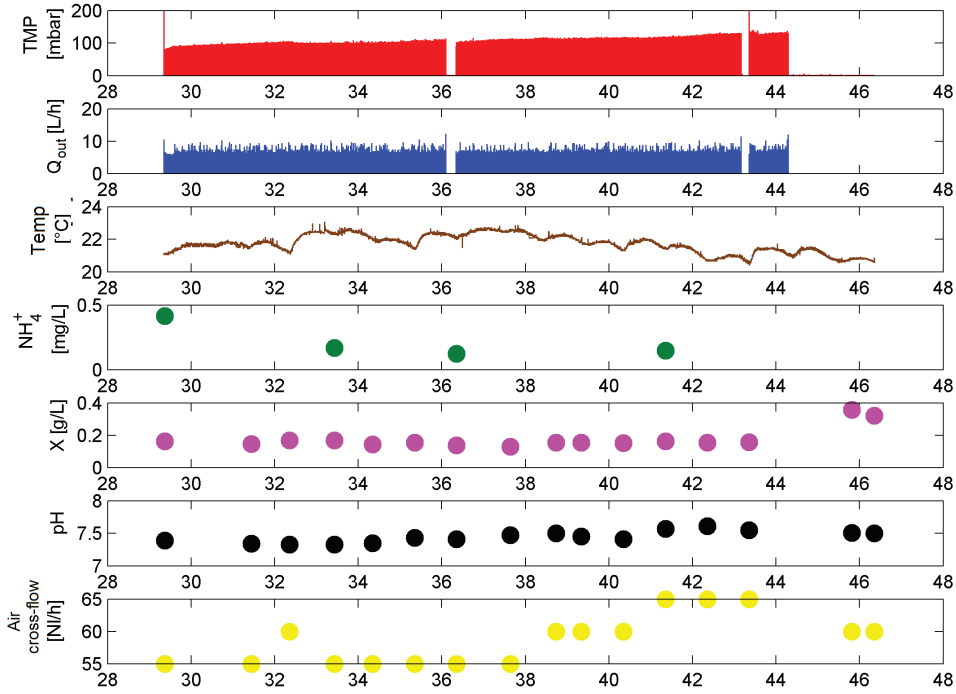


Figure 4.8: Measurements from an experiment in October.

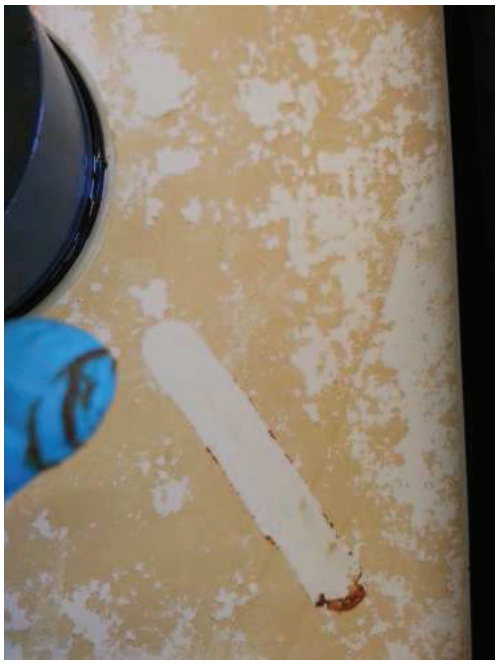


Figure 4.9: Fouling onto membrane surface.

had low concentration of TSS (around 0.2 g/L of TSS) if compared to activated sludge wastewater treatment, probably resulting from the synthetic water concentrations added into the fish tank and lack of carbon in the process. Consequently, a low fouling production was observed, i.e. after five months in use, *TMP* reached 200 *mbar*. Thus an inspection in the membrane apparency took place. Figure 4.9 shows the fouling attached to the membrane.

After the membrane was mechanically cleaned with brushes and the *TMP* dropped from around 200 *mbar* to 45 *mbar*.

The measurements of NH_4^+ concentration was taken using HACH kits $LCK-304$. The ammonia measurements had errors around 3%. The error was monitored twice a year by measuring the same sample three times with the kit. This method was chosen because of the high cost of each measurement.

4.1.5 Critical Flux

To study the filtration characteristics, the "critical flux" procedure was carried out. This involves varying the permeate flow in order to observe the *TMP* behavior. The "critical flux" is overtaken when the relation between the flux and the *TMP* is no longer linear. The step method proposed by Le-Clech et al

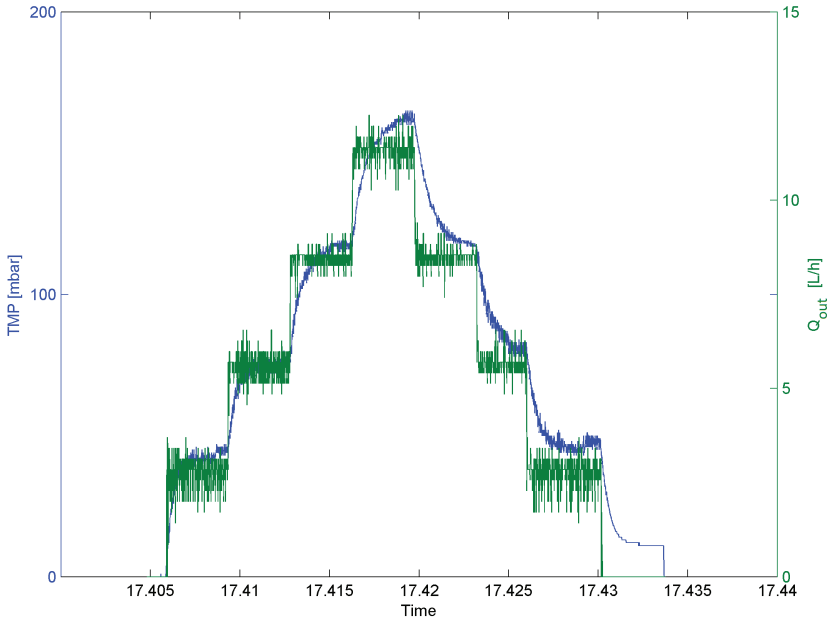


Figure 4.10: Five-minute trial steps varying $8.14 L/m^2h$

(2006) was implemented.

Using the PI controller, the set-point was changed by $8.14 L/m^2h$ over five-minute steps, see Figure 4.10. The test shows that, in the designed operation conditions, the "critical flux" was not reached, probably due to the low concentration of TSS ($0.130[g/L]$), concluding that the reversible layer on the membrane surface was extremely thin while the *TMP* increased because of irreversible sludge deposition.

Note that when the permeate flow is decreased the *TMP* do not follows the same profile as the Q_{out}. This can be explained by the resident air inside the membrane structure, which affect the *TMP* profile.

4.1.6 Air Cross-Flow Study

Two experiments, each carried out over approximately 15 days, were implemented for the study of the fouling evolution. Air cross-flows of $J_{air} = 22.85\, m^3/m^2d$ and $J_{air} = 53.85\, m^3/m^2d$ were selected. For the ease of evaluation of the evolution slope, a second order low pass Butterworth-filter, equation (4.1), with a cut frequency of $\omega_c = 0.0209\ rad/s$ is designed, considering the permeate and relaxation cycles (5:1 min).

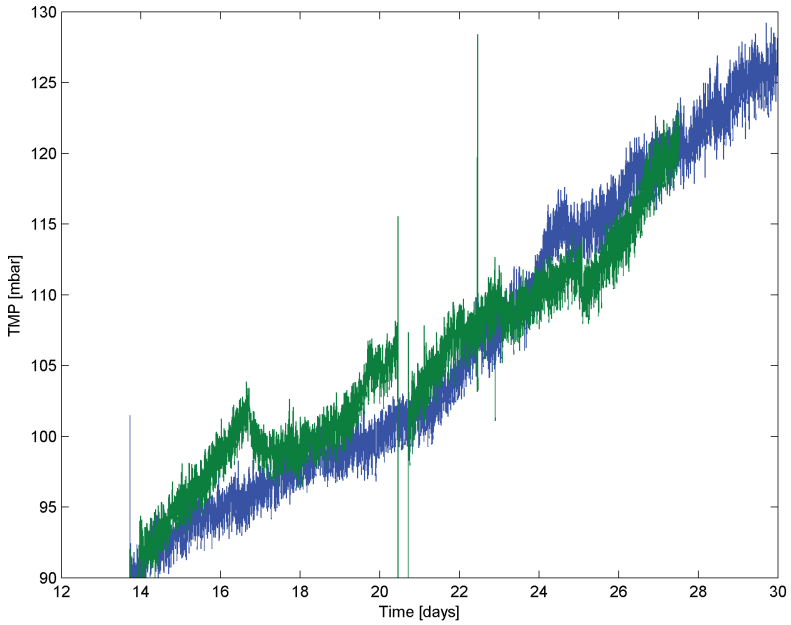


Figure 4.11: Comparison of the different air cross-flow. In blue J_{air} = 53.85 m^3/m^2d and in green J_{air} = 22.85 m^3/m^2d

$$|B(j\omega)|^2 = \frac{1}{1 + (j\omega/j\omega_c)^{2N}} \tag{4.1}$$

Figure 4.11 shows the *TMP* of both experiments. Note that the air cross-flow changes, but the evolution in *TMP* is the same. These tests show that reversible fouling was not present and the greater effect of the irreversible layer in the *TMP* value was evident.

4.1.7 Model Identification and Cross-validation

It is important to remember that experimental sMBR plants are exposed to daily temperature variations which have an influence on the apparent viscosity. The apparent bulk viscosity η can be modeled by equation (4.2) proposed by Rodríguez et al (2010):

$$\eta(Temp) = A_1 e^{\frac{A_2}{Temp}} \tag{4.2}$$

where $Temp$ is the bulk temperature and A_1 and A_2 are apparent viscosity parameters.

Analyzing the process dynamics and the model characteristics, presented in Section 3.2.1, the system can be divided into three parts on account of

the three time-scales of the process. The reversible layer mass attachment is considered an ultra-fast dynamic and its parameters $\theta_{UF} = [K_{air}, \rho_{rev}, m_0]$ are identified using an one-hour data set of measurements. The biological degradation and growth is considered a fast process and its parameters $\theta_F = [Y, \mu_{S,max}, K_S]$ are identified using a three-day data set. The slow dynamic are the long fouling evolution term, the irreversible resistance mechanism and the influence of the temperature on the apparent viscosity. The parameters $\theta_S = [\gamma, A_1, A_2, \rho_{irrev}]$ are identified using a 16-day data set. This feature is used to simplify the identification procedure that is organized in three steps corresponding to the three time-scales.

This procedure uses initial parameter values inspired by physical interpretation, literature study and knowledge about process dynamic behavior. For example: the parameters ρ_{rev} and m_0 influence the *TMP* initial amplitude; the K_{air} influences the detachment by J_{air}; and γ and ρ_{irrev} are linked to the *TMP* slope. Before starting the validation procedure, the data set is analyzed and a data window is selected based on the following properties:

1. The data window should have required data measurements for model input and output comparison, i.e. Q_{out}, J_{air}, X and T for model inputs and *TMP* for model output. These measurements are essential for the process simulation;

2. Few or no data acquisition interruption.

The validation of models, which connect the biological degradation and the filtration mechanism, is extremely important to understand and optimize recirculating aquaculture processes. The recirculating aspect adds more degrees of complexity to the process dynamics making the system surprisingly difficult to operate and to maintain in the desired "operating" zone. Bearing this in mind, the integrated model with simple structure is important for process maintenance.

The parameter identification procedure is based on the following weighted least-squares cost function

$$f_{cost}(\theta) = \sum_{i=1}^{n_t} \Big((\xi_{sim}(i) - \xi_{pilot}(i)) \Big)^T \Omega^{-1} \Big((\xi_{sim}(i) - \xi_{pilot}(i)) \Big) \tag{4.3}$$

is minimized, where $\xi_{pilot} = [S_{pilot}\ X_{pilot}\ TMP_{pilot}]$, $\xi_{sim} = [S_{sim}\ X_{sim}\ TMP_{sim}]$, $\theta = [\beta_0,\ K_{air},\ \rho_{rev},\ m_0,\ Y,\ \mu_S,\ K_{air},\ \gamma,\ A_1,\ A_2,\ \rho_{irrev}]$, n_t is the number of

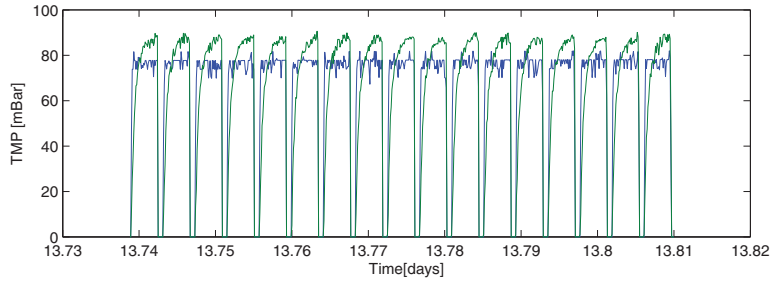


Figure 4.12: *TMP* short-term behavior, ultra-fast dynamic.

measurements and Ω is defined as a scaling matrix that is selected as a diagonal matrix of the square of the maximum values corresponding to each state. The optimization is performed in this study using the Nelder-Mead algorithm as implemented by the *fminsearch* function in *Matlab*.

The lower bound of the covariance matrix $\hat{P}$ of the estimated parameters is obtained by the inverse of the Fisher Information Matrix (FIM) is computed in the same manner described in Section 3.5 with equations (3.46), (3.47) and (3.48).

4.1.7.1 Ultra-fast Dynamic Identification

The ultra-fast dynamic was linked to the reversible sludge attachment and detachment, which influenced the *TMP* measurements. Over this time-scale, neither the biological degradation nor the long-term fouling evolution were taken into account; they were considered constant dynamics due to their slow dynamic behavior. The parameter identification procedure is set to a one-hour data simulation to identify K_{air}, ρ_{rev} and m_0. Figure 4.12 shows that the dynamic of *TMP* measurements (in green) grew slower than the proposed model (in blue). This behavior is linked to the fact that the model did not take into account the air compression aspect inside the tubes of the pilot. This drawback was overcome by using the average values from each cycle. The second column of Table 4.1 shows the identified parameter values found by minimizing the cost function (4.3). The identification result has a correlation factor of $R^2 = 0.8813$. Note that β_0 could not be identified with the set of the experimental data, thus the parameter is fixed at 55000 m^{-1}. A future investigation to find an appropriate experimental data set for this parameter identification should be carried out.

Table 4.1: Identified Parameters

Parameters	**Ultra-Fast Procedure**	**Fast Procedure**	**Slow Procedure**
K_{air} $[g]$	(48.581 ± 2.332)	48.581^{*}	48.581^{*}
ρ_{rev} $[m \cdot g^{-1}]$	$(2.931 \pm 0.168) \times 10^{11}$	$2.931 \times 10^{11*}$	$2.931 \times 10^{11*}$
m_0 $[g]$	$(9.508 \pm 0.133) \times 10^{-1}$	$9.508 \times 10^{-1*}$	$9.508 \times 10^{-1*}$
Y $[-]$	0.4^{*}	(0.232 ± 0.136)	0.232^{*}
$\mu_{S,max}$ $[day^{-1}]$	0.9^{*}	(0.915 ± 0.689)	0.915^{*}
K_S $[g \cdot m^{-3}]$	0.1^{*}	(0.090 ± 0.106)	0.090^{*}
γ $[d^{-1}]$	-0.1^{*}	-0.1^{*}	$-(1.631 \times 10^{-13} \pm 1.640 \times 10^{-5})$
A_1 $[-]$	1.1^{*}	1.1^{*}	$(9.134 \pm 0.023) \times 10^{-1}$
A_2 $[-]$	13.5^{*}	13.5^{*}	(7.842 ± 0.018)
ρ_{irrev} $[m^{-2}]$	$8.0 \times 10^{7*}$	$8.0 \times 10^{7*}$	$(8.329 \pm 0.025) \times 10^{7}$

*Constant value in this identification procedure

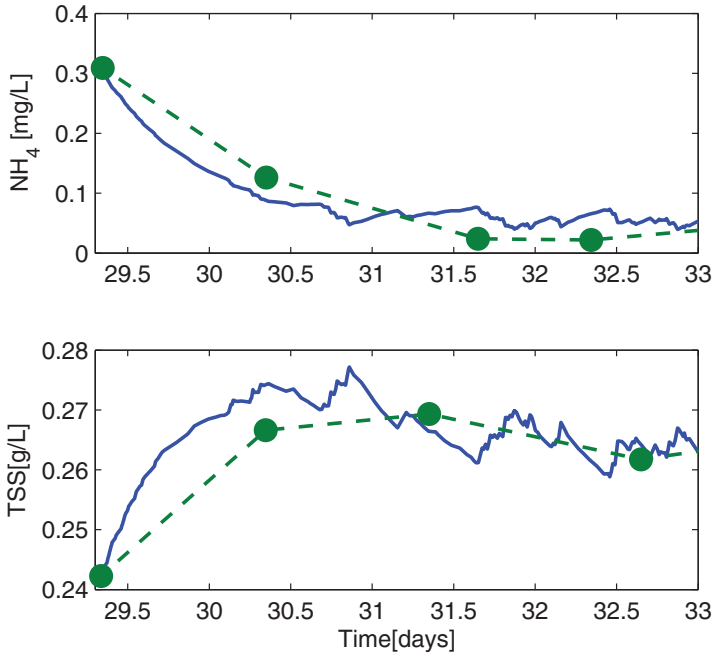


Figure 4.13: Biological degradation direct identification (Fast Dynamic): blue is the model and green is the real data.

4.1.7.2 Fast Dynamic Identification

The fast dynamic comprises the biological aspect and, consequently, the ammonia degradation and biomass growth were taken into account. As the process operates in a stationary regime, with constant ammonia inflow, disturbances were added to the ammonia inflow to extract information about the biological degradation dynamics (see the disturbances on the ammonia plot in figure 4.7 after day 27). The disturbances were provoked adding 0.1 L of a solution with 850 mg/L concentration of ammonia.

The parameters Y, $\mu_{S,max}$ and K_{air} were identified over approximately 3.5 *days* and its values are presented in the third column of Table 4.1.

Note that, the identified parameter ranges are quite similar to values presented in the literature, such as: $\mu_{S,max} = 0.8$, $K_S = 1.0$, $Y = 0.24$ by Henze et al (1987); $\mu_{S,max} = [0.7 - 0.8]$, $K_S = [0.2 - 0.4]$ and $Y = [0.084 - 0.142]$ by Queinnec et al (2006); and $\mu_{S,max} = [0.742 - 1.478]$ by Park et al (2007).

Figure 4.13 shows the simulation results that have a correlation factor of $R^2 = 0.9026$ and $R^2 = 0.9745$ for TSS and ammonia concentration, respectively.

4.1.7.3 Slow Dynamic Identification

The slow dynamic is linked to the long-term fouling evolution, which is expressed using the irreversible sludge layer, the parameter ρ_{irrev}, the long-term sludge cake evolution γ and the apparent viscosity parameters A_1 and A_2. The long-term identification uses a larger data set of 16 *days*.

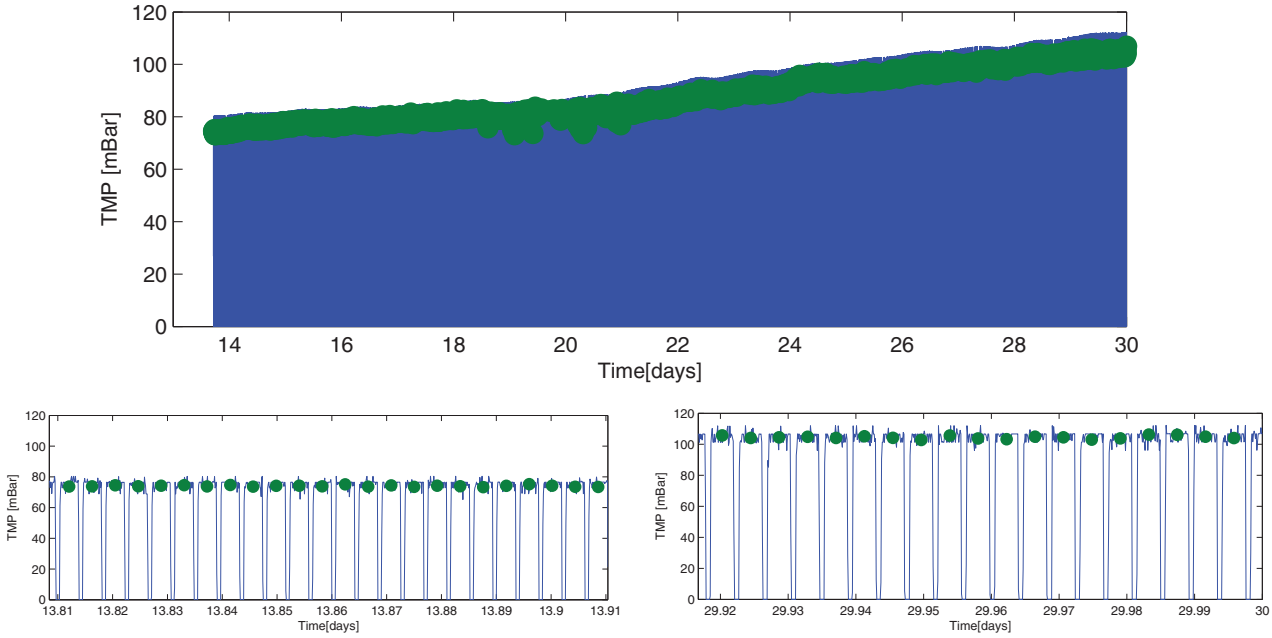


Figure 4.14: Figure on the top shows slow dynamic cross-validation: the blue stands for the model and the green dots are the mean value of each cycle computed from the real data. Figure on bottom-left shows the initial values in detail and Figure on bottom-right shows the end values in detail

The average value of each cycle is computed and used in the identification procedure,see figure 4.14. Their estimated values and sensitivities are shown in Table 4.1. The correlation factor of TMP is $R^2 = 0.8799$.

A parameter identification procedure with all the parameters taken at the same time was carried out. The cost function varies at about 0.061% and the parameter with the largest variation obtained is 0.1% of its value. These results show that the three procedures reached a minimum cost function value.

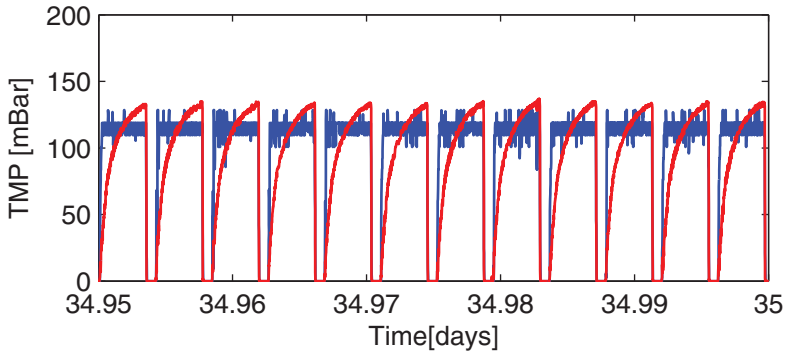


Figure 4.15: Cross-validation of the ultra-fast dynamic.Red line is the experimental data and in blue the model.

4.1.7.4 Cross-validation

Cross-validation was performed using experimental data that was not used in the direct validation. Unfortunately, only the ultra-fast and slow dynamics had data for the cross-validation procedure. For the fast time-scale, more experiments should be carried out. The difficulty lies in selecting the right amount of ammonia to obtain a data set with sufficient information for the parameter identification. The other problem is the very strict duration for thesis research. Further experiments are outlined in Section 6(Directions for Further Research).

This cross-validation of the ultra-fast dynamic is presented in Figure 4.15. The experimental data is represented by the red line and the model by the blue line. Note that over time, an undesirable amount of air inside the membrane structure increases, transforming the shape of the *TMP* to a smoother dynamic.

The cross-validations of the slow dynamic parameters are presented in Figure 4.16; the Figures at the bottom show the simulation in more detail. A fair accuracy factor value is achieved ($R^2 = 0.8493$), showing the possibility to use the model as a predictor in long-term experiments.

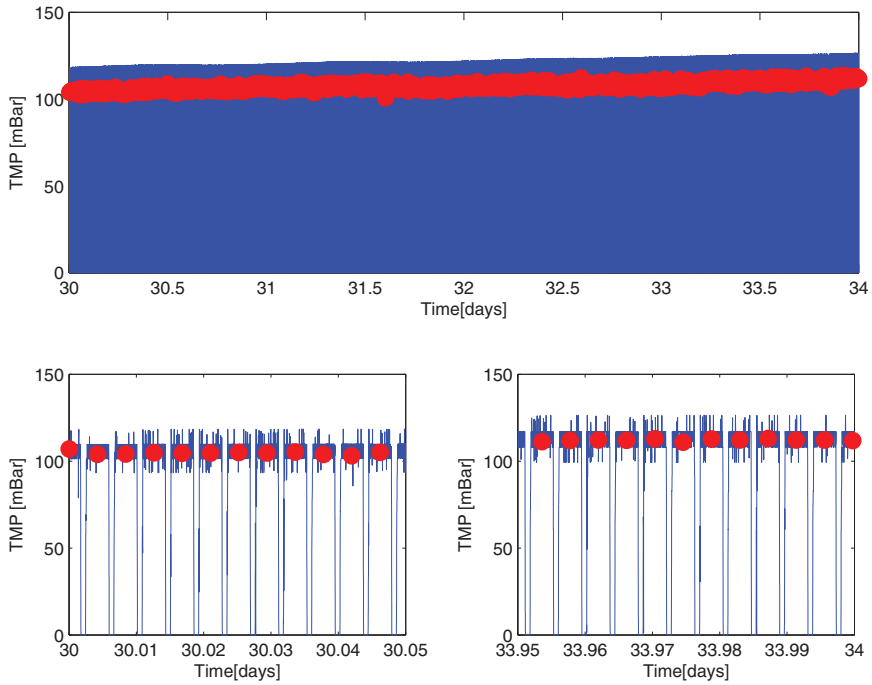


Figure 4.16: Cross-validation of the fast dynamic.Red line is the experimental data and in blue the model.

A recirculating aquaculture plant with a submerged membrane bioreactor has been designed and automated to maintain the ammonia concentration at a low level of 0.1 mgN/L. This system allows experiments to be carried out in a variety of situations and the data collected can be used for the development of dynamic models. The results show that the main factor of fouling formation is the attachment of irreversible sludge layer, caused by the low concentration of total suspended solids. Based on a dynamic integrated model of sMBRs, it is possible to implement advanced control strategies to optimize the process on account of the fouling evolution and biological degradation. Further research into the denitrification process must be carried out in order to achieve a total nitrogen removal from the system.

4.2 Wastewater Treatment Pilot Plant[2]

The submerged membrane bioreactor has been increasingly applied to wastewater treatment, due to its high effluent quality (regarding solid matters), foot-

[2]Experimental data provided by LEQUiA Group, Laboratory of Chemical and Environmental Engineering, University of Girona, Catalonia, Spain

print reduction and the decoupling of the hydraulic and solid retention times (Judd and Judd, 2011).

In this study, attention is focused on the fouling mechanism only, and an even simpler dynamic model is proposed, calibrated and validated with experimental data collected from a pilot plant. The influence of the water temperature variation on the *TMP* is also taken into account, resulting in a more precise fouling build-up prediction.

The fouling dynamic model analyzed here is as follows:

$$\begin{cases} \dfrac{d\beta}{dt} = \gamma\beta & \text{(4.4a)} \\ \dfrac{dm}{dt} = Q_{out}X - J_{air}\mu_{air}(m)m & \text{(4.4b)} \end{cases}$$

$$\mu_{air}(m) = \beta\frac{m}{K_{air} + m}$$

4.2.1 Pilot Plant Description

The experimental pilot plant is an sMBR able to biologically remove organic matter, nitrogen and phosphorous, presented in Figure 4.17. The influent wastewater is obtained directly from the full-scale wastewater treatment plant sewer in Castell d'Aro, Catalonia, Spain, where the MBR pilot plant is located. Specifically, the MBR pilot plant is equipped with a primary settler and a screening system to prevent the entrance of large particles. The bioreactor has a total volume of 2.26 m^3 divided into an anaerobic (14% of the total volume), an anoxic (14%) and an aerobic compartment (23%) and a compartment with submerged microfiltration flat sheet membranes (49%). The sludge retention time of the plant is $25\pm6\,d$, and the hydraulic retention time is $0.50 \pm 0.05\,d$. The total area of the membrane used is 8 m^2 (LF, Kubota, Japan), with a nominal pore size of $0.4\mu\ m$, working at $t_{permeate} = 0,00625\ d$ (9 min) filtration and $t_{relax} = 6.94 \times 10^{-4}\ d$ (1 min) relaxation (see Figure 4.3). The permeate production is around 3.6 m^3/d, and the membrane aeration fluctuates between $27 - 36\ m^3/m^2d$, depending on the fouling behavior. The suspended solids concentration in the membrane compartment ranges from $6 - 10\ g/l$, while in the anaerobic reactor, it varies between $1 - 3\ g/l$. Online data, including temperature, flows, suspended solids concentration (into the membrane and in the anaerobic tank), air-flow rates and dissolved oxygen concentration, are automatically gathered every 10 seconds.

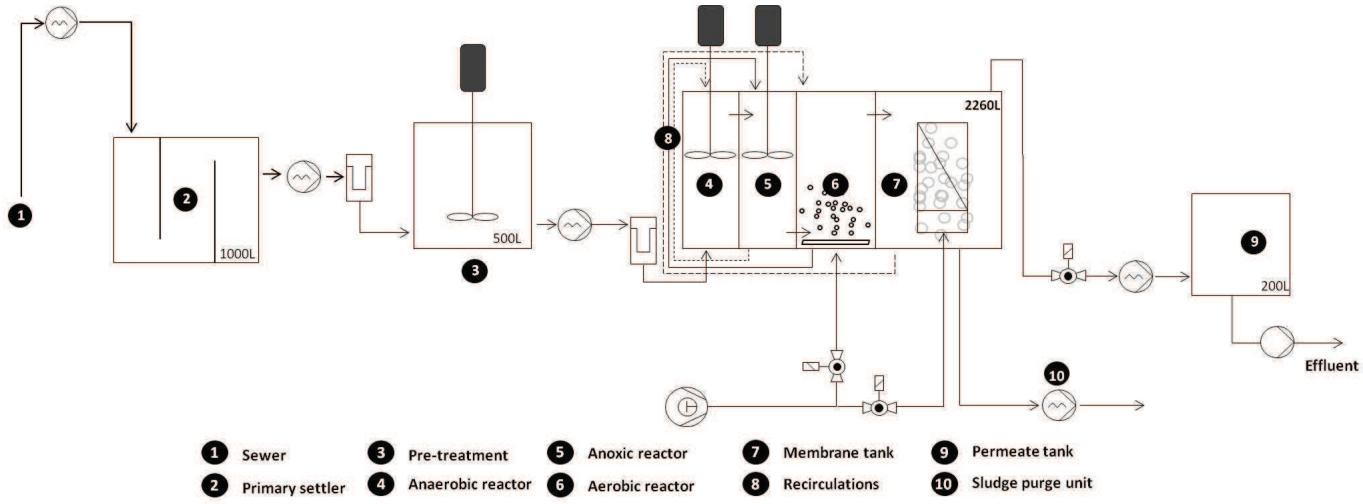


Figure 4.17: Experimental pilot plant schematic.

4.2.2 Recorded Data

The online data acquisition is recorded every **10 seconds**, except Q_w (just daily values recorded), S_{in} and S_{out} (offline measurements). The available data were collected during two years and have been differentiated by chemical cleanings, resulting in 10 periods. (Figures 4.18 and 4.19 show the division of periods).

The large quantity of online data are recorded in seven different excel tables (effluent, waste and air-flow, temperature, total suspended solids concentration, trans-membrane pressure and effluent characteristics) split into months, containing date, time and measurement values. To import these data to the Matlab environment, the tables have been transformed into .csv files, imported to Matlab and organized into one big table with eight columns divided by the periods. The data sets have been validated by a routine that organizes each measurement by the YYMMDDhhmmss (Y- year, M - month, D - day, h - hour, m - minute and s-second). This finds missing data in within ten seconds. If the missing data length is inferior of one minute, the values are created by interpolation.

These recorded data sets are analyzed in order to illustrate well-know dynamic behaviors found in a sMBR processes.

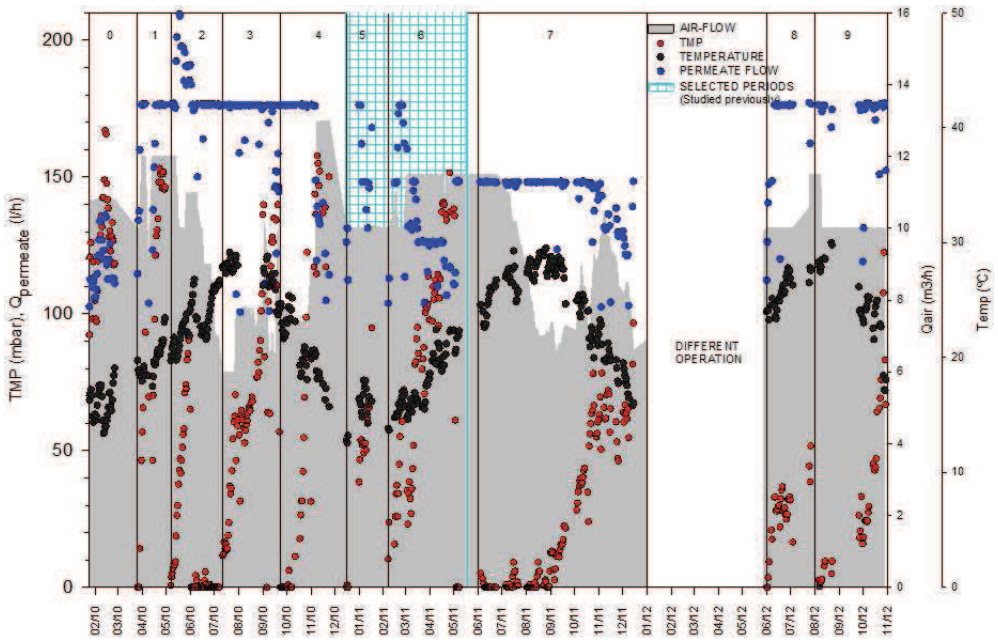


Figure 4.18: Chemical cleaning periods. Plotted values are daily averages: red - *TMP* [mBar]; black - temperature [°C]; blue - permeate flow [L/h]; gray area - membrane airflow [m^3/h].

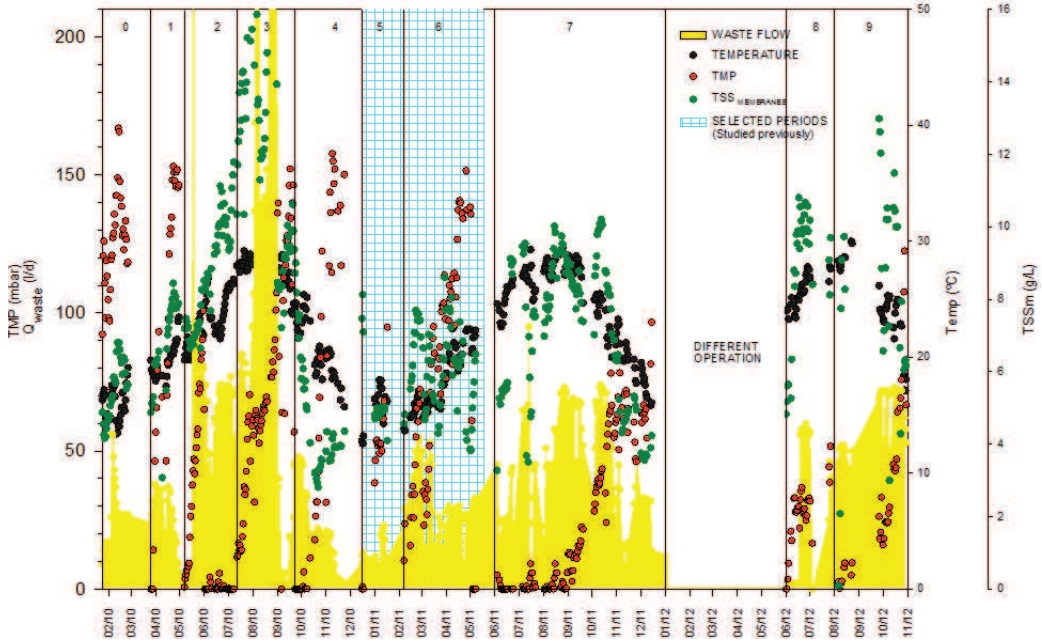


Figure 4.19: Chemical cleaning periods. Plotted values are daily averages: red - *TMP* [mBar]; black - temperature [°C]; green - total suspended solids in the membrane tank [g/L]; yellow - wasteflow rate [L/d]

4.2.3 *TMP* Long-term Exponential-like Behavior

The exponential-like behavior of trans-membrane pressure is well known in the MBR process and is illustrated by Figure 4.20.

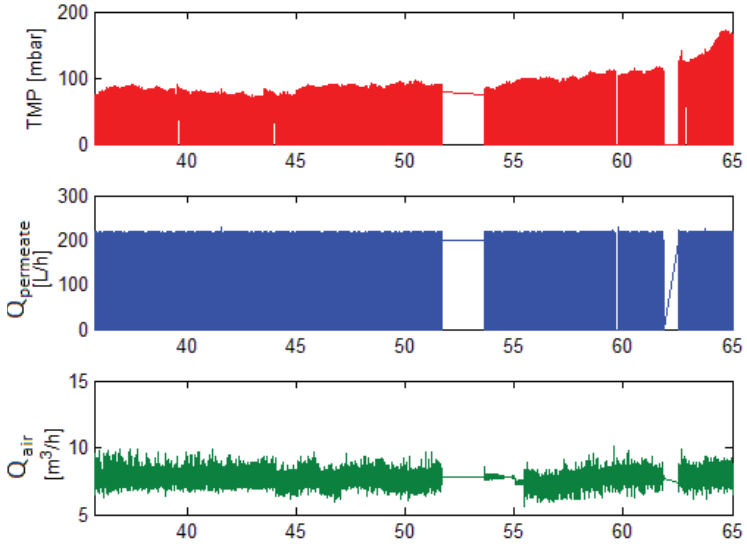


Figure 4.20: An exponential behavior in the *TMP* (data from one month) can be observed.

4.2.4 Permeate and *TMP* Amplitude

Another important and well-known relation is the direct link between *TMP* and permeate amplitude. The permeate flow (Q_{out}) is altered and *TMP* is rapidly affected, as observed in Figure 4.21.

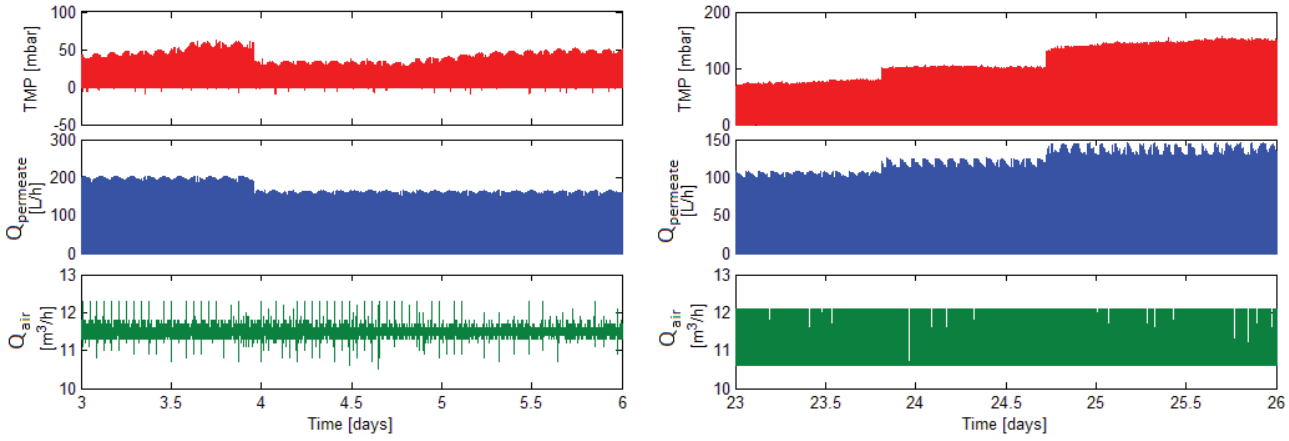


Figure 4.21: Influent of permeate flow over the *TMP*.

4.2.5 Relaxation

In a continuous process operation, the *TMP* starts to increase, as presented in Figure 4.20. One way to control the *TMP* build-up is a longer relaxation cycle, resulting in a greater detachment of the sludge cake. Figure 4.22 shows a longer relaxation period resulting in a *TMP* decay when the permeate cycle restarts.

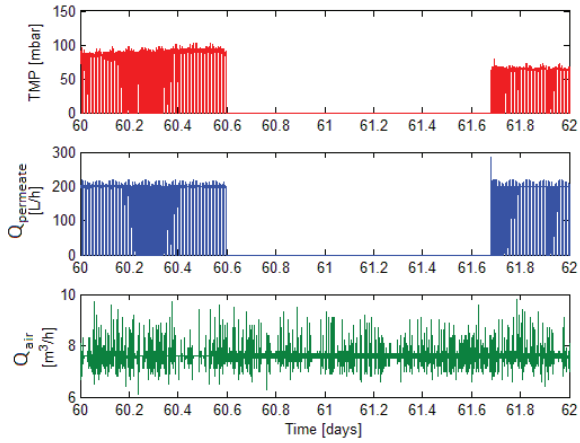


Figure 4.22: Influence of longer relaxation time on the *TMP*.

4.2.6 Temperature Influence

Figure 4.23 shows real data plots of water temperature and *TMP*. Note that the apparent viscosity is inversely proportional to the water temperature, provoking *TMP* oscillations.

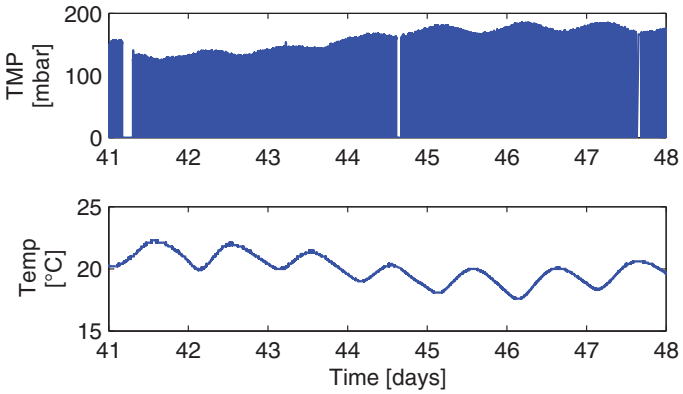


Figure 4.23: The oscillations of the *TMP* and temperature are approximately in the opposition phase.

4.2.7 Air-blowers Temperature

Similarly to water daily temperature variation that affects bulk viscosity, Figure 4.24 shows that the air cross-flow rate injected by the blowers changes the bulk viscosity. This is due to the air temperature that affects water viscosity and the apparent viscosity.

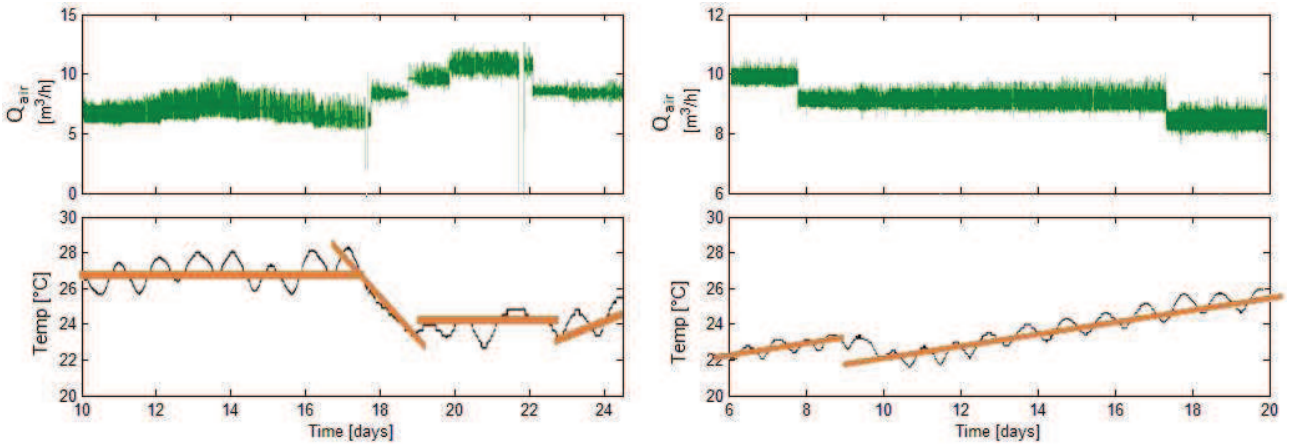


Figure 4.24: Influence of injected air temperature on bulk temperature.

4.2.8 Model Identification and Cross-validation

In order to fit the response of the fouling model to the experimental data collected from the plant, the unweighted least-squares cost function

$$f_{cost}(\theta) = \sum_{i=1}^{n_t} \Big((\xi_{sim}(i)\xi_{pilot}(i)) \Big)^T \Big((\xi_{sim}(i) - \xi_{pilot}(i)) \Big) \tag{4.5}$$

is minimized, where $\xi_{pilot} = [TMP]$, $\xi_{sim} = [TMP_{sim}]$, $\theta = [K_{air}, \rho_{rev}, m_0, \gamma, A_1, A_2]$ and n_t is the number of measurements. The optimization is performed in this study using the Nelder-Mead algorithm, as implemented by the *fminsearch* function in *Matlab*.

As in the previous identification procedure, a lower bound on the covariance matrix $\hat{P}$ of the parameter estimates is obtained by the inverse of the Fisher Information Matrix (FIM) and estimates the parameters confidence interval.

The initial parameter values have been inspired by physical interpretation, literature study and knowledge about process dynamic behavior. γ is linked to the *TMP* slope and A_1 and A_2 define the apparent viscosity. Before starting

the validation procedure, the data set is analyzed and a data window is selected based on the following properties:

1. The data window should have required data for the model input and output comparison, i.e. Q_{out}, J_{air}, X and T for model inputs and TMP for model output. These measurements are essential for the process simulation;

2. Data with TMP lower then 20 $mbar$ are not considered;

3. No or small data acquisition interruption.

Based on the fast and slow dynamics analysis presented in Section 3.2.1, the parameter identification can be organized in two steps corresponding to the two time-scales. The set of parameters θ is divided into two subsets of parameters to be identified. The short-term identification procedure uses $\theta_{short} = [K_{air}, \rho_{rev}, m_0]$ with β and η considered constant values. Note that the apparent viscosity η can be measured and β should be roughly estimated by some preliminary simulations. The identified short-term parameters are used in the long-term identification that has a long-term parameters subset $\theta_{long} = [\gamma, A_1, A_2]$. The β_0 parameter is considered constant with value of $3.0 \times 10^4\ m^{-1}$.

4.2.8.1 Short-term Identification

As presented in Figure 4.25, the fast behavior of cake attachment and detachment, which influence the TMP measurements, is evident. With this, the short-term parameters are estimated and validated analyzing only the fast dynamics of the process (dm/dt). The parameters identification procedure is set to have a half day of data simulation to identify K_{air}, ρ_{rev} and m_0, from days 20.0 to 20.5. Table 4.2 shows the identified parameters values found by minimizing the cost function (4.5).

Table 4.2: Short-term: Identified Parameters

Short-term Parameters	Values
K_{air} $[g]$	(35.0279 ± 0.42762)
ρ_{rev} $[m \cdot g]$	$(4.4164 \pm 2.9958) \times 10^{10}$
m_0 $[g]$	$(9.748 \pm 1.6917) \times 10^{-2}$
β $[m^{-1}]$	5.5×10^4 (Fixed Value)
η $[mbar \cdot s]$	2.66 (Fixed Value)

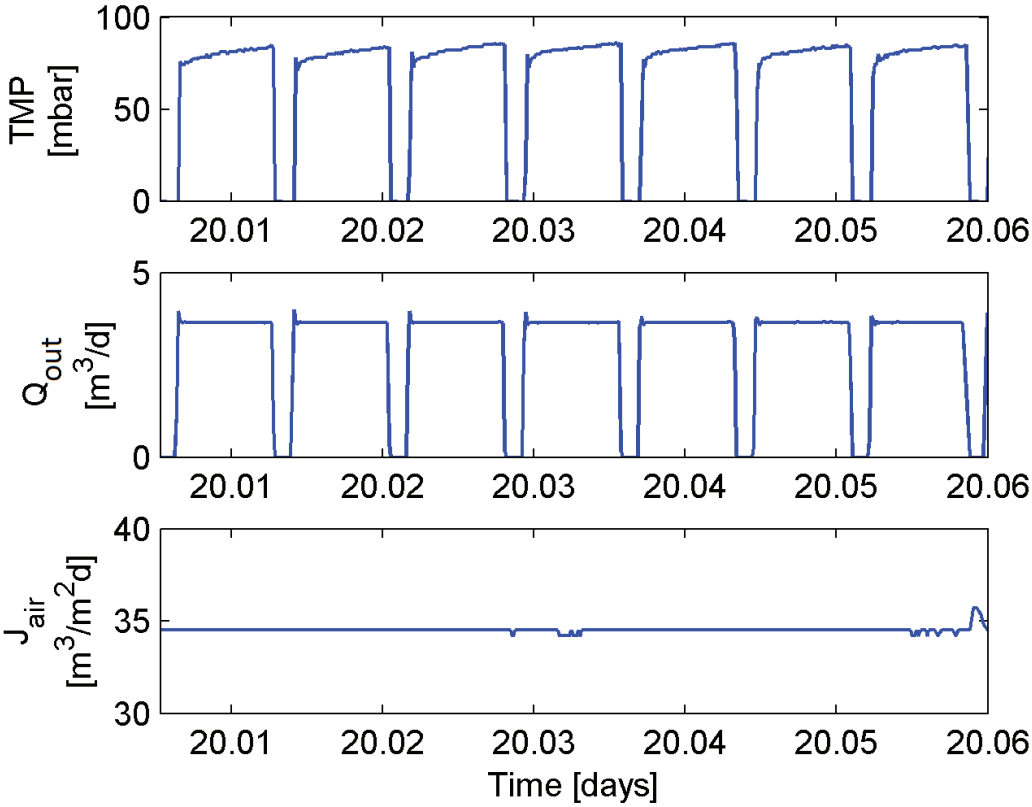


Figure 4.25: *TMP* short-term behavior.

Figure 4.26 shows the simulation results that have a correlation factor of $R^2 = 0.9518$. Following the procedure, the short-term identified parameters are used for the identification of the long-term parameters. Note that the slow phenomena do not interfere in the fast dynamics, meaning that the slow phenomena do not exist in a short period of time, i.e. 0.5 days.

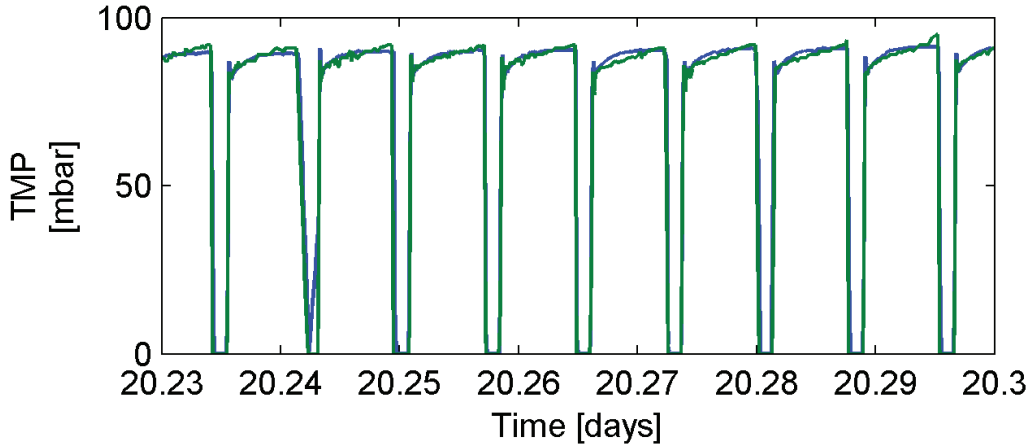


Figure 4.26: Short-term validation : blue is the model and green is the real data.

4.2.8.2 Long-term Identification

For the long-term validation, the larger data set is used, i.e. from days 20 to 50. Equation (4.2) is taken into account and the parameters γ, A_1 and A_2 are thus identified. Their estimated values and sensitivities are shown in Table 4.3.

Table 4.3: Long-term: Identified Parameters

Long-term Parameters	**Values**
K_{air} $[g]$	Short-term identified (see Tab.4.2)
ρ_{rev} $[m/g]$	Short-term identified (see Tab.4.2)
m_0 $[g]$	Short-term identified (see Tab.4.2)
γ $[1/d]$	$-(7.681 \pm 0.002) \times 10^{-2}$
A_1	1.9508 ± 0.3145
A_2	7.0372 ± 3.0632

Figure 4.27 shows the real data TMP, Q_{out}, J_{air}, $Temp$ and X in blue. The model simulation in green. The correlation factor of the TMP is $R^2 = 0.9630$. Note that the model follows the day temperature oscillations. It is important to highlight that if these oscillations are not considered and the process is not analyzed in the long-term, a wrong interpretation of the TMP measurement could be accidentally made: if the TMP decays, this can be explained by the temperature affecting the bulk apparent viscosity and not because of some

implemented control strategy. Taking into account of these natural variations may indeed lead to better fouling control strategies.

The proposed time-scale identification procedure stands for the possible necessity to identify all the parameters taken at the same time and iterate for a new time-scale identification procedure with the identified values. Despite of this, the iteration step is not need due to the cost function found in the identification of all parameters varies at about 0.10%. This result shows the convergence of the cost function in a minimum local.

4.2.8.3 Cross-validation

The cross-validation analysis is performed with a set of data that have not been used for identification purposes. In this study, the cross-validation period is from days 50 to 60. This simulation is presented in Figure 4.27 by the red line, and in more detail in Figures 4.28 and 4.29. Even though these 10 days of data were not used for the identification routine, they still have a *TMP* correlation factor of $R^2 = 0.9512$, showing the capacity of the model to predict *TMP* in a medium-term horizon. It is important to emphasize that although there are small missing data periods, the model continues to predict the process quite well.

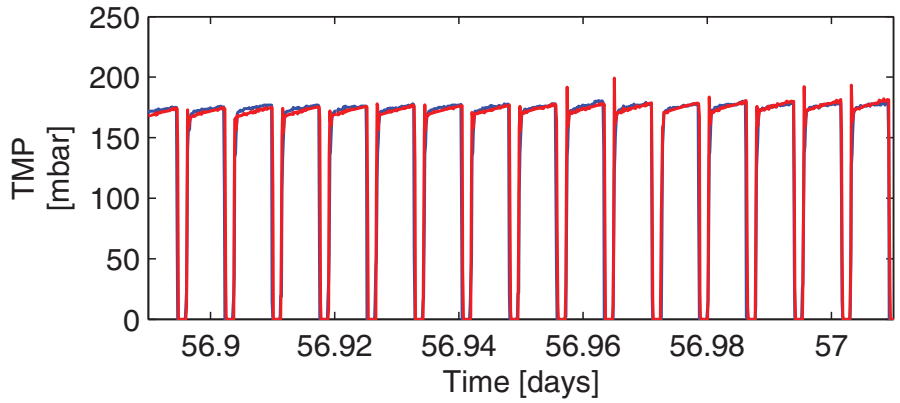


Figure 4.28: Short-term cross-validation. The blue line symbolizes real data and the red line the predicted values

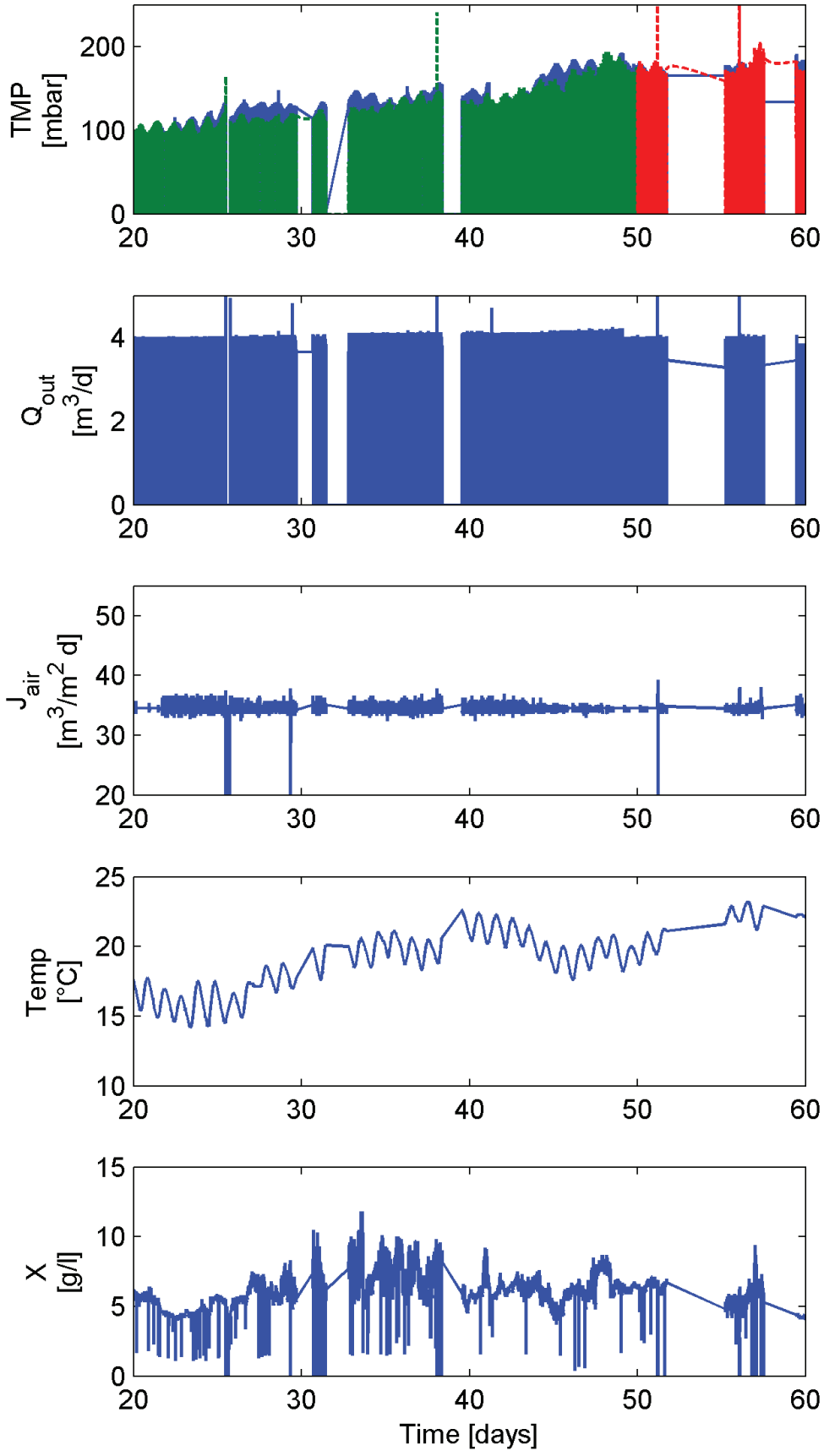


Figure 4.27: Long-term validation: the blue line represents real data, the green line is the identified model and the red line symbolizes the predicted values

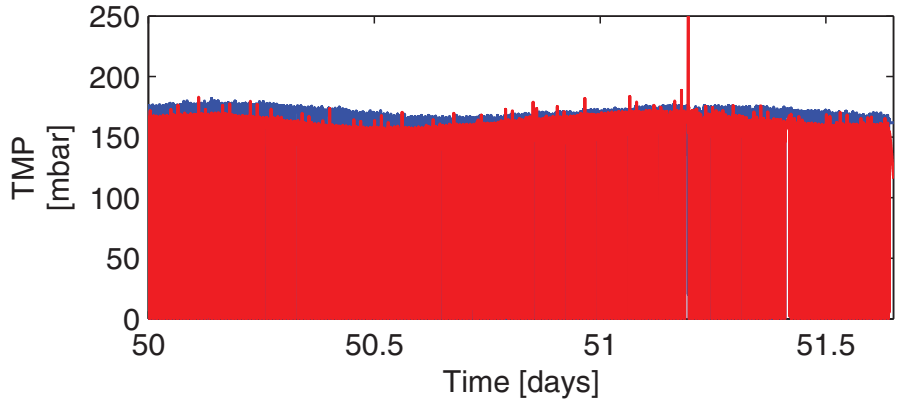


Figure 4.29: Long-term cross-validation detail. The blue line represents real data and the red line predicted values

Figure 4.29 shows a small difference between the experimental data and the model. This could explained by the fact that the proposed model is designed to mimic the main dynamics of the process and some small variation are expected due to the simple model structure. It is important to highlight that the measurement are directly used in the model, no data processing is needed. With that some spikes on the *TMP* estimation are expected. This direct utilization of the measurements, provides the possibility to implement model prediction with online measurements.

The proposed model for an sMBR process has been validated with a large quantity of experimental data, in short and long terms from a WWTP-sMBR. The *TMP* dynamics can be reproduced by the model with an accuracy around $R^2 = 0.95$ validating the model horizon prediction propriety. The time-scale separation based on the fast and slow study simplified and decreased the computational effort on the parameter identification procedure, resulting in the possibility for on-line prediction of *TMP*. As future work, the capacity of the model to predict *TMP* evolution in real-time and *TMP* model-based process control will be studied.

4.3 Analysis of the Identified Parameters

This section presents Table 4.4, which compiles the values of the parameters identified in this chapter and the previous one. An analysis of each parameter is carried out presenting the importance of each for sMBR process modeling.

- β_0: This parameter is identified with GPS-X data,yet it is fixed in the other

two procedures. In the GPS-X simulations, the state m is measured, but not in the others. Thus β_0 is fixed so that the parameter K_{air} can be identified. Experimental trials maybe implemented in order to extract data with sufficient information identify this parameter.

- $\mathbf{K_{air}}$: The values of this parameter have the same magnitude, validating the model structure in three different scenarios.

- $\mathbf{m_0}$: The initial sludge cake mass is set to zero in the GPS-X simulations, but for the experimental data set, m_0 should identified due to the lack of reliable instruments for its measurement. The extremely low value in the RAS-sMBR experiments converge with the experimental results presented in section 4.1.6, showing that the main cause of the fouling is the irreversible fouling, given by equation 2.13.

- $\mathbf{Y}$, $\mu_{\mathbf{S,max}}$ and $\mathbf{K_S}$: The identified parameter ranges are quite similar to values presented in the literature, such as: $\mu_{S,max} = 0.8$, $K_S = 1.0$, $Y = 0.24$ by Henze et al (1987); $\mu_{S,max} = [0.7 - 0.8]$, $K_S = [0.2 - 0.4]$ and $Y = [0.084 - 0.142]$ by Queinnec et al (2006); and $\mu_{S,max} = [0.742 - 1.478]$ by Park et al (2007). It is expected that some values are out of range due to the simplified dynamics imposed into this model.

- γ: The small values identified proves the assumption presented in section 3.2.1. Note that the extremely small value of γ in RAS-sMBR shows that the main mechanism of fouling evolution is the irreversible fouling as m_0 explained before.

- $\mathbf{A_1}$ and $\mathbf{A_2}$: These two parameters are not identified in the simulation with GPS-X as the apparent viscosity is considered constant. Note that the parameter A_1 is larger in the WWTP-sMBR than in the RAS-sMBR. In the case of RAS-sMBR, variations of the water temperature inside the laboratory are not so significant as in plants exposed to daily temperature variations. These oscillations can even be compared, as seen in the *TMP* graphs 4.7,4.8 and 4.27.

- $\rho_{\mathbf{irrev}}$: This parameter is used only in the RAS-sMBR and is directly linked to the fouling evolution. In the other experiment, this parameter is not identified because irreversible resistance is not considered.

- **Data Length**: The length of data used for identifying the parameters are similar in the GPS-X and RAS-sMBR processes, but a larger data window is need to have a acceptable confidence interval for ultra-fast parameters of WWTP-sMBR. A larger quantity of data is needed due to the different measurement sampling time that is bigger in WWTP-sMBR (10 seconds) than in RAS-sMBR (one second), resulting in a identification horizon ten times larger for the WWTP-sMBR than the others.

Even though the model has a very simple structure, the parameters are still interconnecting the mathematical model with physical and biological aspects. It is evident that more experimental data and identification should be carried out for a better understanding of all mechanisms and the validation of the model. Nevertheless, identification and the experimental results presented show the relevance of this simple integrated dynamic model for the design of advanced control strategies in order to optimize this processes.

Table 4.4: Identified Parameters from GPS-X, RAS-sMBR and WWTP-sMBR.

	Parameters	Ultra-Fast Parameters	Fast Parameters	Slow Parameters
GPS-X	$\beta_0\ [m^{-1}]$	$(5.531 \pm 0.643) \times 10^4$		
	$K_{air}\ [g]$	$(4.596 \pm 0.134) \times 10^1$		
	$Y\ [-]$		$(8.985 \pm 0.016) \times 10^{-1}$	
	$\mu_{S,max}\ [d^{-1}]$		(2.265 ± 0.343)	
	$K_S\ [g \cdot m^{-3}]$		0.1^*	
	$\gamma\ [d^{-1}]$			(0.001 ± 0.535)
	Data Length $[d]$	0.02	6	20
RAS-sMBR	$\beta_0\ [m^{-1}]$	$5.5 \times 10^{4*}$		
	$K_{air}\ [g]$	$(4.858 \pm 0.232) \times 10^1$		
	$\rho_{rev}\ [m \cdot g^{-1}]$	$(2.917 \pm 0.168) \times 10^{11}$		
	$m_0\ [g]$	$(9.415 \pm 0.176) \times 10^{-1}$		
	$Y\ [-]$		(0.2323 ± 0.1368)	
	$\mu_{S,max}\ [d^{-1}]$		(0.9152 ± 0.688)	
	$K_S\ [g \cdot m^{-3}]$		(0.090 ± 0.106)	
	$\gamma\ [d^{-1}]$			$-(1.613 \times 10^{-13} \pm 1.64 \times 10^{-5})$
	$A_1\ [-]$			$(9.134 \pm 0.023) \times 10^{-1}$
	$A_2\ [-]$			(7.821 ± 0.017)
	$\rho_{irrev}\ [m^{-2}]$			$(8.328 \pm 0.025) \times 10^7$
	Data Length $[d]$	0.04	3.67	16.28
WWTP-sMBR	$\beta_0\ [m^{-1}]$	$5.5 \times 10^{4*}$		
	$K_{air}\ [g]$	$(3.502 \pm 0.047) \times 10^1$		
	$\rho_{rev}\ [m \cdot g^{-1}]$	$(4.416 \pm 2.637) \times 10^{10}$		
	$m_0\ [g]$	$(9.748 \pm 1.4893) \times 10^1$		
	$\gamma\ [d^{-1}]$			$-(0.0768 \pm 0.0024)$
	$A_1\ [-]$			(1.950 ± 0.314)
	$A_2\ [-]$			(7.037 ± 3.063)
	Data Length $[d]$	0.4		30

*Constant value

Chapter 5

Control Strategies for sMBRs

The grueling task of mathematical modeling living organisms and the small quantity of reliable instrumentation suited to real-time monitoring on the market can be considered as the main cause for introducing modern optimization and control strategies to bioprocesses, which are considered non-trivial tasks (Van Impe et al, 1998).

Normally, a controller is designed when the process outputs do not fulfill the expectations in a certain sense (i.e. effluent quality, volume quantity, *TMP*, etc.). Generally, the objective of a designed controller is to perform modifications in the system to alter its dynamics, driving the process towards a region of interest (Distéfano, 1974).

The sMBR control problem can be divided into open- and closed-loop controllers, which acts in the filtration, biological or both processes (Ferrero et al, 2011). The open-loop controller is normally obtained by process trials, resulting in a fixed time history for actuators. The closed-loop controllers use process measurements to compute a control action that is introduced to the system through an actuator (e.g. pump, valve, timer, etc.).

In sMBR processes, the connections between filtration, fouling formation and biotransformation elevate the complexity in the design and application, of a controller in this case, even more.

In Section 3.2.1, the benefit to decouple the process in three time-scales is analytically demonstrated. The possibility to split the process has been instinctively used by the sMBR process operators, when only the biological degradation or filtration are taken into account. This fact allowed open-loop techniques to be designed, in order to control the fouling separately from the biological degradation. One of these techniques imposes to increase effluent flow steps and monitors *TMP* stability at each step. When the *TMP* is no

longer stable (no linear relation) at each flux step and increases rapidly to indicate rapid accumulation of foulants, this is usually referred as the *critical-flux* (Le-Clech et al, 2006).

Open-loop strategies, such as physicochemical pretreatment process, can also be applied. This procedure is widely and successfully used due to its low cost and relatively easy operation with coagulation regents, ozone and bio-filters (Gao et al, 2011).

Implementing closed-loop strategies on sMBRs is not so simple. Nonetheless, one of the strategies is to optimize filtration efficiency by controlling the concentration profile of the sludge cake layer (reversible layer), which is indirectly measured by the *TMP* and can be positively influenced by a suitable air-flow regime along the membrane. The formation of the concentration profile directly influences the sludge cake layer upon total filtration resistance. One mode, to enhance the sludge cake detachment from membrane surface, applies on air pulsing strategy. Another mode, adds more power in the shearing air blowers to enhance shearing forces onto membrane surface, but this results in a higher energetically expensive process (Ferrero et al, 2011; Wintgens et al, 2003).

The biological aspect is normally optimized using one or more closed-loop controllers to control the exchange of biodegradable nutrients between tanks. This is achieved by changing the SRT and HRT of the process. In most cases, the design of the closed-loop controller takes ideal filtration into account, i.e. a membrane with no efficiency degradation, as presented by Maere et al (2011).

Some authors make reference to these strategies as a way to optimize the sMBR processes, however this cannot be considered as global optimization, which takes into account the whole process, but rather as an optimization for one part of the system. Due to the process 'living' aspect, the process characteristics may change easily due to environmental conditions (influent characteristics, water temperature, etc.).

In the following two studies, a nonlinear model predictive control (NMPC) and a partial state-feedback linearizing controller based on a quadratic control-Lyapunov function are proceeded using the proposed integrated model in order to stabilize the fouling evolution.

5.1 NMPC to a WWTP fitted with an sMBR

The objective of this study is to design a nonlinear model predictive control (NMPC) to a wastewater treatment plant (WWTP) with a submerged membrane biorector in order to minimize the irreversible resistance while keeping the trans-membrane pressure, which is a good indicator of membrane fouling, at an acceptable level. To this end, the manipulated variables are the permeate flow and the air scouring flow, which allow the material layer formed on the membrane (in short, the "sludge cake") to be detached. The NMPC structure is tested in simulation, considering a detailed simulator as the reference process and the proposed reduced-order model as the predictor.

The macroscopic model structure of proposed model (2.16), characterized by a modest size, allows the nonlinear model predictive control (NMPC) application that has been used in industrial process control with an impressive success rate in the last decades (Kouvaritakis and Cannon, 2001). In the present case, NMPC can be used to act on the irreversible fouling resistance of the membrane while maintaining the trans-membrane pressure (*TMP*) at an acceptable level using the combination of permeate flow and air scouring flow (or air cross-flow).

The detailed biological sub-model proposed by Mannina et al (2011) is a modified version of the well-known ASM1 (Henze et al, 2000), which takes the influence of SMPs into account. In short, the model uses Monod-type kinetics for the degradation of the different substrates and mass balance equations for the different substrate modeling biomass growth, biomass decay, ammonia and carbon removal processes. For a better readability the filtration sub-model presented section 3.4 is revisited with more details. The detailed filtration sub-model is an improved version of the model proposed by Li and Wang (2006). This model is a resistance in series model with total resistance modeled as follows:

$$R_{total,Mannina} = R_m + R_p + R_{sc} + R_{dc} \tag{5.1}$$

where R_m is the intrinsic membrane resistance, R_{irrev} is the irreversible resistance, which can only be removed by chemical cleaning while R_{rev} denotes the reversible resistance that is affected by the air cross-flow.

The specific pore-blocking resistance R_p is proportional to the amount of permeate produced and is computed through the terms of the filtrate volume

(r_p).

$$R_p = r_p \sum J t_f \tag{5.2}$$

J $[m^3/m^2 d]$ is the filtration flux, t_f is the duration of the filtration period. The stable sludge cake resistance R_{sc} and the dynamic sludge cake resistance R_{dc} are presented in equations (5.3a) and (5.3b).

$$R_{sc} = r_{sc} \cdot M_{sc} \tag{5.3a}$$

$$R_{dc} = r_{dc} \cdot M_{dc} \tag{5.3b}$$

These expressions include M_{sc} $[kg/m^2]$ that denotes the stable sludge cake mass and M_{dc} $[kg/m^2]$ the dynamic sludge cake mass onto membrane surface.

$$\begin{cases} \dfrac{dM_{sc}}{dt} = \dfrac{24 C_{ss} J^2}{24J + C_d d_p G} - \dfrac{\beta_b (1-\alpha_b) G M_{sc}^2}{\gamma_b V_f t + M_{sc}} & (5.4a) \\ \dfrac{dM_{dc}}{dt} = \dfrac{-\beta_b (1-\alpha_b) G M_{dc}^2}{\gamma_b V_f t + M_{dc}} & (5.4b) \end{cases}$$

where C_{ss} $[kg/m^3]$ is the sludge concentration, C_d is the coefficient of the drag and lift force, $d_p[m]$ is the particle size, β_b is the erosion rate coefficient of the dynamic sludge film, α_b is the stickiness of the biomass particle, γ_b $[kg/m^3 s]$ is the compression coefficient for the dynamic sludge film, V_f is water production within a filtration period of an operation cycle, t $[d]$ is time and G $[s^{-1}]$ is the shear intensity

$$G = \sqrt{\frac{\rho_w \cdot g \cdot Q_{air}}{\mu_w}} \tag{5.5}$$

where ρ_w and μ_w are the density and viscosity, respectively, of the sludge mixture, Q_{air} is the air cross-flow and g is the gravitational constant. All parameters are presented in the first column of Table 3.1.

5.1.1 NMPC-sMBR Process Control

The main motivation behind the development of a simple dynamic model is the potential of applying advanced model-based control as NMPC. The advantage of this control technique is its ability to handle model nonlinearity and various types of constraints on the actuators and state variables (Santos et al, 2012).

NMPC uses a model to predict the trajectory of the system on a prediction horizon and computes an optimal control sequence on a sliding horizon (Allgöwer et al, 2004). The first important element is therefore a nonlinear model in the form:

$$\dot{x} = f(x(t), u(t)), \quad x(0) = x_0, \tag{5.6}$$

together with constrains in the form $u(t) \in \mathbf{U}$, $\forall t \geq 0, x(t) \in \mathbf{X}$, $\forall t \geq 0$ where $x(t) \in \mathbb{R}^n$ and $u(t) \in \mathbb{R}^m$ are the vector of states and inputs, respectively. The sets $\mathbf{U}$ and $\mathbf{X}$ are compact and can be represented by $\mathbf{U} := u \in \mathbb{R}^m | u_{min} \leq u \leq u_{max}$, and $\mathbf{X} := x \in \mathbb{R}^n | x_{min} \leq x \leq x_{max}$ with the constant vector u_{min}, u_{max} and x_{min}, x_{max}.

The NMPC control moves are usually the results of a finite horizon open-loop optimal control problem, which is solved at every sampling instant. In generic notation, the NMPC problem can be expressed as:

$$\min_{\phi_u(\cdot)} J_{NMPC}(x(t), \phi_u(\cdot))$$

$$\text{s.t. } \dot{\phi_x}(\tau) = f(\phi_x(\tau), \phi_u(\tau)), \phi_x(t) = x(t), \tag{5.7a}$$

$$\phi_u(\tau) = \phi_u(t + T_c), \forall \tau \in [t + T_c, t + T_p], \tag{5.7b}$$

with the cost function

$$J_{NMPC}(x(t), \phi_u(\cdot)) := \int_t^{t+T_p} F(\phi_x(\tau), \phi_u(\tau)) d\tau;$$

where $\phi_u(\tau) \in \mathbf{U}$, $\forall \tau \in [t, t + T_c]$, $\phi_x(\tau) \in \mathbf{X}, \forall \tau \in [t, t + T_p]$, T_p and T_c are the prediction and control horizon with $T_c \leq T_p$. $\phi_x(\cdot)$ denotes the new value of the state $x(\cdot)$ computed by the closed loop equation $\dot{\phi_x}$ using the new input value ϕ_u found by the optimization problem for each instant over the moving finite horizon T_c (see figure 5.1).

The cost function, equation (5.8), is chosen based on the process desired performance and the first choice for the cost function is often the quadratic function. Positive weighting matrices (Ω_1 and Ω_2) can also be included in the cost function:

$$F(x, u) = (x - x_{ref})^T \Omega_1 (x - x_{ref}) + (u - u_{ref})^T \Omega_2 (u - u_{ref}). \tag{5.8}$$

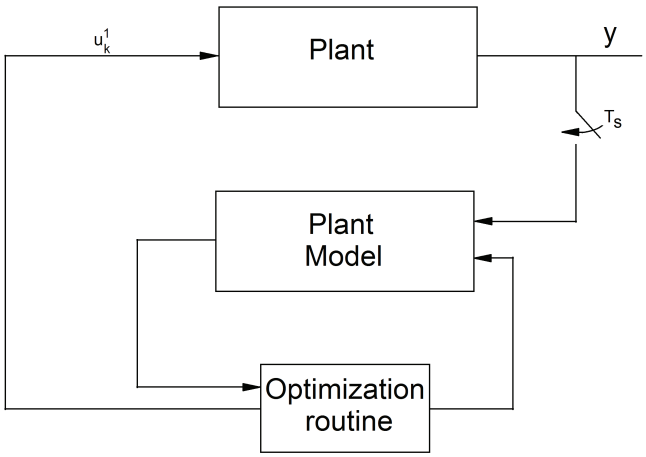


Figure 5.1: NMPC-Scheme

Table 5.1: Input concentrations of the sMBR and physical model parameters

Compound	Units	Value	Compound	Units	Value
S_I	$[gCOD\ m^{-3}]$	30.00	S_S	$[gCOD\ m^{-3}]$	0.77
X_I	$[gCOD\ m^{-3}]$	3554.43	X_S	$[gCOD\ m^{-3}]$	59.35
X_{BH}	$[gCOD\ m^{-3}]$	3572.44	X_{BA}	$[gCOD\ m^{-3}]$	311.33
X_P	$[gCOD\ m^{-3}]$	2373.11	S_O	$[g\ m^{-3}]$	2.19
S_{NO}	$[gN\ m^{-3}]$	11.54	S_{NH}	$[gN\ m^{-3}]$	0.33
S_{ND}	$[gN\ m^{-3}]$	0.63	X_{ND}	$[gN\ m^{-3}]$	4.40
V	$[m^3]$	0.19	A	$[m^2]$	0.93
			r_p	$[m^-2]$	1.4×10^{14}

where x_{ref} and u_{ref} are the desired reference of a state and an input, respectively.

5.1.2 Simulation Results

Both models, the descriptive model from Mannina et al (2011) and the simplified model, equation (2.16), are implemented in the *Matlab* environment. The *TMP* is computed controlling the Q_{out}, i.e. $TMP = \frac{Q_{out}}{A}\eta R_{total}$ and J_{air}. The biological process inputs and the descriptive model parameters can be found in Table 5.1.

First, the parameters of the simplified model are identified based on some prior experiments (see Pimentel et al (2015b) for the details of the parameter estimation procedure or Section 3.5, which is based on a time-scale separa-

tion). The identified parameters are presented in Table 5.2.

Table 5.2: Parameter Calibration

Parameters	Values
K_{air} $[g]$	9.3367×10^6
ρ_{rev} $[m \cdot g^{-1}]$	2.0229×10^{10}
m_0 $[g]$	4.4869
γ $[d^{-1}]$	0.0194
Y $[-]$	1.8558
$\mu_{S,max}$	0.0781

Following the model calibration, the NMPC methodology is applied using the simplified model (2.16) as a predictor. The cost function is defined as:

$$F(x,u) = (\Omega_1 Q_{out} t^2)^2 + (\Omega_2 (TMP - TMP^*))^2 \tag{5.9}$$

where the effluent multiplied by the square of the time is minimized in order to significantly reduce the irreversible resistance and at the same time maintain the trans-membrane pressure at desired set-point TMP^* and Ω_i are the scaling factors. Note that the irreversible resistance depend on the permeate flow and time that should be minimized to enlarge the periods between chemical cleaning. The following constraints are added: (i) $Q_{out} \geq 0$ for the physical range of the permeate pump and (ii) $J_{air} \geq 0$ for the cross-flow range. The methodology is applied using the *Matlab* code presented by Grüne and Pannek (2011).

The results presented in Figure 5.2 are obtained assuming that all the state variables are measured. The NMPC uses a sampling time of one day, while a prediction horizon $T_p = 3$ days and a control interval of $T_c = 1$ day.

The first plot in Figure 5.2, represents TMP computed with the total resistance equation (5.1). Note that, in blue, it is possible to see the influence of the reversible resistance and, in green, the influence of the irreversible resistance on the TMP value. The set-point TMP^* is represented by a red line, which is set to 100 $mbar$. To maintain the desired set-point, the controller increases the air cross-flow (Q_{air}/A or J_{air}) and, at the same time, maintains the permeate flow (Q_{out}) in a constant value. These input values are presented in the last two plots of Figure 5.2. The decay of sludge cake mass, observed in the second plot, shows that the sludge cake resistance (R_{rev}) is much more important than the irreversible resistance at the beginning of the

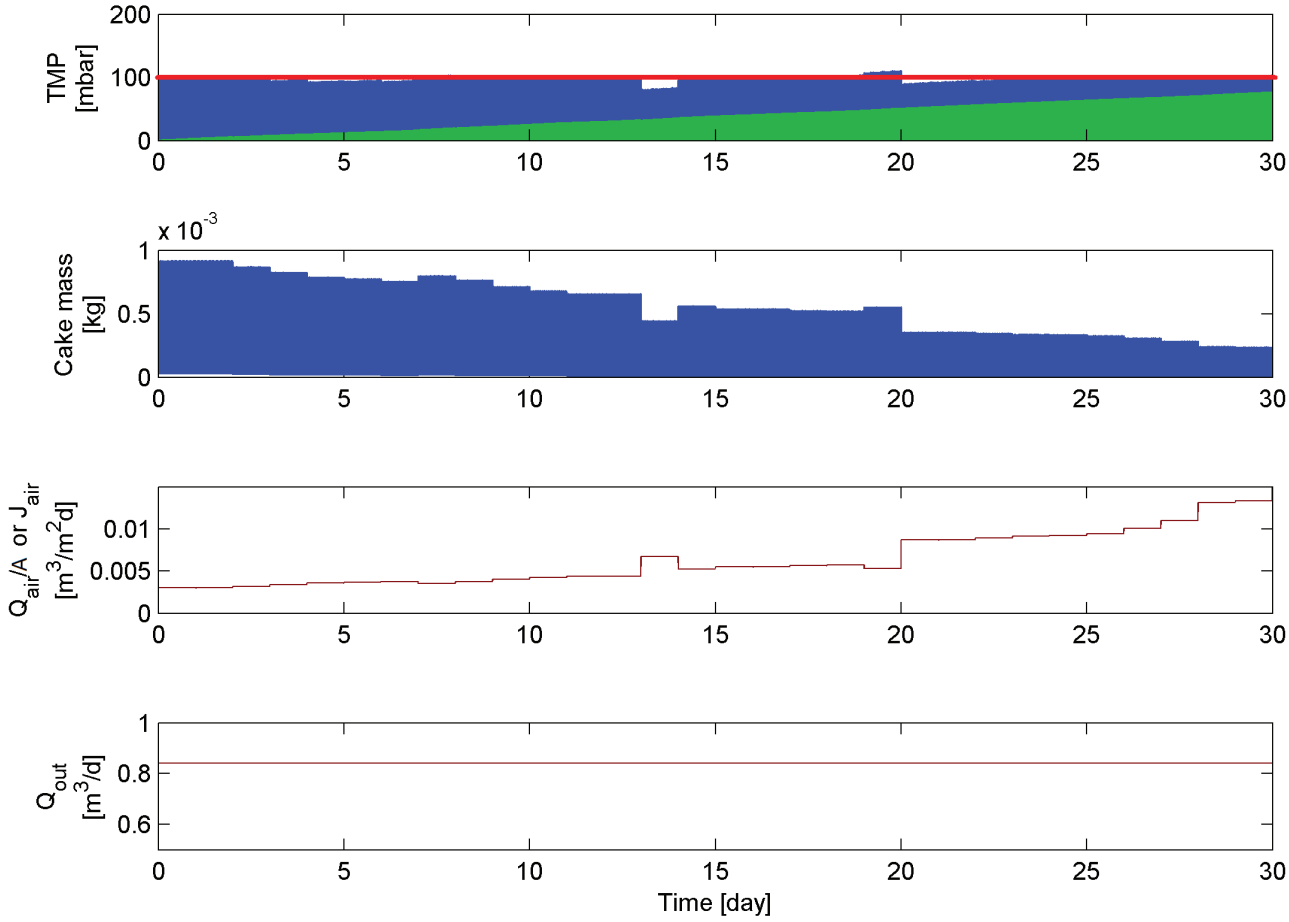


Figure 5.2: The NMPC acting on the descriptive process.

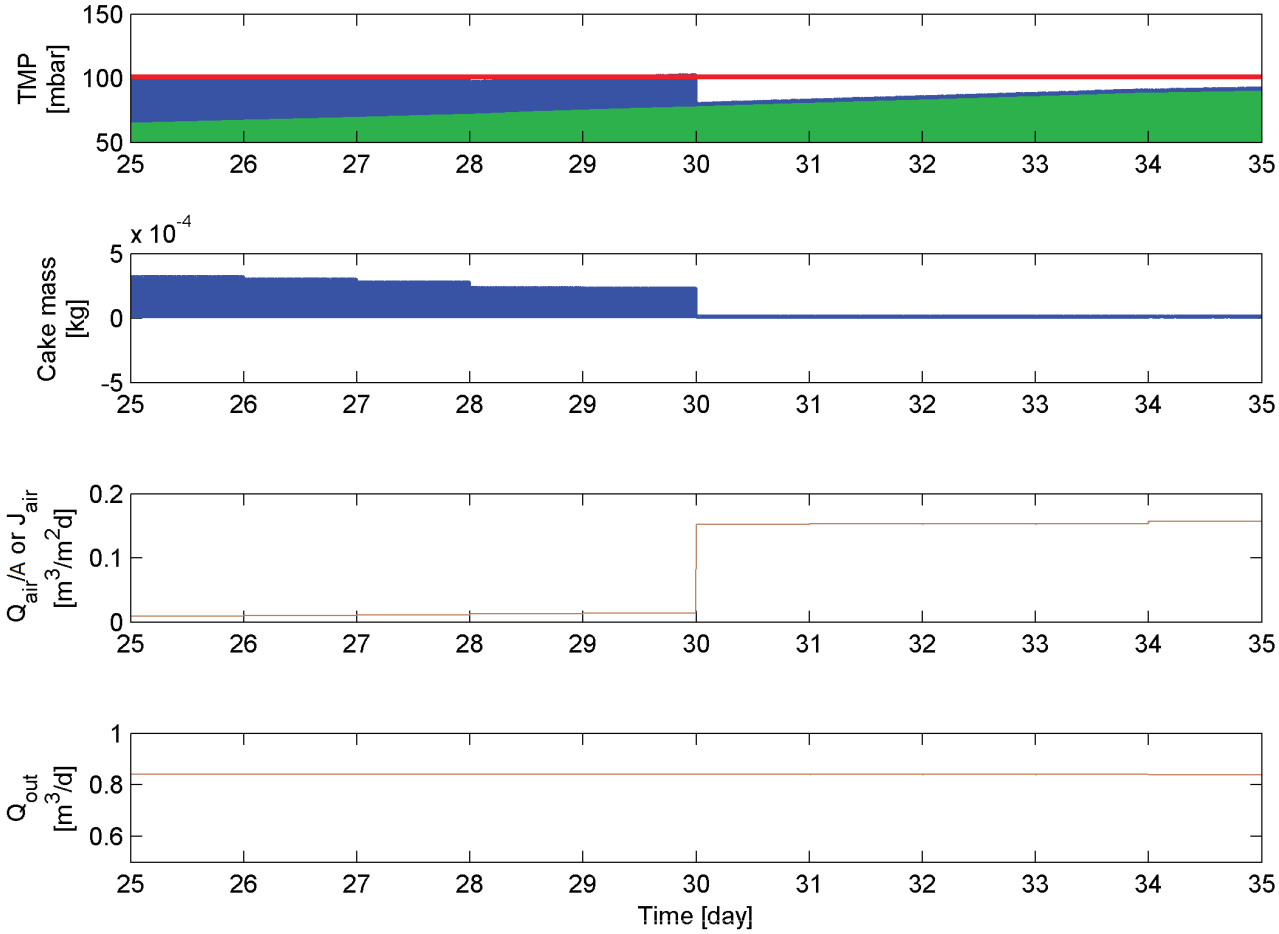


Figure 5.3: Blue is the sludge cake influence on *TMP* and green is the irreversible resistance on *TMP*.

process, matching the observations of Mannina et al (2011). It is important to highlight that the controller actions maintain the desired set-point even though some nonlinearities are not modeled in the simplified model.

The behavior of the controller when the irreversible resistance becomes more important than the sludge cake is shown in Figure 5.3. This occurs around day 30 where the sludge cake mass is extremely small, see second plot in Figure 5.3. To keep the *TMP* at the selected set-point the controller acts vigorously by changing the air cross-flow, as seen in the third plot. The reversible cake reaches its minimum value. When the maximum *TMP* value is reached, a chemical cleaning is required, or a larger trans-membrane pressure has to be selected.

The results show that the process can be regulated until the irreversible resistance takes the main role in the fouling resistance. When this state is

reached, a chemical cleaning is required, or a larger trans-membrane pressure has to be accommodated.

5.2 Partial state-feedback linearizing control based on a quadratic control-Lyapunov function

Linearizing feedback has been largely studied since the 90s and its applications have been proposed to many different fields, including aeronautics, robotics and bioprocesses. However, its main drawbacks lie in the model quality which should closely represent real process dynamics (Slotine and Li, 1991).

The objective of this approach is via feedback to transform a nonlinear dynamic system in a fully or partially linear system (in closed-loop), allowing linear behavior. Figure 5.4 illustrates this strategy, where the signal v is the resulting linear system, u is the linearizing input and y is the output signal.

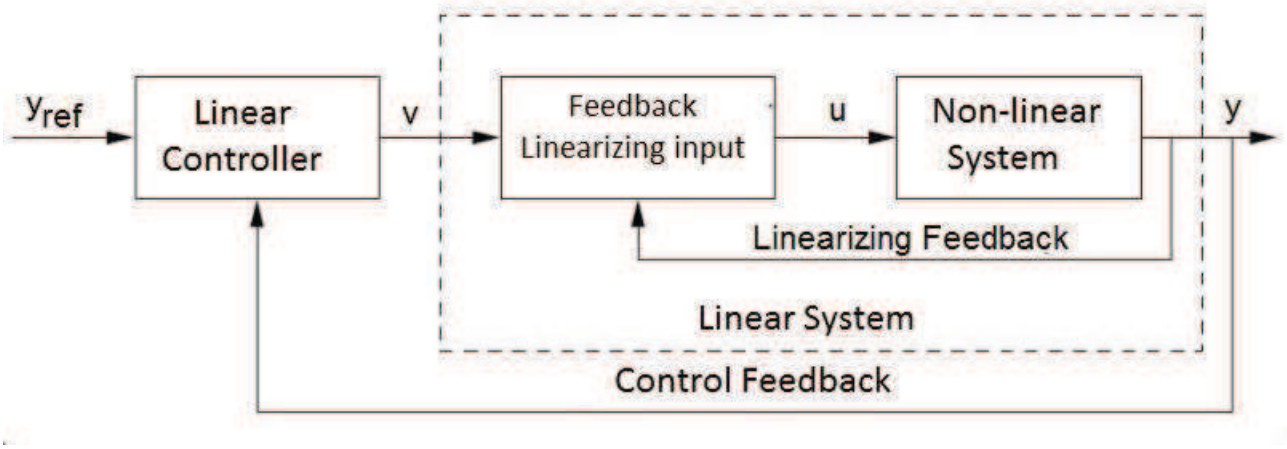


Figure 5.4: Linearizing control structure

In short, there are two ways to obtain a linear dynamic for feedback. The first is called the input-state feedback (or *input-state linearization*) where all state-variable dynamics of the system are linearized. The second is performed from an input-output point of view (*input-output linearization*). This approach emphasizes the linearization map between the input v and the output y of the system. Essentially, linear dynamics are obtained by canceling of nonlinearities by applying a nonlinear control signal at the input u. It can be said that its main drawback is the need of exact cancellation of nonlinearities, therefore

it is necessary to have a perfect knowledge of the dynamics system. When the system dynamics to be linearized are uncertain, the system response may perform poorly or even become unstable when applying a linear controller to the outer-loop process (Henson and Seborg, 1997).

To avoid (or reduce) some of the abovementioned problems, a partial linearizing feedback may be applied where only desired nonlinearities are canceled:(*i*) in order to increase the robustness of the control law; and (*ii*) to reduce the number of states to be used in the implementation of feedback (Freeman and Kokotović, 1997).

The linearizing feedback law can be applied to a nonlinear system when this is represented in a controllable canonical form (or "companion form"). A system in controllable canonical form can be represented as like so:

$$\begin{bmatrix} \dot{\xi}_1 \\ \vdots \\ \dot{\xi}_{r-1} \\ \dot{\xi}_r \\ \dot{\zeta} \end{bmatrix} = \begin{bmatrix} \xi_2 \\ \vdots \\ \xi_r \\ f(\xi) + b(\xi)u \\ g(\xi, \zeta) \end{bmatrix} \tag{5.10}$$

where $\xi = [\ y \ \ dy(t)/dt \ \ \cdots \ \ d^{r-1}y(t)/dt^{r-1}\ ]'$ and $\zeta \in \mathbb{R}^{nr}$ compose the state vector, $\mathrm{u} \in \mathbb{R}$ is the control signal, y the output of interest (to be linearized by feedback), $f(\xi)$ and $b(\xi)$ nonlinear functions in ξ and $g(\xi, \zeta)$ is a nonlinear function in (ξ, ζ). The dynamic $\dot{\zeta} = g(0, \zeta)$ is known as zero dynamic system and the r index is known as a relative degree of the system. To demonstrate this method easily, the following is assumed: (*a*) a nonlinear system to be linearized by feedback should be represented in the controllable canonical form; and (*b*) vector $b(\xi) \neq 0$ for every ξ of interest; and (*c*) the zero-dynamic is asymptotically stable throughout the area of interest. From these simplifying assumptions, input-output linearizing feedback is given by:

$$\mathrm{u}(t) = \frac{1}{b(\xi)}\Big(\mathrm{v}(t) - f(\xi)\Big) \tag{5.11}$$

where $\mathrm{v}(t)$ is the new entry system with a linear mapping output $\mathrm{y}(t)$.

An arbitrary linear dynamic can then be imposed by a control law:

$$\mathrm{v}(t) = -\Big(k_1\xi_1 + k_2\xi_2 + \cdots + k_r\xi_r\Big) \tag{5.12}$$

where k_i are constants that define the resulting linear dynamic.

5.2.1 Formula for Feedback

An universal feedback formula approach was proposed by Sontag (1998), which uses the control-Lyapunov function in order to construct a feedback stabilizer. The advantage of this methodology lies on the fact that is not necessary to rewrite the system in a specific form as the canonical form or find a linearizing input feedback. Nevertheless, the task to find a control-Lyapunov function is not trivial. Note that this method:(i) is for scalar input only and (ii) does not allow input constraints to be considered. Nonetheless, inspired by this method, we propose in Section 5.2.1.2 the design of a control law that satisfies the inputs constraints, playing with the fact that two control variables are available with our model.

5.2.1.1 Control-Lyapunov Function

In control theory, a control-Lyapunov function $\mathbf{V}(x,u)$, considering x as the states and u the input, is a generalization of the notion of the Lyapunov function $\mathbf{V}(x)$ used in stability analysis (Sontag, 1998).

Definition 5.2.1. *A local control-Lyapunov function for the system Σ (relative to the equilibrium state x^0) is a continuous function $\mathbf{V} : \mathcal{X} \to \mathbb{R}$ for which there is some neighborhood $\mathcal{O}$ of x^0 such that the following properties hold:*

1. $\mathbf{V}$ *is* **proper at** x^0, *that is,*

$$x \in \mathcal{X} \mapsto \mathbf{V}(x) \leq \varepsilon$$

is a compact subset of $\mathcal{O}$ for each $\varepsilon > 0$ small enough.

2. $\mathbf{V}$ *is* **positive definite** *on $\mathcal{O}$:*

$$\mathbf{V}(x^0) = 0, \text{ and } \mathbf{V}(x) > 0 \text{ for each } x \in \mathcal{O}, x \neq x^0.$$

3. *For each $x \neq x^0$ in $\mathcal{O}$ there is some time $\varphi \in \mathcal{T}, \varphi > 0$, and some control $u \in \mathcal{U}^{[0,\varphi)}$ admissible for x such that, for the path $\xi = \psi(x,u)$ corresponding to this control and this initial state,*

$$\mathbf{V}(\xi(t)) \leq \mathbf{V}(x) \forall t \in [0,\varphi)$$

and

$$\mathbf{V}(\xi(\varphi)) < \mathbf{V}(x).$$

A **global control-Lyapunov function for** Φ *(relative to* x^0*) is a continuous* $\mathbf{V}$ *which is (globally) proper, that is, the set*

$$\{x \in \mathcal{X} \text{ such that } \mathbf{V}(x) \leq L\} \tag{5.13}$$

is compact for each $L > 0$*, and such that (2) and (3) are satisfied with* $\mathcal{O} = \mathcal{X}$*. For systems without control, it is said simply (local or global)* **Lyapunov function** *(Sontag, 1998).*

5.2.1.2 Partial state-feedback linearization

From these definitions of the control-Lyapunov function, a linearizing partial state-feedback controller is designed based on the universal formula of feedback. The following input-output system is represented:

$$\begin{cases} \dot{x} = f(x,u),\ x \in \mathbb{R}^n, u \in \mathbb{U} \\ y = h(x), y \in \mathbb{R}^p \end{cases} \tag{5.14}$$

where $\mathbb{U} \subseteq \mathbb{R}^m$ is a non-empty compact set and $h(x)$ is its output dynamics.

The objective is to globally stabilize y around the reference value called y^*. The dynamics of y are united:

$$\dot{y} = \frac{\partial h}{\partial x} f(x,u) = g(x,u) \tag{5.15}$$

For this a function $\mathbf{V}(\cdot)$ is chosen where $\mathbf{V} : \mathbb{R}^p \mapsto \mathbb{R}^+$ such that $\mathbf{V}^{-1}(0) = \{y^*\}$, $\mathbf{V}(y) \to +\infty$ when $\|y\| \to +\infty$. The state feedback is designed as $u = \phi(x)$ such that $\mathbf{V}(\cdot)$ is a partial control-Lyapunov function for the closed-loop system, when the following inequality is fulfilled:

$$\frac{\partial \mathbf{V}}{\partial y} g(x, \phi(x)) = -W(y) \tag{5.16}$$

where $W(\cdot) \geq 0$ and $W^{-1}(0) = \{y^*\}$.

A linearizing feedback is such that $W(y) = \lambda \mathbf{V}(y)$ where λ is a positive constant.

The particular case of $p = dim(y) = 1$ and $dim(u) = 2$ is considered for an output dynamic of the following form:

$$\dot{y} = G_1(x)u_1 - G_2(x)u_2 \tag{5.17}$$

with $G_1(x) > 0$, $G_2(x) > 0$ $\forall x \in \mathbb{D}$ invariant domain of the x-dynamics, when the input constraints are $u_1 \geq 0$ and $u_2 \geq 0$.

The following partial state-feedback linearization law is proposed:

$$\left\{ \begin{array}{l} \phi_1(x) = -\lambda \frac{\mathbf{V}(y)}{\mathbf{V}'(y)G_1(x)} \\ \phi_2(x) = 0 \end{array} \right| \text{when } \mathbf{V}'(y) \leq 0 \tag{5.18}$$

$$\left\{ \begin{array}{l} \phi_1(x) = 0 \\ \phi_2(x) = \lambda \frac{\mathbf{V}(y)}{\mathbf{V}'(y)G_2(x)} \end{array} \right| \text{when } \mathbf{V}'(y) \geq 0 \tag{5.19}$$

where $\mathbf{V}'(y) = \frac{\partial \mathbf{V}}{\partial y}$, ϕ_1 is the new input u_1 and ϕ_2 is the new input u_2.

If the constraints u_1,u_2 are:

$$u_1 \geq \underline{u_1} > 0 \;\; u_1 \geq \underline{u_2} > 0 \tag{5.20}$$

and $\varpi = \max\left[\underline{u_1} \max_x G_1(x), \underline{u_2} \max_x G_2(x)\right]$, the static feedback is considered as follows:

$$\phi_1(x) = \left[\begin{array}{c} \left(-\lambda \frac{\mathbf{V}(y)}{\mathbf{V}'(y)} + \varpi\right) \frac{1}{G_1(x)} \\ \frac{\varpi}{G_2(x)} \end{array} \right] \text{when } \mathbf{V}'(y) \leq 0 \tag{5.21}$$

$$\phi_2(x) = \left[\begin{array}{c} \frac{\varpi}{G_1(x)} \\ \left(\lambda \frac{\mathbf{V}(y)}{\mathbf{V}'(y)} + \varpi\right) \frac{1}{G_2(x)} \end{array} \right] \text{when } \mathbf{V}'(y) \geq 0 \tag{5.22}$$

where $\phi_1(x) \geq \underline{u_1}$, $\phi_2(x) \geq \underline{u_2}$ and Φ is continuous at $y = y^*$. Several functions $\mathbf{V}()$ can be considered. In the next Section only a quadratic function is considered. A first preliminary study about the influence of the choice of the function $\mathbf{V}()$ has been conducted and is reported in the Appendix.

5.2.2 Stabilizing Sludge Cake Mass

Considering the fast and slow dynamics analysis, the cake build-up can be controlled as a decoupled process. The stabilization of the cake build-up, around a certain value m^*, is one of the most important tasks in the submerged

membrane bioreactor operation and maintenance in order to prevent low effluent flow and the decrease of filtration efficiency.

A quadratic candidate-Lyapunov function

$$\mathbf{V}(m) = \frac{1}{2}(m - m^*)^2, \tag{5.23}$$

where m is the cake mass and its dynamic is ruled by equation (5.24) and m^* is the desired reference value, is chosen.

$$\frac{dm}{dt} = Q_{out}X - J_{air}\mu_{air}(m)m \tag{5.24}$$

When equation (5.24) is analyzed, two inputs can be distinguished which then act to prevent cake build-up: the permeate pump flow Q_{out}, which is linked to the particle attachment, and the air cross-flow J_{air}, which is linked to the cake detachment. Both inputs are positive and bounded. In this study, the irreversible layer is neglected. These two inputs are used for the sludge cake stabilization around the m^*, considered a positive nonzero value.

The following two linearizing inputs are obtained when equations (5.18) and (5.19) are applied to the system:

$$u_{Q_{out}} = \frac{-\lambda(m - m^*)X + J_{air}\mu_{air}(m)}{X}\ ,\ u_{J_{air}} = \frac{\lambda(m - m^*) + Q_{out}X}{\mu_{air}(m)m} \tag{5.25}$$

In order to maintain positivity of the process inputs, the control law must be divided into two cases: $m \geq m^*$ and $m \leq m^*$. In the first case, J_{air} should be more vigorous to detach the sludge mass from the membrane surface, and , in second case, Q_{out} should be more vigorous.

$$\begin{cases} m \geq m^* \quad u_{Q_{out}} = 0 \quad u_{J_{air}} = \frac{\lambda(m-m^*)}{\mu_{air}(m)m} \\ m \leq m^* \quad u_{J_{air}} = 0 \quad u_{Q_{out}} = \frac{-\lambda(m-m^*)}{X} \end{cases} \tag{5.26}$$

In this case, the objective of the controller driving m to m^* is fulfilled, but when m^* is reached Q_{out} and J_{air} are set to zero. This is a undesired behavior, because process stops once the set-point is reached.

It is much more convenient to design a control law which drives m to the set-point and, at the same time, maintain $u_{Q_{out}} > 0$ and $u_{J_{air}} > 0$.

The next control law, equation (5.27), has constant values of Q_{out} and J_{air}.

$$\begin{cases} m \geq m^* & u_{Q_{out}} = \bar{u}_{Q_{out}} \qquad u_{J_{air}} = \frac{\lambda(m-m^*)+\bar{u}_{Q_{out}}X}{\mu_{air}(m)m} \\ m \leq m^* & u_{J_{air}} = \bar{u}_{J_{air}} \quad u_{Q_{out}} = \frac{-\lambda(m-m^*)+\bar{u}_{J_{air}}\mu_{air}(m)m}{X} \end{cases} \tag{5.27}$$

Analyzing equations (5.25), it is possible to rewrite two positive control laws depending on the sludge cake mass set-point.

$$\begin{cases} m > m^* & \bar{u}_{Q_{out}} = \frac{\omega}{X} \qquad \bar{u}_{J_{air}} = \frac{\lambda(m-m^*)+\omega}{\mu_{air}(m)m} \\ m < m^* & \bar{u}_{J_{air}} = \frac{\omega}{\mu_{air}(m)m} \quad \bar{u}_{Q_{out}} = \frac{-\lambda(m-m^*)+\omega\mu_{air}(m)m}{X} \end{cases} \tag{5.28}$$

When applied to equation (5.24), the process dynamic is reduced to a linear dynamic $\frac{dm}{dt} = -\lambda(m - m^*)$. An $\omega > 0$ is added in the control law to have both inputs bigger than zero during all the process. This is more convenient than turning off the permeate pump or air cross-flow blowers when sludge cake mass reaches the set-point. Note that this constant does not interfere in the control law performances.

It is important to highlight that due to the process characteristics, the sludge cake mass can have values close to zero, but it is physically impossible for it to have $m = 0$ due to environmental and membrane material composition characteristics (see Chapter 1). This tendency guarantees that the linearizing inputs will never reach infinite values (see $\bar{u}_{J_{air}}$ in the denominators equation (5.25)).

Figure 5.5 shows the inputs of the process, Q_{out} and J_{air}, actuating to maintain the sludge cake mass at the desired value (m^*). The process starts with a sludge cake mass of 0.5 g with a set-point at 0.4 g until day 10, where it is changed to 0.5 g. Since there are two different actuators, λ should be distinguished between both inputs. $\lambda = 50$ for J_{air} and $\lambda = 1$ for Q_{out}. Note that both inputs remain constant in the short-term aspect. After 17 *days*, the slow fouling evolution becomes more important and the controller should increase the J_{air} value to maintain the sludge cake constant.

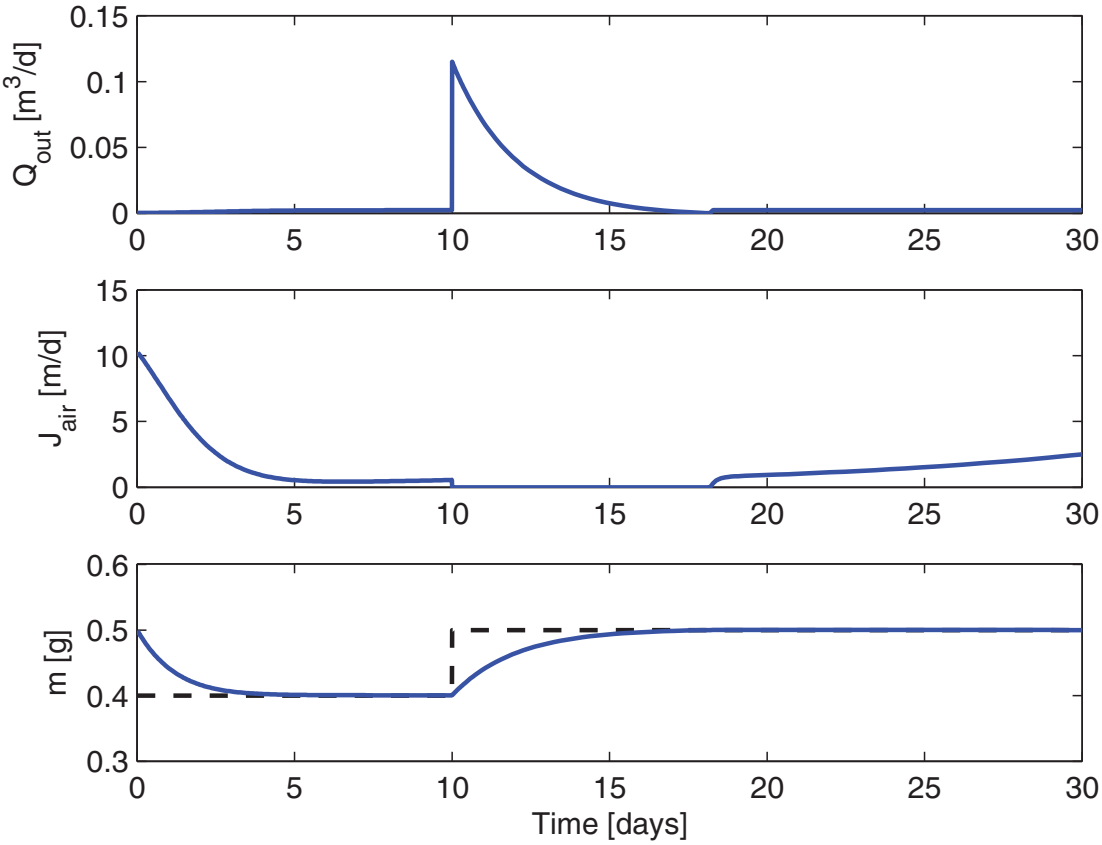


Figure 5.5: Quadratic Lyapunov Controller. The set-point (m^*) value in black.

Chapter 6

Conclusions & Directions for Further Research

The purpose of this thesis was to develop a link between sMBR processes and advanced tools for model analysis and process control design. This was performed by proposing a simplified dynamic model for a submerged membrane bioreactor. The analytical analysis of the model was achieved by applying a singular perturbation method, leading to a specific identification procedure based on model time-scales. Real data obtained from two different water treatment processes have been used for the identification procedure. On account of its simple dynamic, the proposed model showed satisfactory results when the design of nonlinear control laws were implemented, using either analytical techniques to derive globally stabilizing feedback law or numerical techniques, such as model-based predictive control.

sMBR Simple Model: sMBR models studied in literature usually have large quantities of parameters and states, mainly intended to process description and cognition. These complex models are extremely difficult to use when the objective is to manipulate the model and to cast it into nonlinear controller frameworks while interfering in the use and implementation of nonlinear tools to improve the sMBR process robustness and efficiency. The simple model proposed appeared to be sufficient for process prediction and control strategies, as presented in the thesis chapters.

Model Analytical Analysis: Another advantage of a simple dynamic model is the feasibility to apply analytical tools to better understand the process dy-

namic and equilibrium point behaviors. Based on the equilibrium point analysis a coupling between the total suspended solids concentration and the sludge cake build-up is clear. This resulted in the study of the process time-scales showing the viability for dynamic decoupling. The application of the fast and slow dynamics analysis allowed three time-scales to be distinguished (sludge cake build-up, biological degradation and long-term fouling evolution) simplifying even more the model.

Three Time-scales Parameter Identification: This procedure takes advantage of the decoupled aspect of the sMBR process in order to identify the parameters of each time-scale. Compared to all parameter identifications at the same time, the three time-scales parameter identification procedure has lower computational effort, where subsets of parameters are estimated first and the full set of parameters are then re-estimated starting from the previous estimates, which are then much closer to the optimum and severely decrease the computational efforts.

Advanced Control Strategies for sMBR: In the same way that the simple model can be analytically analyzed, advanced control strategies can easily be designed. In this thesis, two controllers are designed to demonstrate the advantages of the simple model when an NMPC and a Lyapunov linearizing-feedback controller are applied.

- An NMPC was applied to a submerged membrane bioreactor process intended to stabilize the trans-membrane pressure at a desired value. The irreversible and reversible resistances have been used in order to optimize the process. The results show that after a certain amount of time, the process cannot be stabilized anymore due to the irreversible resistance. The process input values of Q_{out} and J_{air} lead us to believe that the set-point should be changed or the chemical cleaning procedure should be carried out. Hence, it is possible to control the process and, at the same time, monitor the input variations that try to predict the next cleaning procedure needed.
- Similarly, a Lyapunov linearizing-feedback controller was applied to a submerged membrane bioreactor process intended to globally and asymptotically stabilize the sludge cake mass to the desirable set-point.

Model Validation with Experimental Data: The simple model was validated with two different water treatment experimental data sets from a wastewater treatment plant and a recirculating aquaculture process. In both validations, the time-scales identification procedure was applied, showing its reliability.

- **Wastewater Treatment Plant:** The proposed model for an sMBR process was validated with a large quantity of real data, in the short and the long term. The *TMP* dynamics was reproduced by the model with an accuracy around $R^2 = 0.95$, validating the model horizon prediction propriety. The time-scale separation based on the fast and slow study simplified and decreased the computational effort on the parameter identification procedure, resulting in the possibility for an online prediction of *TMP*.
- **RAS-sMBR:** The parameter identification of biological degradation, fouling long-term evolution and cake build-up are identified. The respective accuracy factors of $R^2 = 0.8988$, $R^2 = 0.8763$ and $R^2 = 0.8929$ were found. The favorable behavior of the model showed the great versatility on different process applications with sMBRs.

Note that both processes had different characteristics, which not prevented the simple dynamic model to have high accuracy factors.

RAS-sMBR Pilot Plant: A recirculating aquaculture plant with a submerged membrane bioreactor was designed and automated to maintain the ammonia concentration at a low level of 0.1 mgN/L. The data acquisition structure was validated and the data was used for model identification. The results show that the main factor of fouling formation was the attachment of irreversible sludge layer, caused by the low concentration of total suspended solids.

Directions for Further Research

Model Modularity: Model modularity is illustrated when temperature, which influence bulk apparent viscosity, is added to the model. Another mechanism that can be added to the model is the substrate biodegradations by the biofilm formed onto the filter surface.

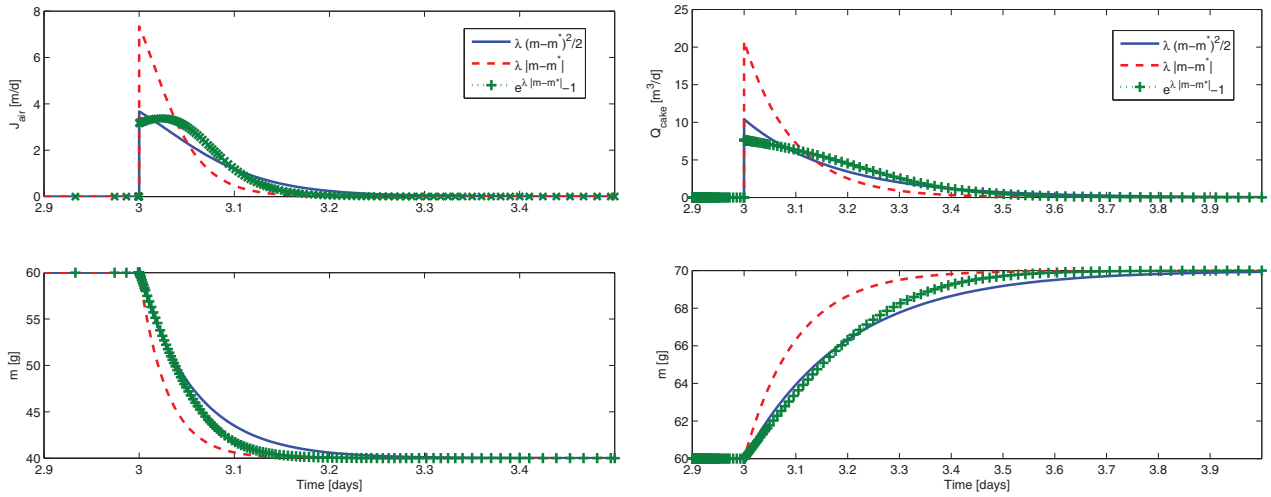


Figure 6.1: Three different control-Lyapunov functions comparison

Modeling Complete Nitrogen Removal Process: The biological model can be extended for a complete nitrogen removal process, adding to it the denitrification aspect on the model dynamics.

Further Experimental Data: The thesis duration was not sufficient for the acquisition of large experimental data sets, especially for biological validation (fast identification procedure). Experiments with different concentrations of ammonia and TSS should be taken into account and new direct and indirect validations should be performed for model validation.

NMPC: (i)An NMPC comprising the biodegradation process can be implemented, intended for global optimization on sMBR processes; (ii)The BSM1-MBR can be considered as the model to be controlled by the NMPC using the simple model proposed.

Different control-Lyapunov Functions for Cake Stabilization: In order to take advantage of the universal formula for feedback, three different Lyapunov functions were tested for the stabilization of the cake build-up. Figure 6.1 presents different dynamic responses to reach the same desired set-point with three distinct Lyapunov-functions. It could be interesting to study these differences in order to choose the best Lyapunov-function performance for several scenarios depending on the position of the state in the state-space.

RAS-sMBR: (i) Based on the validation of a generic simple integrated model for sMBRs, it is possible to implement advanced control strategies to optimize the pilot plant on account of the fouling evolution and biological degradation; (ii)Further research into the denitrification process can be carried out in order to achieve total nitrogen removal from the system.

TMP Prediction for the Wastewater Treatment Pilot Plant: (i) An investigation of the capacity of the model to predict *TMP* evolution in real-time can be executed; (ii) A *TMP* model-based process control can also be applied to the process.

Air-blowers Temperature: In the wastewater pilot plant data study, the influence of the air-temperature, injected by the air-blowers, into the *TMP* is presented. In some cases the variation of the temperature is $\Delta T = \pm 3°C$ affecting the *TMP* to ± 20 *mbar*, i.e. $\pm 22\%$ of the *TMP*. This link between air temperature and *TMP* could be used to optimize the permeate efficiency in order to warm the air injected into the sMBR, resulting in and increase in the sMBR bulk temperature and a decrease in its apparent viscosity and the *TMP*.

Control-Lyapunov Laws: Implement the analytical proof that for all initial conditions with dilution rate positive, the design of a controller increases the performance of the process compared to the process in batch mode.

Nomenclature

A	membrane area [m^2]
A_1	apparent viscosity model parameter [−]
A_2	apparent viscosity model parameter [−]
α	waste flow factor
α_b	stickness of the biomass particle
ASM1	activated sludge model number 1
β	resistance of detachable cake by air cross-flow [m^{-1}]
β_0	initial conditions of β dynamic [m^{-1}]
β_b	erosion rate coefficient of the dynamic sludge film
BOD	biological oxygen demand
CAS	conventional activated sludge
CEB	chemically enhanced backwash
C_d	coefficient of the drag and lift force
CIP	cleaning in place
COD	chemical oxygen demand
CT	capillary tube
C_{SS}	sludge concentration [kg/m^2]
δ_R	total resistance disturbance
d_p	particle size
η	apparent viscosity [$mbar \cdot d$]
ϵ	small positive parameter
F/M ratio	food/maintenance ration
FC	filter cartridge
f_{cost}	function cost
FIM	fisher information matrix
FS	flat sheet
G	shear intensity
g	gravitational constant
γ	efficiency of the J_{air} in long-term evolution [d^{-1}]

γ_b	compression coefficient for the dynamic sludge film
HS	hollow fiber
J	filtration flux
J_{air}	air cross-flow $[m^3/m^2d]$
K_{air}	half saturation of airflow$[g]$
K_S	half saturation of substrate$[g/m^3]$
λ	controller gain
m	reversible fouling mass state $[g]$
m^*	desired mass cake set-point
m_0	initial reversible fouling attached to the membrane $[g]$
MBR	membrane bioreactor
MF	microfiltration
MWCO	molecular weight cutoff
μ	Monod's Law $[d^{-1}]$
μ_{air}	Monod-Like saturation resistance of J_{air} $[m^{-1}]$
$\mu_{S,max}$	maximum growth rate$[d^{-1}]$
μ_w	viscosity of the sludge mixture
MT	multitubular
M_{dc}	dynamic sludge cake $[kg/m^2]$
M_{sc}	stable sludge cake $[kg/m^2]$
NF	nanofimtration
n_t	number of measurements
Ω	scaling matrix
$\hat{P}$	covariance matrix
PES	polyethersulfone
ϕ	permeate flow factor
PLC	Programmable Logic Controller
q_a	air cross-flow by Busch et al (2007b)
Q_{air}	air cross-flow by Mannina et al (2011)
Q_{in}	inflow$[m^3/d]$
Q_{out}	permeate flux $[m^3/d]$
Q_r	recirculation flux $[m^3/d]$
Q_w	waste flux $[m^3/d]$
σ_j	standard deviation of the element j^{th}
R^2	correlation factor
R_b	biofilm layer resistance $[m^{-1}]$
R_c	sludge cake layer resistance $[m^{-1}]$

R_{cp}	condensation polarization resistance [m^{-1}]
R_{irrev}	irreversible fouling resistance [m^{-1}]
R_m	intrinsic membrane resistance [m^{-1}]
R_p	pore-blocking resistance [m^{-1}]
R_{rev}	reversible fouling resistance [m^{-1}]
R_{rev}	scaling resistance [m^{-1}]
R_{total}	total fouling resistance [m^{-1}]
$R_{total,Busch}$	total fouling resistance proposed by Busch et al (2007b) [m^{-1}]
$R_{total,Mannina}$	total fouling resistance proposed by Mannina et al (2011) [m^{-1}]
RO	reverse osmosis
ρ_{irrev}	specific irreversible fouling resistance in terms of the filtrate volume [m^{-2}]
ρ_{rev}	specific reversible resistance[$m \cdot g^{-1}$]
ρ_w	density of the sludge mixture
S	substrate concentration [g/m^3]
S_{in}	input substrate concentration [g/m^3]
Σ	estimated covariance matrix
S_S	readly biodegrable substrate[g/m^3]
sMBR	submerged membrane bioreactor
SRT	sludge retention time
SW	spiral-wound
$Temp$	bulk temperature [°C]
t	time
θ	parameters vector
$t_{permeate}$	duration of the permeate cycle [d]
t_{relax}	duration of the relaxation cycle [d]
t_f	duration of the filtration period [d]
TMP	trans-membrane pressure [$mbar$]
$Temp$	bulk temperature [°C]
TSS	total suspended solids [g/m^3]
V	tank volume[m^3]
$\mathbf{V}(\cdot)$	control-Lyapunov function
V_f	water production within a filtration period of an operation cycle
UF	ultrafiltration
Y	yield coefficient of the substrate consumption [−]
Y_m	vector of process outputs
X	solid matter concentration [g/m^3]

X_{BA} autotrophic biomass $[g/m^3]$
X_{BH} heterotrophic biomass $[g/m^3]$
X_S slowly biodegradable biomass $[g/m^3]$

Bibliography

Acharya C, Nakhla G, Bassi A (2006) Simultaneous nitrification denetrification in an aerobic MBR treating high strength pet food wastwater. In: 2006 Water Environment Foundation

Alex J, Benedetti L, Copp J, Gernaey K, Jeppsson U, Nopens I, Pons M, Rosen C, Steyer J, Vanrolleghem P (2008) Benchmark simulation model no. 1 (BSM1). Tech. rep., IWA Taskgroup on Benchmarking of Control Strategies for WWTPs

Allgöwer F, Findeisen R, Nagy ZK (2004) Nonlinear model predictive control: from theory to application. Journal of the Chinese Institute of Chemical Engineers 35:299 – 315

Atasi K, Crawford G, Hudkins JM, Livingston D, Reardon R, Schmidt H (2006) Membrane systems for wastewater treatment. WEFPress

Atkinson S (2006) Research studies predict strong growth for MBR markets. Membrane Technology 2:8 – 10

Benyahia B, Sari T, Harmand J, Cherki B (2011) Modeling of the soluble microbial products (SMP) in anaerobic membrane bioreactor (AMBR): Equilibria and stability of the AM2b model. In: Proceedings of the 18th IFAC World Congress

Bernard O, Sallet G, Sciandra A (1998) Nonlinaer observers for a class of biological system: Application to validation of a phytoplanktonic growth model. IEEE Transactions on Automatic Control 43:1056 – 1065

Braak E, Alliet M, Schetrite S, Albasi C (2011) Aeration and hydrodynamics in submerged membrane bioreactors. Journal of Membrane Science 379:1 – 18

Broeckmann A, Buscha J, Wintgens T, Marquardt W (2006) Modeling of pore blocking and cake layer formation in membrane filtration for wastewater treatment. Desalination 189:97 – 109

Busch J, Cruse A, Marquardt W (2007a) Run-to-run control of membrane filtration processes. AIChE Journal 53 (9):2316 – 2328

Busch J, Cruse A, Marquart W (2007b) Modeling submerged hollow-fiber membrane filtration for wastewater treatment. Journal of Membrane Science 288:94 – 111

Charfi A, Amar NB, Harmand J (2012) Analysis of fouling mechanisms in anaerobic membrane bioreactors. Water Research 46:2637 – 2650

Chellam S (2005) Artificial neural network model for transient crossflow microfiltration of polydispersed suspensions. Jounal of Membrane Science 258:35 – 42

Chen L, Tian Y, Cao C, Zhang S, Zhang S (2012) Sensitivity and uncertainty analyses of an extended ASM3-SMP model describing membrane bioreactor operation. Journal of Membrane Science 389:99 – 109

Choi YJ, Oh H, Lee S, Nam SH, Hwang TM (2012) Investigation of the filtration characteristics of pilot-scale hollow fiber submerged MF system using cake formation model and artificial neural networks model. Desalination 297:20–29

Cicek N (2003) A review of membrane bioreactors and their potential application in the treatment of agriculture wastewater. Canadian Biosystems Engineering 45:6.37 – 6.49

Crab R, Avnimelech Y, Defoirdt T, Bossier P, Verstraete W (2007) Nitrogen removal techniques in aquaculture for a sustainable production. Aquaculture 270:1–14

Dalmau M, Rodriguez-Roda I, Ayesa E, Odriozola J, Sancho L, Comas J (2013) Development of a decision tree for the integrated operation of nutrient removal MBRs based on simulation studies and expert knowledge. Chemical Engineering Journal 217:174 – 184

David R (2008) Modélisation dynamique et commande des procédés d'épuration biologique des auex usées à boues activées. PhD thesis, Faculté Polytechnique de Mons

Di Bella G, Mannina G, Viviani G (2008) An integrated model for physical-biological wastewater organic removal in a submerged membrane bioreactor: Model development and parameter estimation. Journal of Membrane Science 322:1–12

Distéfano N (1974) Nonlinaer Processes in Engineering. Adademic Press

Dochain D, Vanrolleghem PA (2001) Dynamical modelling and estimation in wastewater treatment processes. IWA Publishing

Eding E, Kamstra A, Verreth J, Huisman E, Klapwijk A (2006) Design and operation of nitrifying trickling filters in recirculating aquaculture: A review. Aquacultural Engineering 34(3):234 – 260

ERemigi (2008) Summer school on modelling MBR processes: MBR modelling - hands-on. Tech. rep., www.mbr-network.eu

Fenu A, Guglielmi G, Jimenez J, Spérandio M, Saroj D, Lesjean B, Brepols C, Thoeye C, Nopens I (2010) Activated sludge model (ASM) based modelling of membrane bioreactor (MBR) processes: A critical review with special regard to MBR specificities. Water Research 44:4272 – 4294

Fernández XR, Rosenthal I, Anlauf H, Nirschl H (2011) Experimental and analytical modeling of the filtration mechanisms of a paper stack candle filter. Chemical Engineering Research and Design 89:2776–2784

Ferrero G, Moncús H, Buttuglieri G, Gabarron S, Comas J, Rodríguez-Roda I (2011) Development of a control algorithm for air-scour reduction in membrane bioreactors for wastewater treatment. Journal of Chemical Technology and Biotechnology 86 (6):784 – 789

Freeman R, Kokotović P (1997) Robust Nonlinear Control Design. Birkhäuser

Gander M, Jefferson B, Judd S (2000) Aerobic MBRs for domestic wastewater treatment: a review with cost consideration. Separation Purification Technology 18:119 – 130

Gao W, Liang H, , Ma J, Han M, lin Chen Z, shuang Han Z, bai Li G (2011) Membrane fouling control in ultrafiltration technology for drinking water production: A review. Desalination 272:1–8

Gehlert G, Abdulkadir M, Fuhrmann J, Hapke J (2005) Dynamic modeling of an ultrafiltration module for use in a membrane bioreactor. Journal of Membrane Science 248:63 – 71

Geissler S, Wintgens T, Melin T, Vossenkaul K, Kullmann C (2005) Modelling approaches for filtration processes with novel submerged capillary modules in membrane bioreactors for wastewater treatment. Desalination 178:125 – 134

Gemende B, Gerbeth A, Pausch N, von Bresinsky A (2008) Tests for application of membrane technology in a new method for intensive aquaculture. Desalination 224:57 – 63

Gershanovich A, Pototskij I (1992) The peculiarities of non-faecal nitrogen excretion in sturgeons (pisces; acipenseridae) -1. the influence of ration size. Comparative Biochemistry and Physiology Part A 103(3):609–612

Grüne L, Pannek J (2011) Nonlinaer Model Predictive Control: Theory and Algorithms. Springer

Henson M, Seborg D (1997) Feedback linearizing control, in Nonlinear process control. Prentice Hall

Henze M, Jr CLG, Gujer W, Marais G, Matsuo T (1987) A general model for single-sludge wastewater treatment system. Water Research 21:505 – 515

Henze M, Gujer W, Mino T, van Loodrecht M (eds) (2000) Activated sludge models ASM1, ASM2, ASM2d and ASM3. IWA Publisher

Henze M, van Loosdrecht MC, Ekama GA, Brdjanovic D (eds) (2011) Biological wastewater treatment - Principles, Modeling and Design. IWA Publisher

Ho CC, Zydney AL (2000) A combined pore blockage and cake filtration model for protein fouling during microfiltration. Journal of Colloid and Interface Science 232:389 –399

Howell JA (2004) Future of membranes and membrane reactor in green technologies and for water resue. Desalination 162:1–11

Hutchinson W, Jeffrey M, O'Sullivan DD, Casement D, Clarke S (2004) Recirculating Aquaculture Systems: Minimum Standards for Design, Construction and Management. Inland Aquaculture Association of South Australia, 2004.

Hydromantis - Environmental Software Solution, Inc (2012) GPS-X, version 6.2.0. Software

IWA Group (2014) Membrane bioreactors: A global picture. URL http://www.iwawaterwiki.org/xwiki/bin/view/Articles/Membranebioreactors

Jan Kincl PD, Cakl J (2009) Filtration model for hollow fiber membranes with compressible cake formation. Desalination 240:99 – 107

Jang N, Ren X, Cho J, Kim IS (2006) Steady-state modeling of bio-fouling potentials with respect to the biological kinetics in the submerged membrane bioreactor (SMBR). Journal of Membrane Science 284:352 – 360

Jeison D (2007) Anaerobic membrane bioreactors for wastewater treatment - feasibility and potential application. PhD thesis, Wageningen Universiteit

Jones D, Sleeman B (2003) Differential equations and mathematical biology. Chapman & Hall/CRC

Jørgensena MK, Buggea TV, Christensena ML, Keiding K (2012) Modeling approach to determine cake buildup and compression in a high-shear membrane bioreactor. Journal of Membrane Science 409 - 410:335 – 345

Judd C (2014) The mbr site. URL http://www.thembrsite.com

Judd S, Judd C (2011) The MBR book, principles and applications of membrane bioreactors in water and wastewater treatment, second edition edn. Elsevier

Khalil HK (2002) Nonlinear System, 3rd edn. Prentice Hall

Khan SJ, Visvanathan C, Jegatheesan V (2009) Prediction of membrane fouling in MBR systems using empirically estimated specific cake resistance. Bioresource Technology 100:6133 – 6136

Klamkin MS (1995) Mathematical modelling: Classroom notes in applied mathematics. SIAM

Kokotović P, Khalil HK, O'Reilly J (1986) Singular pertubation methods in control: analysis and design. Academic Press INC.(London)LTD

Kouvaritakis B, Cannon M (2001) Nonlinear predictive control: Theory and Practice. IEE Control Series, 61

Kuberkar VT, Davis RH (2000) Modeling of fouling reduction by secondary membranes. Journal of Membrane Science 168:243 – 258

Lapolli FR, Leon AC, Tavares CRG, Campos J (1998) Tratamento de água residuárias através de membranas. Tech. rep., Departamento de Engenharia Sanitária e Ambiental Universidade Federal de Santa Catarina

Le-Clech P, Chen V, Fane TA (2006) Fouling in membrane bioreactors used in wastewater treatment. Journal of Membrane Science 284:17 – 53

Lee Y, Cho J, Seo Y, Lee JW, Ahn KH (2002) Modeling of submerged membrane bioreactor process for wastewater treatment. Desalination 146:451 – 457

Li X, Wang X (2006) Modelling of membrane fouling in a submerged membrane bioreactor. Journal of Membrane Science 278:151 – 161

Lu SG, Imai T, Ukita M, Sekine M, Higuchi T, Fukagawa M (2001) A model for membrane bioreactor processes based on the concept of formation and degradation of soluble microbial production. Water Research 35:2038 – 2048

Maere T, Moerenhout S, Judd S, Nopens I (2011) BSM-MBR: A benchmark simulation model to compare control and operation strategies for membrane bioreactors. Water Research 45 (6):2181 – 2190

Mailier J, Goffaux G, Vande Wouwer A (2010) Analysis of nonlinear software sensor applied to bioprocesses. Presentation Benelux

Mangold M, Ginkel M, Gilles E (2004) A model library for membrane reactor implemnted in the process modelling tool ProMot. Computational Chemical Engeeniring 28 (3):319 – 332

Mannina G, Di Bella G, Viviani G (2011) An integrated model for biological and physical process simulation in membrane bioreactor. Journal of Membrane 376:56 – 69

Marriott J, Sørensen E (2003) A general approach to modeling membrane modules. Chemical Engineering Science 58:4975 – 4990

McKay M, Conover W, Beckman R (1979) A comparison of three methods for selecting values of input variables in the analysis of output from a computer code. Technometrics 221:239 – 245

Merlo RP, Adham S, Gagliardo P, Trussell RS, Trussell R, Watson M (eds) (2000) Application of membrane bioreactor (MBR) technology for water reclamation, vol 27, Proceedings of the Water Environment Federation, WEFTEC 2000: Session 11 through Session 20, Water Environment Federation

Murray JD (2002) Mathematical Biology - I: an introduction. Springer-Verlag

Naessens W, Maere T, Nopens I (2012a) Critical review of membrane bioreactor models - Part 1: Biokinetic and filtration models. Bioresource Technology 122:95 – 106

Naessens W, Maere T, Ratkovich N, SVedantam, Nopens I (2012b) Critical review of membrane bioreactor models - Part 2: Hydrodynamic and integrated models. Bioresource Technology 122:107 – 118

Ng AN, Kim AS (2007) A mini-review of modeling studies on membrane bioreactor (MBR) treatment for municipal wastewater. Desalination 212:261 – 281

Park S, Bae W, Chung J, Baek SC (2007) Empirical model of the ph dependence of the maximum specific nitrification rate. Process Biochemistry 42:1671 – 1676

Peiris RH, Budman H, Moresoli C, Legge RL (2010) Optimization of membrane filtration process for drinking water treatment using fluorescentebase measurement. In: Proceedings of the 9th International Symposium on Dynamics and Control of Process System

Perko L (1991) Differential equations and dynamic systems. Springer-Verlag

Piedrahita RH (2003) Reducing the potential environmental impact of tank aquaculture effluents through intensification and recirculation. Aquaculture 226:35–44

Pimentel GA, Dalmau M, AVargas, Comas J, Rodriguez-Roda I, Vande Wouwer ARA (2015a) Validation of a simple fouling model for submerged membrane bioreactor. In: Submitted to MathMod2015

Pimentel GA, Vande Wouwer A, Harmand J, Rapaport A (2015b) Design, analysis and validation of a simple dynamic model of a submerged membrane bioreactor. Water Research Journal 70:97–108

Polyakov YS (2006) Deadened outside-in hollow fiber membrane filter: Mathematical model. Journal of Membrane Science 279:615 – 624

Pulefou T, Jegatheesan V, Steicker C, Kim SH (2008) Applications of submerged membrane bioreactor for aquaculture effluent reuse. Desalination 221:534 – 542

Queinnec I, Ochoa JC, Paul E, Wouwer AV (2006) Dynamic modelling of a biofilter used for nitrification of drinking water at low influent ammonia concentrations. In: International Symposium on Advanced Control of Chemical Processes

Robles A, Ruano M, Ribes J, Seco A, Ferrer J (2013a) A filtration model applied to submerged anaerobic MBRs (SAnMBRs). Journal of Membrane Science 444:139 – 147

Robles A, Ruano M, Ribes J, Seco A, Ferrer J (2013b) Mathematical modelling of filtration in submerged anaerobic MBRs (SAnMBRs): Long-term validation. Jounal of Membrane Science 446:303 – 309

Rodríguez FA, Martinez-Toledo M, González-López J, Hontoria E, Poyatos J (2010) Performance of bench-scale membrane bioreactor under real work conditions using pure oxygen: Viscosity and oxygen transfer analysis. Bioprocess and Biosystems Engineering 33:885 – 892

Saksena V, O'Reilly J, Kokotović PV (1984) Singular perturbation and time scale methods in control theory: Survey 1976 - 1983. Automatica 20:273 – 293

Santos L, Dewasme L, Coutinho D, Wouwer AV (2012) Nonlinear model predictive control of fed-batch cultures of micro-organisms exhibiting overflow metabolism. Computers and Chemical Engineering 39:143–151

Sari T (2005) Contôle non linéaire et application. Éditeurs des sciences et des arts - Hermman

Sarioglu M, Insel G, Artan N, Orhon D (2009) Model evaluation of simultaneous nitrification and denitrification in membrane bioreactor operated without an anoxic reactor. Journal of Membrane Science 337:17–27

Sarioglu M, Insel G, Orhon D (2012) Dynamic in-series resistance modeling and analysis of a submerged membrane bioreactor using a novel filtration mode. Desalination 285:285 – 294

Sartorius C, Walz R, Orzanna R (2013) Lead market for membrane bio-reactor (MBR) technology - china s second-mover strategy for the development and exploitation of its lead market potential. Tech. rep., Fraunhofer Institute for Systems and Innovation Research ISI, Karlsruhe

Shirazi S, Lin CJ, Chen D (2010) Inorganic fouling of pressure-driven membrane processes - a critical review. Desalination 250:236 – 248

Sjöberg J, Zhang Q, Ljung L, Benveniste A, Delyon B, Glorennec PY, ans Anatoli Juditsky HH (1995) Nonlinear black-box modeling in system identification: a unified overview. Automatica 31 (12):1691 – 1724

Slotine J, Li W (1991) Applied nonlinear control. Prentice Hall

Smith HL, Waltman P (1995) The theory of the chemostat. Cambridge University press

Sontag ED (1998) Mathematical control theory. Springer

Spérandio M, Espinosa MC (2008) Modelling an aerobic submerged membrane bioreactor with asm models on a large range of sludge retention time. Desalination 231:82–90

Muñoz Tamayo R, Laroche B, Leclerc M, Walter E (2009) Ideas:a parameter identification toolbox with symbolic analysis of uncertainty and its application to biological modelling. In: 15th Symposium on System Identification

Tchobanoglous G, Burton FL, Stensel HD (2003) Wastewater engineering - treatment and reuse. McGranw Hill

Thomas SL, Piedrahita RH (1998) Apparent ammonia-nitrogen production rates of white sturgeon (acipenser transmontanus) in commercial aquaculture systems. Aquacultural Engineering 17:45–55

Tien C, Ramarao BV (2011) Revisiting the laws of filtration: An assessment of their use in identifying particle retention mechanisms in filtration. Journal of Membrane Science 383:17 – 25

Van Impe JF, Vanrolleghem PA, Iserentant DM (1998) Advanced instrumentation, data interpretation, and control of biotechnological processes. Kluwer Academic Publishers

Viadero Jr RC, Noblet JA (2002) Membrane filtration for removal of fine solid from aquaculture process water. Aquacultural Engineering 26:151 – 169

Viadero Jr RC, Cunningham JH, Semmens KJ, Tierney AE (2005) Effluent and production impacts of flow-through aquaculture operations in west virginia. Aquacultural Engineering 33:258 – 270

Wintgens T, Rosen J, Melin T, Brepols C, Brensla K, Engelhardt N (2003) Modelling of membrane bioreactor system for municipal wastewater treatment. Journal of Membrane Science 216:55–65

Wu J, He C, Zhang Y (2012) Modeling membrane fouling in a submerged membrane bioreactor by considering the role of solid, colloidal and soluble components. Journal of Membrane Science 397 - 398:102 – 111

Yang W, Cicek N, Ilg J (2006) State-of-the-art of membrane bioreactors: Worldwide research and commercial application in north america. Journal of Membrane Science 270:201–211

Zarragoita-González A, Schetrite S, Alliet M, Jáuregui-Haza U, Albasi C (2008) Modeling of submerged membrane bioreactor: Conceptual study about link between activated sludge biokinetics, aeration and fouling process. Journal of Membrane Science 325:612 – 624

Zuthi M, Ngo H, Guo W (2012) Modelling bioprocesses and membrane fouling in membrane fouling in membrane bioreactor(mbr): A review toward finding an integrated model framework. Bioresource Technology 122:119 – 129

Appendix A

About Lyapunov Controllers for Bioreactors

A.1 Biological Stabilization Based on Lyapunov Controllers Theory

In this section is presented a special case of bioprocess with no membrane in order to stabilize the substrate concentration. This is a preliminary work that intends to be extended later for the MBRs models developed in this thesis. The solid retention time (SRT) is controlled by actuating the waste flow rate Q_w when Q_{out} is zero. It is possible to model this scenario by the chemostat process (equation (A.1)), where the representation is in Figure A.1.

$$\begin{cases} \dfrac{dS}{dt} = -\mu(S)X + D(S_{in} - S) & \text{(A.1a)} \\ \dfrac{dX}{dt} = (\mu(S) - D)X & \text{(A.1b)} \end{cases}$$

$$\text{where } \mu(S) = \mu_{S,max}\frac{S}{K_S + S}$$

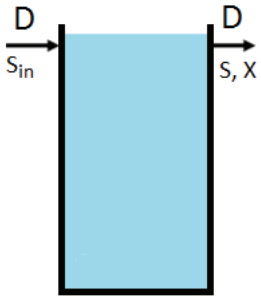


Figure A.1: Chemostat process representation.

A controller based on the universal formula for feedback, proposed by Sontag (1998), is designed to control the chemostat to a desired substrate concentration (S^*). This procedure uses a control-Lyapunov function in order to design a feedback stabilizer for S when

$$\dot{\mathbf{V}}(S) = \mathbf{V}'(S)\dot{S} = -\lambda \mathbf{V}(S) \tag{A.2}$$

where λ is the gain imposed on the dynamic and $\mathbf{V}'(S) = \frac{\partial \mathbf{V}}{\partial S}$.

When applying (A.1a) to (A.2)

$$-\mathbf{V}'(S)\mu(S)X + \mathbf{V}'(S)D(S_{in} - S) = -\lambda \mathbf{V}(S) \tag{A.3}$$

and considering the dilution rate D as the process input, the control law is expressed as follows:

$$D = \frac{\mathbf{V}'(S)\mu(S)X - \lambda \mathbf{V}(S)}{\mathbf{V}'(S)(S_{in} - S)} = \phi(S, X). \tag{A.4}$$

The value of $\phi(S, X)$ is positive if

$$\phi(S, X) \geq 0 \Longleftrightarrow X \geq \frac{\lambda \mathbf{V}(S)}{\mathbf{V}'(S)\mu(S)} = \lambda \gamma(S) \tag{A.5}$$

Note that the expression of this feedback has no reason to be non-negative. When it is negative one has to use a "saturation" of the expression i.e. to choose a null control, which no longer guarantees a convergence with an exponential decay λ of the function $\mathbf{V}$. The objective of this Section is to investigate the role of the choice of the function $\mathbf{V}(\cdot)$ on the positivity of this formula on the domain.

The closed-loop equilibrium may be expressed as follows:

$$\phi(S, X) = X - \lambda \gamma(S) \tag{A.6}$$

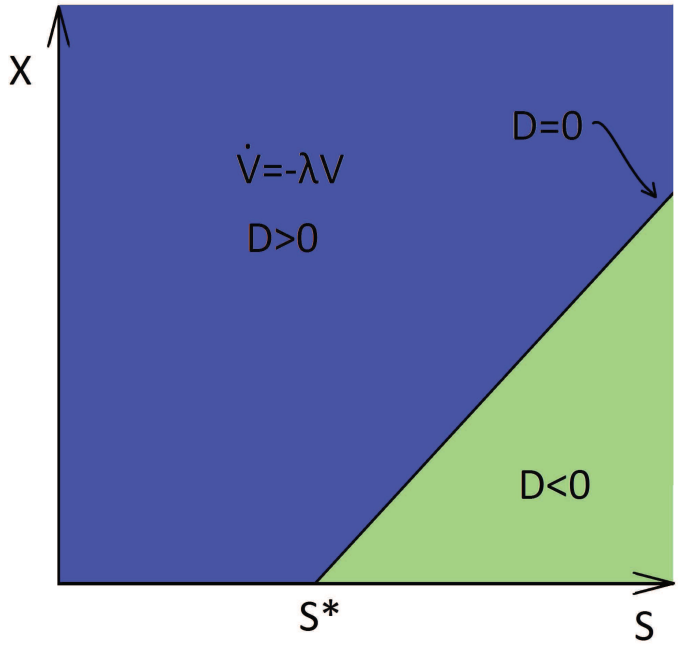


Figure A.2: Area where the initial conditions will result in a positive control law (blue zone) or where the control law has negative values (light green zone)

Note that when $X \geq \gamma(S)$, the dilution rate is always positive $\phi \geq 0$. Figure A.2 shows two areas, positive and negative dilution rate and its boundary.

The positive dilution rate depends on the gain λ and the control-Lyapunov function, imposed to the controller. Therefore, it is possible to conclude if the initial set values of S and X fulfill the following inequality the closed-loop process has always a positive dilution rate:

$$\frac{\partial \phi}{\partial S}\dot{S} + \frac{\partial \phi}{\partial X}\dot{X} \geq 0 \tag{A.7}$$

where applying (A.6) to (A.7) results

$$\dot{X} - \lambda \gamma'(S)\dot{S} \geq 0 \tag{A.8}$$

$\dot{S}$ and $\dot{X}$ are the closed-loop derivatives, which are expressed such as:

$$\begin{cases} \dot{S} = -\lambda \dfrac{\mathbf{V}(S)}{\mathbf{V}'(S)} \\ \dot{X} = \lambda \mu(S)\gamma(S) - \lambda \left[\mu(S)\gamma - \dfrac{\mathbf{V}(S)}{\mathbf{V}'(S)} \right] \dfrac{\lambda \gamma(S)}{(S_{in} - S)} \end{cases}$$

A.1.1 Comparison of two Control-Lyapunov Functions

Based on the fact that the selection of the Lyapunov function $\mathbf{V}$ and the decay speed λ change the admissible region of the initial condition, a study comparing the quadratic and the exponential Lyapunov-function ($\mathbf{V}_{quad}$, $\mathbf{V}_{exp}$) is proceeded.

$$\mathbf{V}_{quad} = \frac{1}{2}(S - S^*)^2, \quad \mathbf{V}_{exp} = \exp(k|S - S^*|) - 1 \tag{A.10}$$

Quadratic Function Considering

$$\lambda_1\gamma(S) = \lambda_1\left(\frac{(S - S^*)^2}{(S - S^*)\mu(S)}\right) = \lambda_1\left(\frac{(S - S^*)}{\mu(S)}\right) \tag{A.11}$$

and $D > 0, \forall S_0 < S^*$, but $\forall S_0 > S^*$ the region of $D > 0$ is in functions of λ. This will be illustrated in Section A.1.2.

Exponential Function Considering

$$\lambda_2\gamma(S) = \lambda_2\left(\frac{1 - \exp(-k|S - S^*|)}{k\ sign(S - S^*)\mu(S)}\right) \tag{A.12}$$

In the same manner as the quadratic function, $D > 0, \forall S_0 > 0$, but $\forall S_0 > S^*$, D is ruled by the controller gains k and λ_2.

These two studies show the potential of selecting the Lyapunov-functions with different properties with regard to the initial conditions of the process and the desired speed of convergence and/or less inlet substrate consumption, as well as the ability to cope with input constraint (positivity of the input variable).

A.1.2 Simulation Tests

To illustrate the analytical results aforementioned simulation were proceeded. Figure A.3 shows the phase-plot, on the left, and the plot of dilution rate over the time, on the right. S^* is set to 0.4 mg/L. Three different initial values of S and X, represented by big dots, were selected. The quadratic Lyapunov law is used with $\lambda_1 = 1$. The blue-lines in the plot, represent when all the

trajectory of each dilution rate D is positive. In green, when there is at least one point of negative dilution rate in all trajectory.

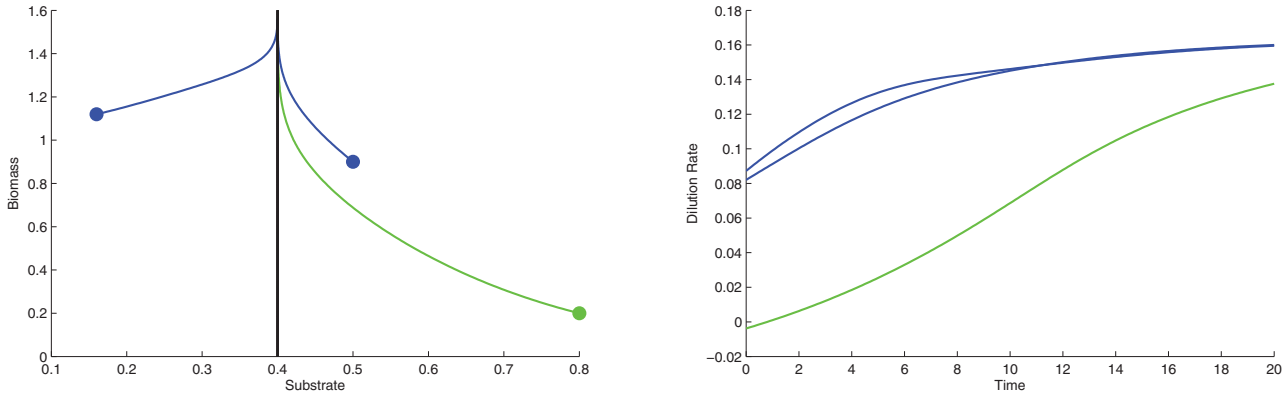
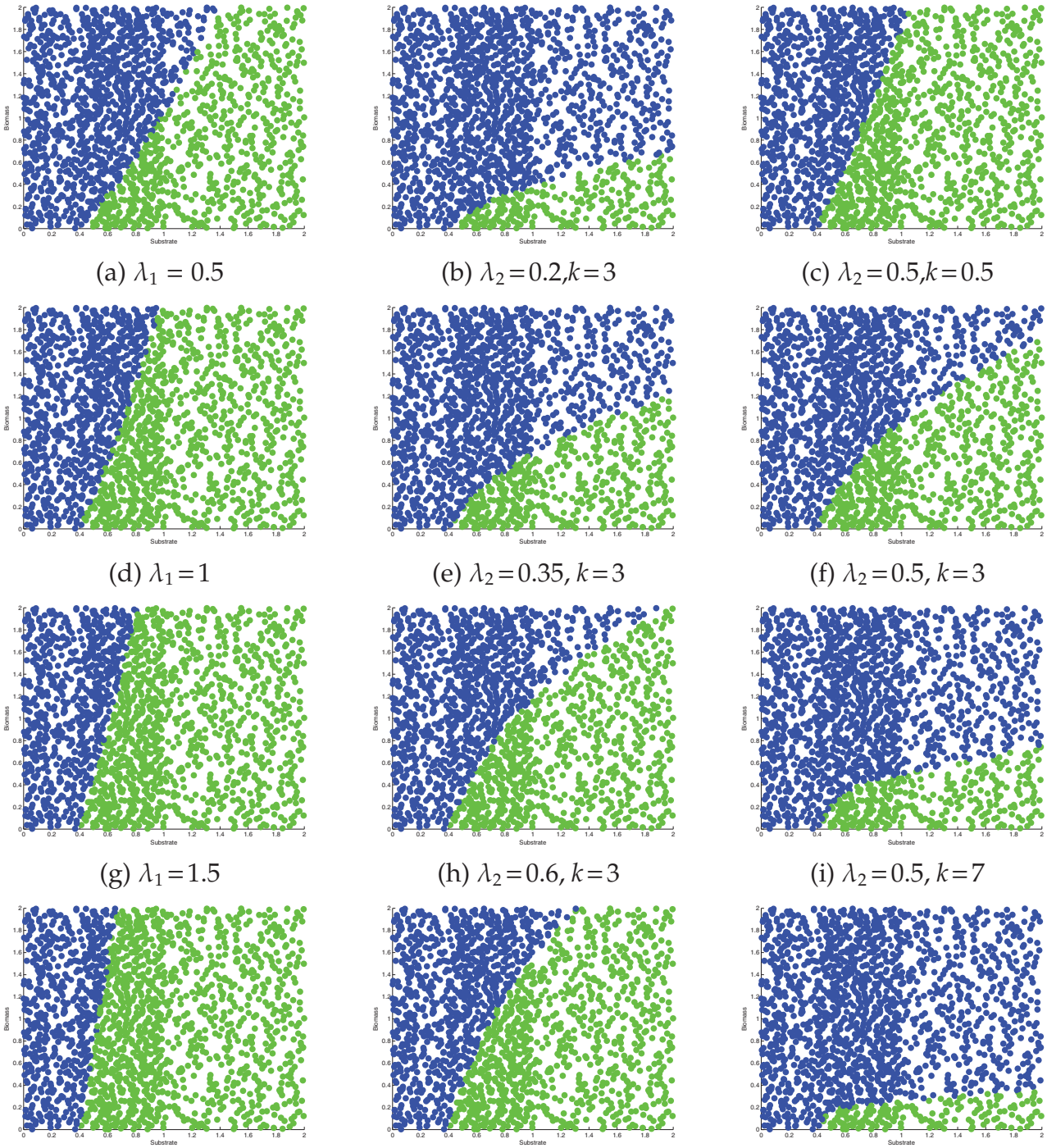


Figure A.3: Quadratic Lyapunov Functions with $\lambda_1 = 1$.

To have a larger perspective of the positive and negative zones, simulations were carried out using ScicosLab and 1700 different initial conditions (S_0,X_0) generated by the Latin HyperCube sampling (LHS) method (McKay et al, 1979). Figure A.4 shows the initial values of S and X (big dots) obtained with LHS.

Analyzing the columns from top to bottom, it is possible to see that: in column one the λ_1 that increases; in column two, the λ_2 that increases, and in column three, k increases.

The combination of λ_2 and k, and values of λ_1 are clearly related to the area of actuation of the exponential and quadratic functions. These prospections depict the dependence of the process to the initial conditions. Therefore, a different control-law can be designed or selected in order to obtain a positive influent flow through a larger area.



(a) $\lambda_1 = 0.5$ (b) $\lambda_2 = 0.2, k = 3$ (c) $\lambda_2 = 0.5, k = 0.5$

(d) $\lambda_1 = 1$ (e) $\lambda_2 = 0.35, k = 3$ (f) $\lambda_2 = 0.5, k = 3$

(g) $\lambda_1 = 1.5$ (h) $\lambda_2 = 0.6, k = 3$ (i) $\lambda_2 = 0.5, k = 7$

(j) $\lambda_1 = 2.5$ (k) $\lambda_2 = 0.8, k = 3$ (l) $\lambda_2 = 0.5, k = 14$.

Figure A.4: Each point means initial conditions, where abscissas are the substrate concentration (S) and the ordinate are the biomass concentrations(X). Blue: positive dilution rate in all trajectory. Green: at least one point of negative dilution rate.